IN-24
168479

FRACTURE CRITERIA FOR DISCONTINUOUSLY REINFORCED METAL MATRIX COMPOSITES

NASA Grant NAG-1-724

SEMI-ANNUAL REPORT

Period of Performance

February 16, 1988 thru August 15, 1988

SUBMITTED TO

NASA-Langley Research Center
Hampton, Virginia

By

H. J. Rack, J. G. Goree, J. Albritton
and P. Ratnaparkhi

Department of Mechanical Engineering
Clemson University
Clemson, South Carolina 29634-0921

FRACTURE CRITERIA FOR DISCONTINUOUSLY REINFORCED METAL MATRIX COMPOSITES

NASA Grant NAG-1-724

SEMI-ANNUAL REPORT

Period of Performance

February 16, 1988 thru August 15, 1988

SUBMITTED TO

NASA-Langley Research Center
Hampton, Virginia

By

H. J. Rack, J. G. Goree, J. Albritton
and P. Ratnaparkhi

Department of Mechanical Engineering
Clemson University
Clemson, South Carolina 29634-0921

ABSTRACT

This report summarizes the progress achieved during the period September 16, 1987 to August 15, 1988 on NASA Grant NAG-1-724, "Fracture Criteria for Discontinuously Reinforced Metal Matrix Composites". Appended to the report are copies of three manuscripts prepared by the authors under NASA funding during the performance period.

INTRODUCTION

Renewed interest in light-weight, ceramic reinforced metal matrix composites for high performance applications has recently resulted in the development of continuous and discontinuously reinforced silicon carbide reinforced aluminum alloy metal matrix composites (1,2). While these materials offer the potential of achieving outstanding strength and stiffness properties, their successful design application will require development of suitable damage tolerance design criteria. These criteria should also include development of relatively simple and inexpensive mechanical tests that can be used for materials qualification and acceptance.

Historically, damage tolerant design fail-safe design of metallic primary-airframe-structure has evolved from a consideration of whole-life fatigue to assesment of the influence of load spectrum on fatigue crack growth and fracture resistance, the latter utilizing the concepts embodied within linear elastic fracture mechanics (LEFM). The applicability of this approach to fail-safe design of monoque metallic structure has been repeatedly demonstrated through both laboratory and service experience.

One of the fundamental precepts included in the utilization of linear elastic fracture mechanics for airframe fail-safe design is that the description of the critical fracture event depends only on the local stress state in the vicinity of the crack tip, even if the stresses remote from the

crack tip are very much different. This approach leads directly to the acceptance of the parameter K_{IC}, the Mode I plane strain fracture toughness, as a material property, similar to the yield strength, whose value does not depend upon specimen configuration. Indeed, determination of K_{IC} has been standardized through use of ASTM E-399 procedures.

However, the rather simple, but classic experiments of Reedy (3), have shown that linear elestic fracture mechanics failure criteria are not appropriate for continuously reinforced unidirectional metal matrix composites. His results showed, for example, that drastically different values of K_{IC} can be obtained in unidirectional boron/aluminum composites through variation in test coupon configuration. For samples oriented so that the pre-crack was perpendicular to the fiber axis, K_{IC} = 77 ksi$\sqrt{in}$ for a center-cracked panel, 59 ksi$\sqrt{in}$ for a three-point bend sample and 34 ksi$\sqrt{in}$ for a compact-tension sample. Microscopic examination further indicated that the mode of crack growth in this material was also sample dependent.

Crack growth in the three-point bend and compact-tension samples typically involved crack splitting and branching along the fiber-matrix interface, while crack propagation in the center-cracked samples proceeded across the fibers in a self-similar manner.

Early fracture toughness measurements in whisker reinforced aluminum metal matrix composites suggest that the results may also be specimen dependent. For example, plane strain fracture toughness values between 5 and 30 ksi$\sqrt{in}$ have been reported (4-8) for whisker reinforced 6061 and 2124 aluminum. In addition, these investigators have noted the great difficulty encountered in pre-cracking L-T compact-tension samples. Indeed, almost all data were obtained utilizing L-T center-cracked panels. If confirmed, these observations cast doubt on the general applicability of linear elastic

fracture mechanics to discontinuously reinforced whisker metal matrix composites.

The first phase of this investigation, as reported previously (9), was designed to examine what effect sample configuration has on the details of initial crack propagation in discontinuously whisker reinforced aluminum metal matrix composites. Care was taken to allow direct comparison of fracture toughness values utilizing differing sample configurations and orientations, holding all materials variables constant, e.g., extrusion ratio, heat treatment, chemistry, etc.

The second phase of this investigation, initiated during this report period, extended the phase 1 study to consider (a) the effect of lower volume fraction, 5 and 10 volume percent, reinforcement content, (b) whisker orientation and (c) matrix plasticity on the fracture behavior of SiC whisker reinforced aluminum metal matrix composites. A comparison of the results obtained from 10 and 20 volume percent SiC whisker reinforced 2124-F is summarized in Appendix C, a paper to be published in the "Proceedings of the Seventh International Conference on Fracture, 1989(ICF7)", being held in Houston, Texas, March 20-24, 1989. Fractographic studies of the 10 and 20 volume percent SiC whisker reinforced fracture toughness measurements presented in Appendix C have been completed. Finally, detailed aging studies of unreinforced, 5, 10 and 20 volume percent SiC whisker reinforced 2124 has been initiated to provide selection criteria for further fracture toughness and plane strain tensile studies.

EXPERIMENTAL PROCEDURES

2124 reinforced with 0, 5, 10 and 20 volume percent SiC whiskers are being utilized in this investigation. These materials were fabricated

following the generalized procedures described in Appendix B. Essentially this process involves wet blending helium inert gas atomized powder and SiC whiskers, drying, cold compaction and vacuum hot pressing in the mushy zone to either 8 inch (5 volume percent) or 6 inch (0, 10, 20 volume percent) diameter billets. Following homogenization, the billets were extruded to 5 inch wide by 0.5 inch thick planks.

Optical microscopy of the 0.5 inch thick extrusions indicated that the SiC whiskers were relatively evenly distributed throughout the aluminum matrix, see for example Figure 1. A comparison of Figure 1 with those previously presented for the 10 and 20 volume percent reinforced composites (9) indicates that the use of F-8 whiskers in the 5 volume percent composite virtually eliminates the large SiO_2 and SiC particulate inclusions normally associated with these composites. It is anticipated that the elimination of these inclusions will enhance the tensile ductilities to be measured in this investigation and allow a truer examination of the effects of whisker reinforcement on the fracture process.

Whisker alignment and length-to-diameter measurements are being made on the 5, 10 and 20 volume percent composites. Figure 2 schematically defines the two orientations being examined, the surface plane and thru thickness direction. Initially, samples were prepared utilizing standard metallographic procedures, the final step being etching with 10 percent bromine in ethanol. A minimum of 30 scanning electron microgarphs at 3500 and 6500X were taken for data collection and analysis, with care being taken to select areas representative of the bulk. A minimum of 500 whisker orientation and 250 whisker length measurements were made on each of the orientations examined. The whisker length-to-diameter, l/d, ratio was finally determined assuming that the whisker diameter was 0.5 μm.

Figure 1 - Optical Micrograph of Extruded 2124 Reinforced with 5 V/O F-8 SiC Whiskers.

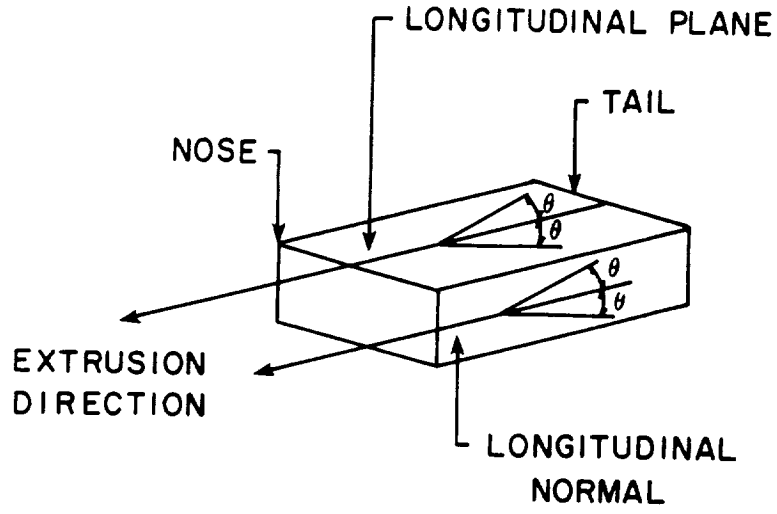

A. ORIENTATION RELATIVE TO EXTRUSION DIRECTION

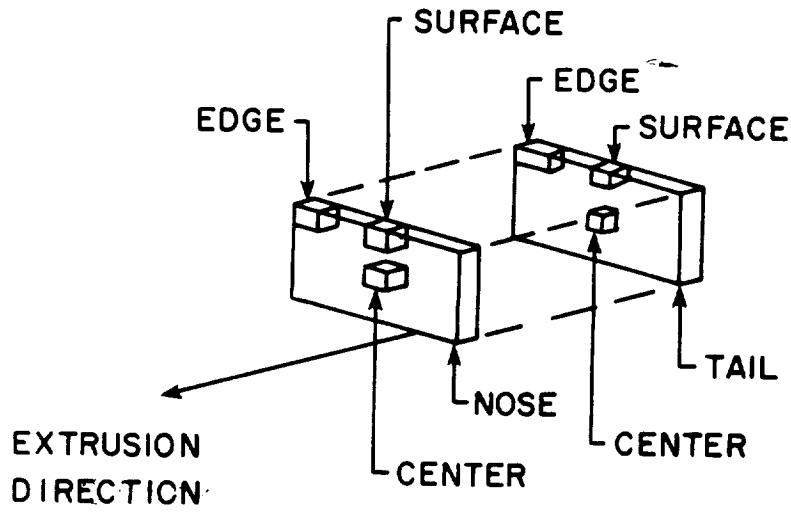

B. SPECIMEN LOCATION

Figure 2 - Schematic Diagram Illustrating Whisker Orientation Definition.

Quantitative analysis of the 10 and 20 volume percent SiC whisker reinforced extrusions (9) showed that the 11.5:1 extrusion ratio used in fabricating these composites resulted in a distinct alignment of the SiC whiskers with respect to the extrusion direction in both the transverse (T) and the thru-thickness (S) planes. Furthermore, the degree of alignment, as depicted by the standard deviation of the whisker orientation with respect to the extrusion direction, was a function of the volume percent SiC, the 20 volume percent reinforced composite exhibiting a higher degree of alignment, particularly in the thru-thickness plane.

Continuing quantitative characterization of the 10 and 20 volume percent SiC whisker reinforced extrusions indicates that the whisker length-to-diameter ratio (l/d) distribution is relatively insensitive to the overall volume fraction of the composite, Figure 3. In addition, many whiskers having l/d ratio's below 10. For example, Figure 4(a) shows that approximately 70 percent of the whiskers in the 10 volume percent reinforced extrusion had l/d ratio's below 10, while Figure 4(b), shows that in the 20 volume percent extrusion, approximately 75 percent of the whiskers had l/d ratio's below 10. It should be noted that these composites had been fabricated utilizing a common lot of SiC whiskers (10).

These quantitative measurements of whisker orientation and l/d ratio are currently being extended to a recently fabricated 5 volume fraction SiC whisker reinforced extrusion where F-8, an enhanced grade of whisker, and a higher extrusion ratio, 20:1, have been employed.

Heat Treatment Response

The heat treatment response of 0, 5, 10 and 20 volume percent SiC whisker reinforced 2124 is being examined utilizing Rockwell hardness, eddy current, X-ray small angle scattering and transmission electron microscopy.

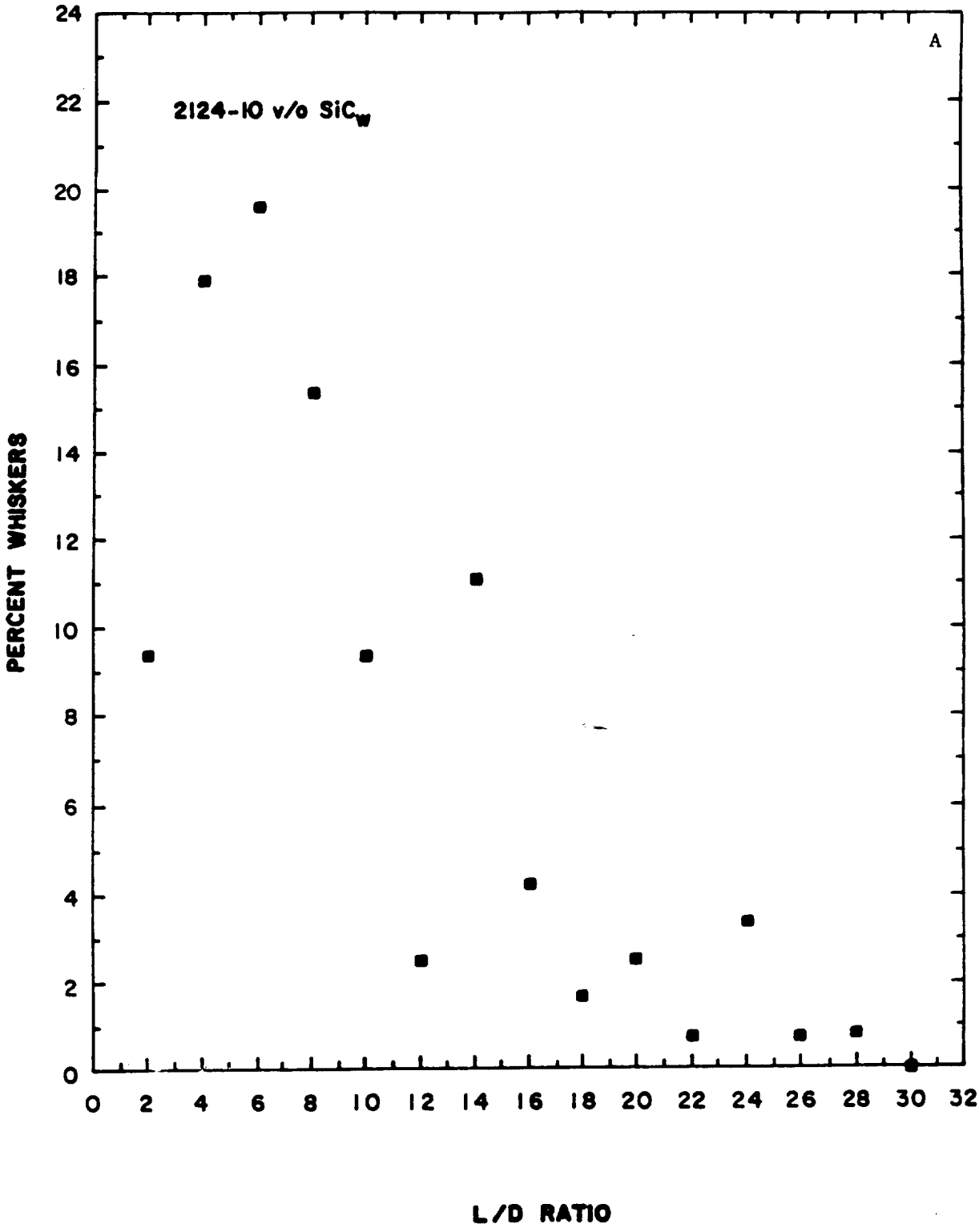

Figure 3 - SiC Whisker Length-to-Diameter Ratio's for (a) 2124-10 V/O SiC Whiskers and (b) 2124-20 V/O SiC Whiskers.

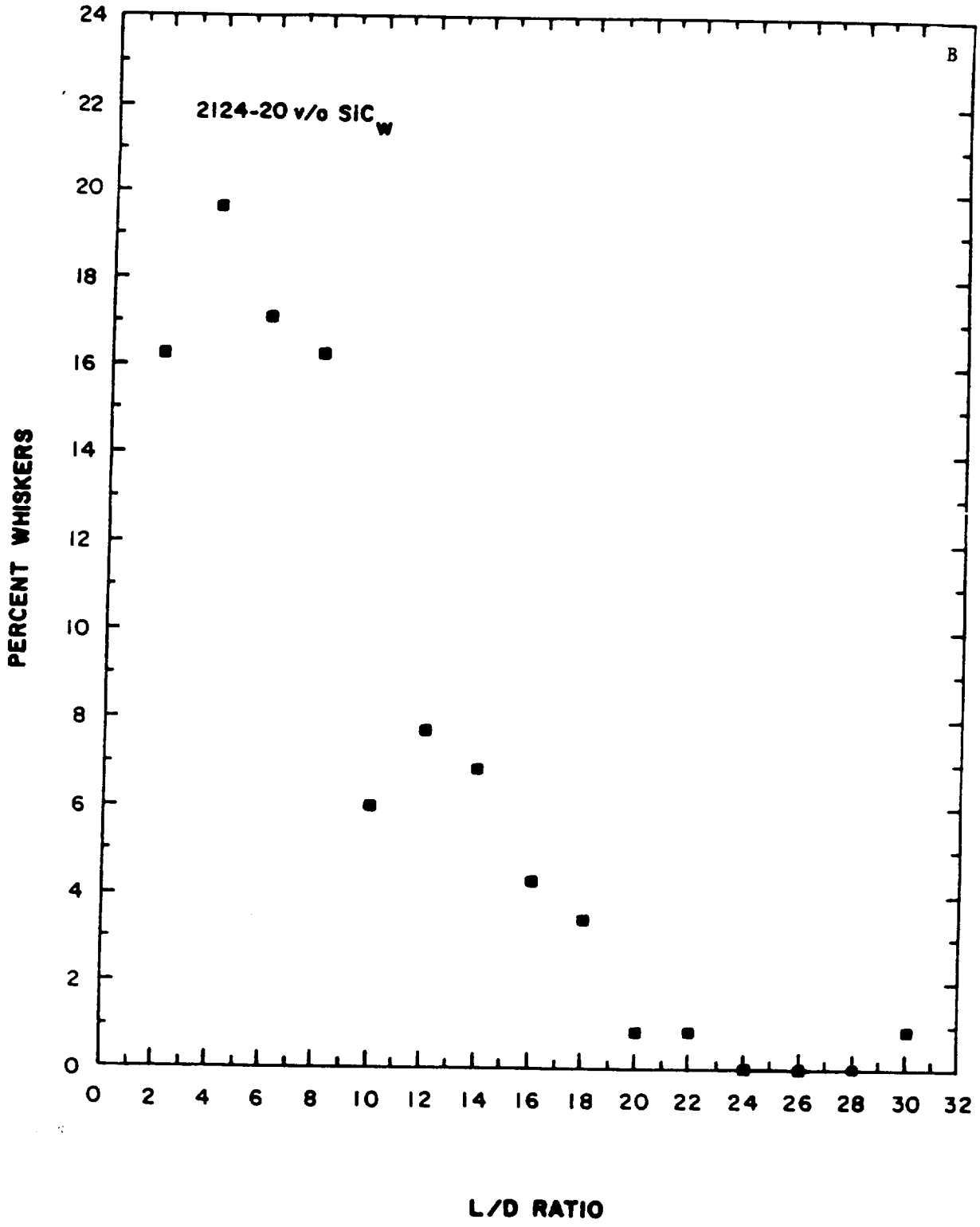

Figure 3 - Continued

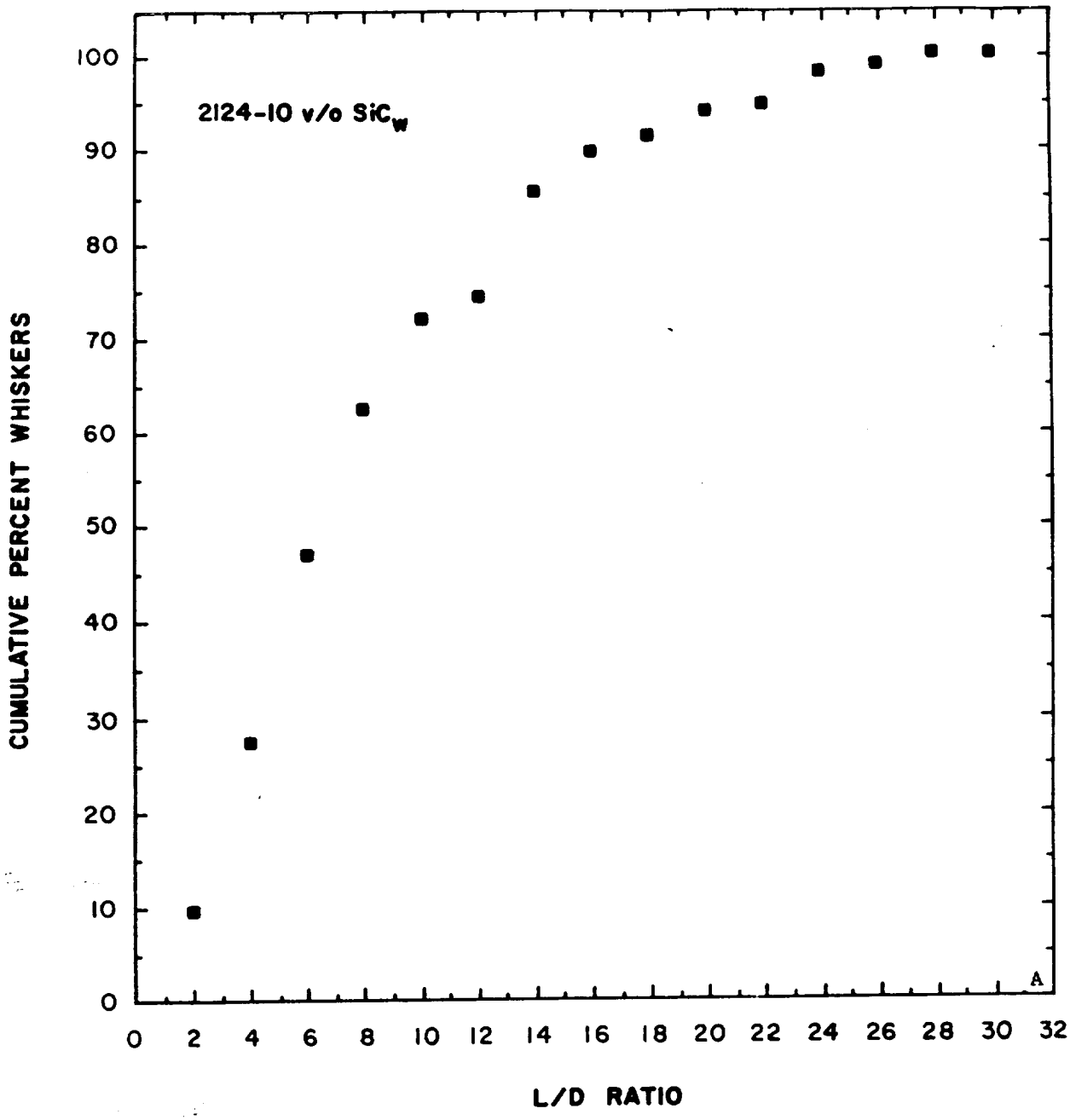

Figure 4 - Cumulative Distribution of SiC Whisker L/D Ratio's in (a) 2124-10 V/O F-9 SiC and (b) 2124-20 V/O F-9 SiC Whiskers.

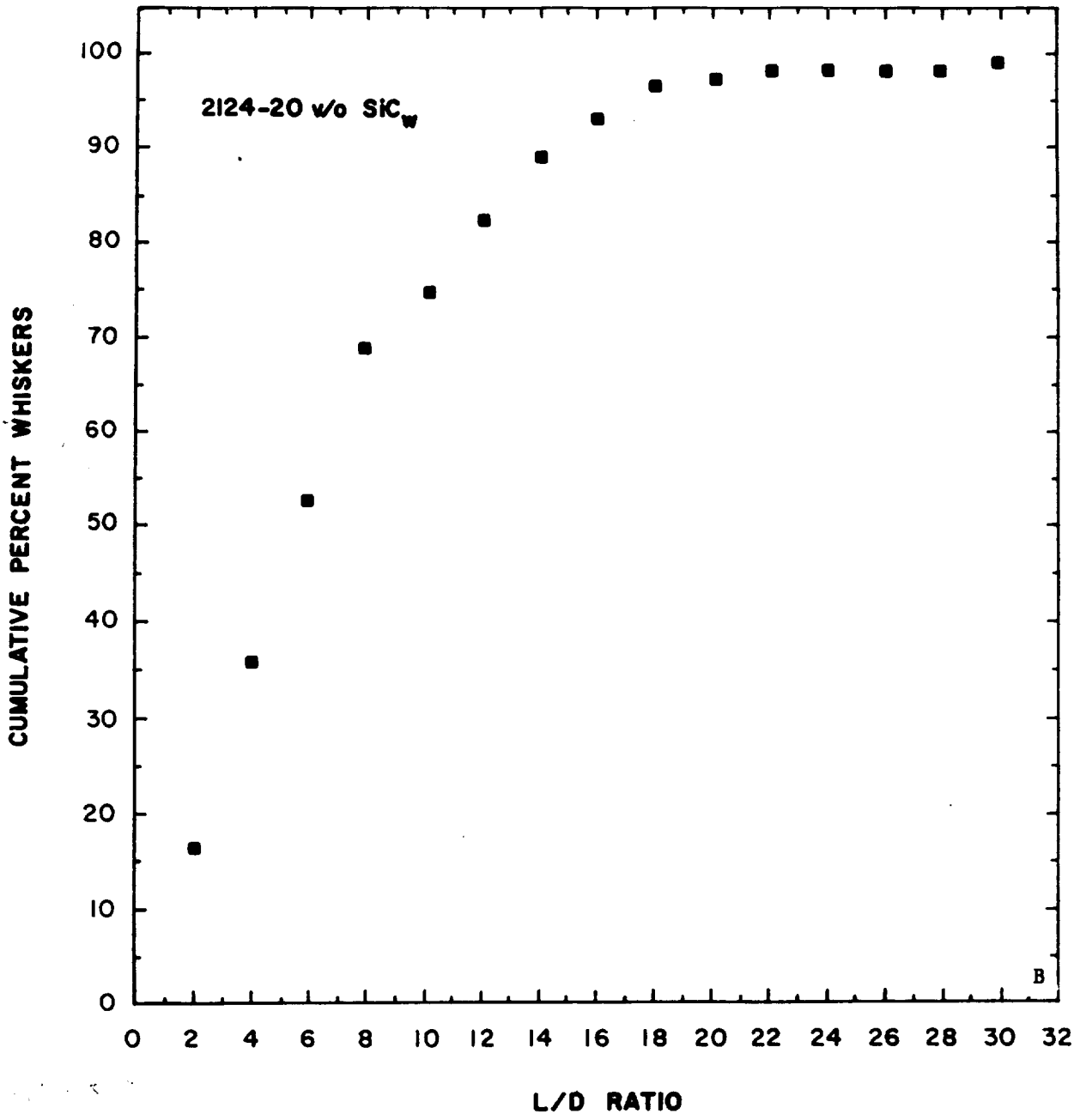

Figure 4 - Continued

All measurements utilized samples approximately 0.5 inch by 0.625 inch by 0.5 inch thick, with the hardness and eddy current measurements being made parallel to the extrusion direction. Samples were solution treated at 495°C for 1 hour, water quenched and aged, the elapsed time between quenching and aging never exceeding 5 min.

Aging temperatures between 75 and 175°C are being examined, aging times extending to 1000+ hours. Following aging the samples were air cooled to 25°C, ground thru 600 grit and tested. The hardness values reported are the average of 5 readings.

Table 1 lists the aging treatments being examined utilizing small angle X-ray and transmission electron microscopy. These samples were selected from the hardness and eddy current results and are intended to clarify the details of aging in SiC whisker reinforced 2124. The small angle scattering studies are being conducted in cooperation with Dr. Stephen Spooner of Oak Ridge National Laboratory utilizing the National X-Ray and Neutron Diffraction facility available at ORNL. Samples for both X-ray and transmission electron microscopy are being prepared from hardness samples and ground to 0.002 inch thick. The transmission electron microscopy samples are then being thinned electrochemically utilizing a dual jet Fischione apparatus, a 5 percent perchloric acid solution in ethanol, operated at -30°C, prior to examination with a JEOL 100C.

Mechanical Property Response

All fracture toughness testing conducted to date have utilized the as-extruded (F) temper. The details of specimen preparation, test procedures and results are given in Appendix C. Extension of these results to include orientational, test temperature and heat treatment effects is currently underway. Specimens have been heat treated, machining to a center cracked panel and plane strain tensile configurations is underway.

Table 1

X-Ray and Transmission Electron Microscopy

	V/O SiC	Aging Temperature(°C)	Aging Times(hrs.)
X-Ray	0	150	1,2,4,8,16,32
	5	150	½,1,2,4,8,16
	10	150	½,1,2,4,8
	20	150	½,1,2,4
Transmission	0	150	32,128
	5	150	1,64,256

The test matrix to be examined is listed in Figures 5 and 6. Both fracture toughness and plane strain tensile measurements are being fabricated, the later being included to provide the necessary data for modeling of the fracture event. In addition, the MTS 880 system being used for this program is undergoing modification and integration with a high speed micro-processor to allow pre-cracking under K control, this enhanced procedure being designed to overcome some of the pre-cracking problems encountered in phase 1 of this study.

Finally, selected 10 and 20 volume percent SiC whisker 2124-F samples have been examined after failure utilizing a JEOL 848 scanning electron microscope to ascertain the microscopic crack path with respect to the whisker orientation. Once the measurements outlined in Figures 5 and 6 are completed, selected samples of these conditions will be included in the fractographic investigation.

EXPERIMENTAL RESULTS AND DISCUSSION

Aging Response

Figures 7 thru 10 summarize the Rockwell B hardness and eddy current response of the 0, 5, 10 and 20 volume percent SiC whisker reinforced composites. Previous studies of 2124 (11,12) indicate that maximum hardness in this alloy is associated with the combined precipitation of GPB and S'. Detailed examination of the present results suggests that the effect of whisker reinforcement on the aging response is quite complex, depending upon reinforcement level, aging temperature and aging time. Preliminary analysis indicates:

1. Aging at 175°C, the highest temperature examined, results in either a single maxima (unreinforced, 20 V/O reinforced) or two maxima

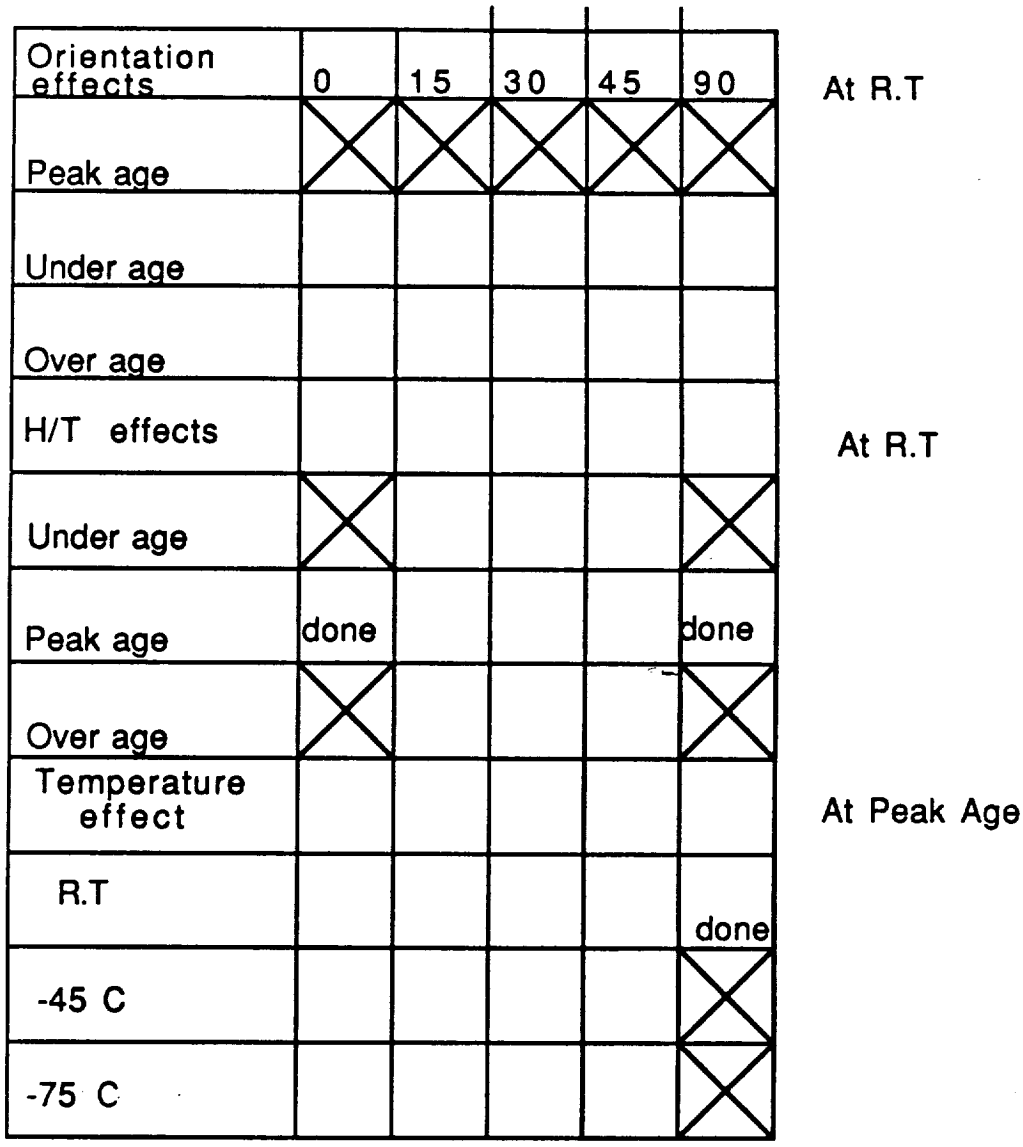

Figure 5 - Fracture Toughness Test Matrix for 5 V/O F-8 SiC Reinforced 2124 Aluminum.

Heat treat effects					
At R.T	0	15	30	45	90
Under age	X				X
Peak age	X				X
Over age	X				X
Temperature effects					
R.T					done
-45 C					X
-75 C					X

Figure 6 - Plane Strain Tensile Test Matrix for 5 V/O F-8 SiC Reinforced 2124 Aluminum.

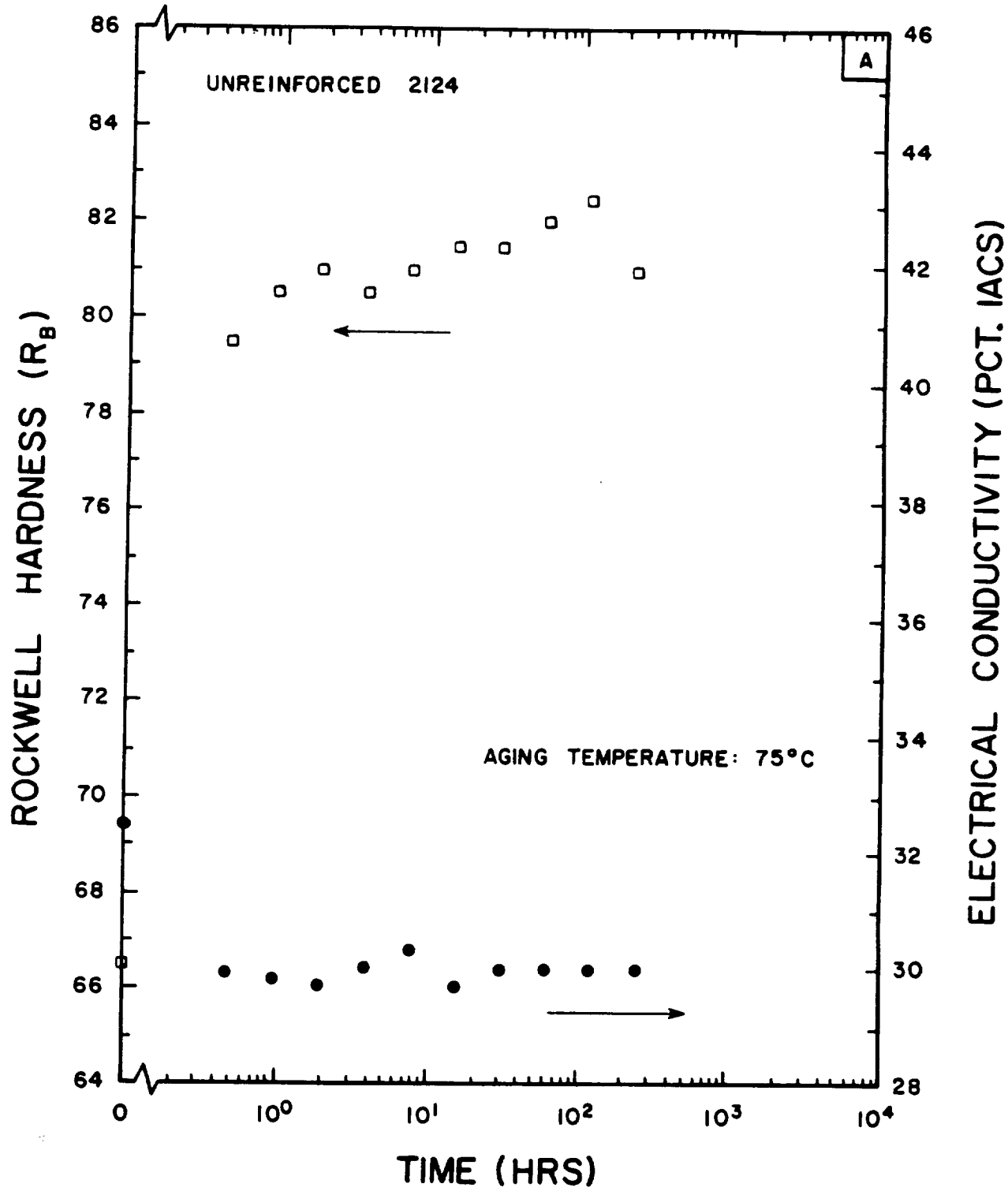

Figure 7 - Aging Resonse of 2124 Aluminum Solution Treated at 495°C for 1 hour, Water Quenched and Aged at (a) 75°C, (b) 100°C, (c) 125°C, (d) 150°C and (e) 175°C.

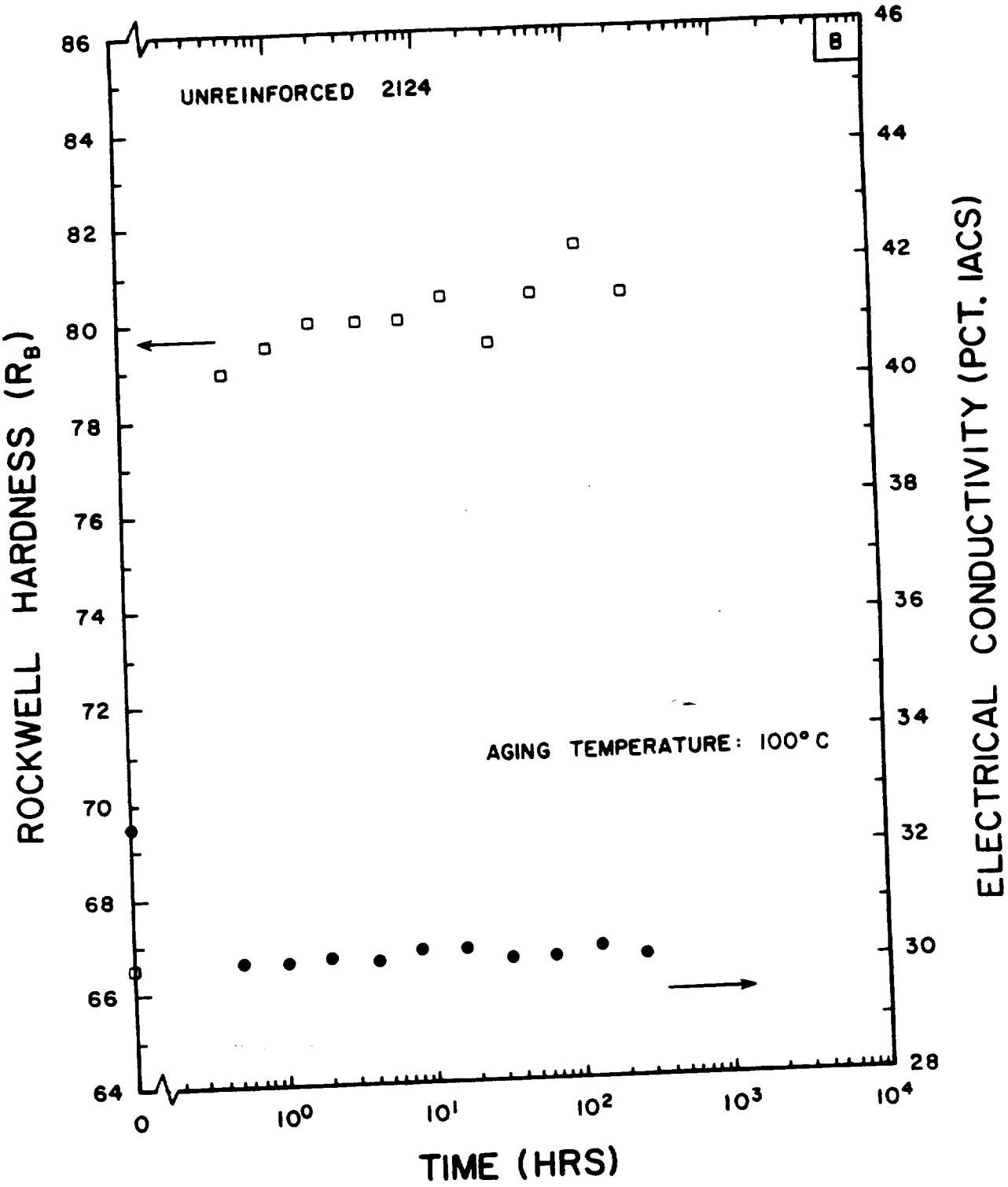

Figure 7 - Continued

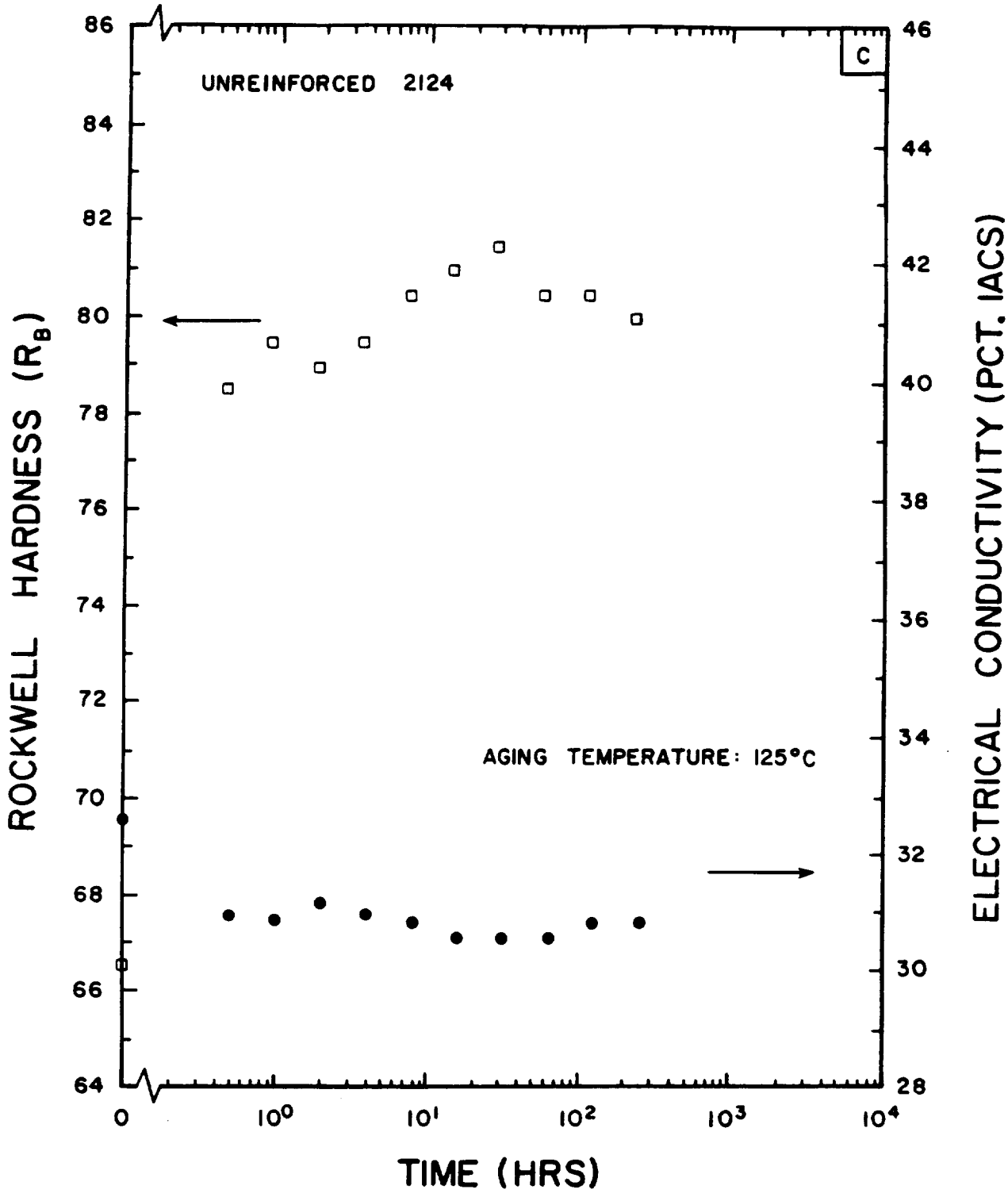

Figure 7 - Continued

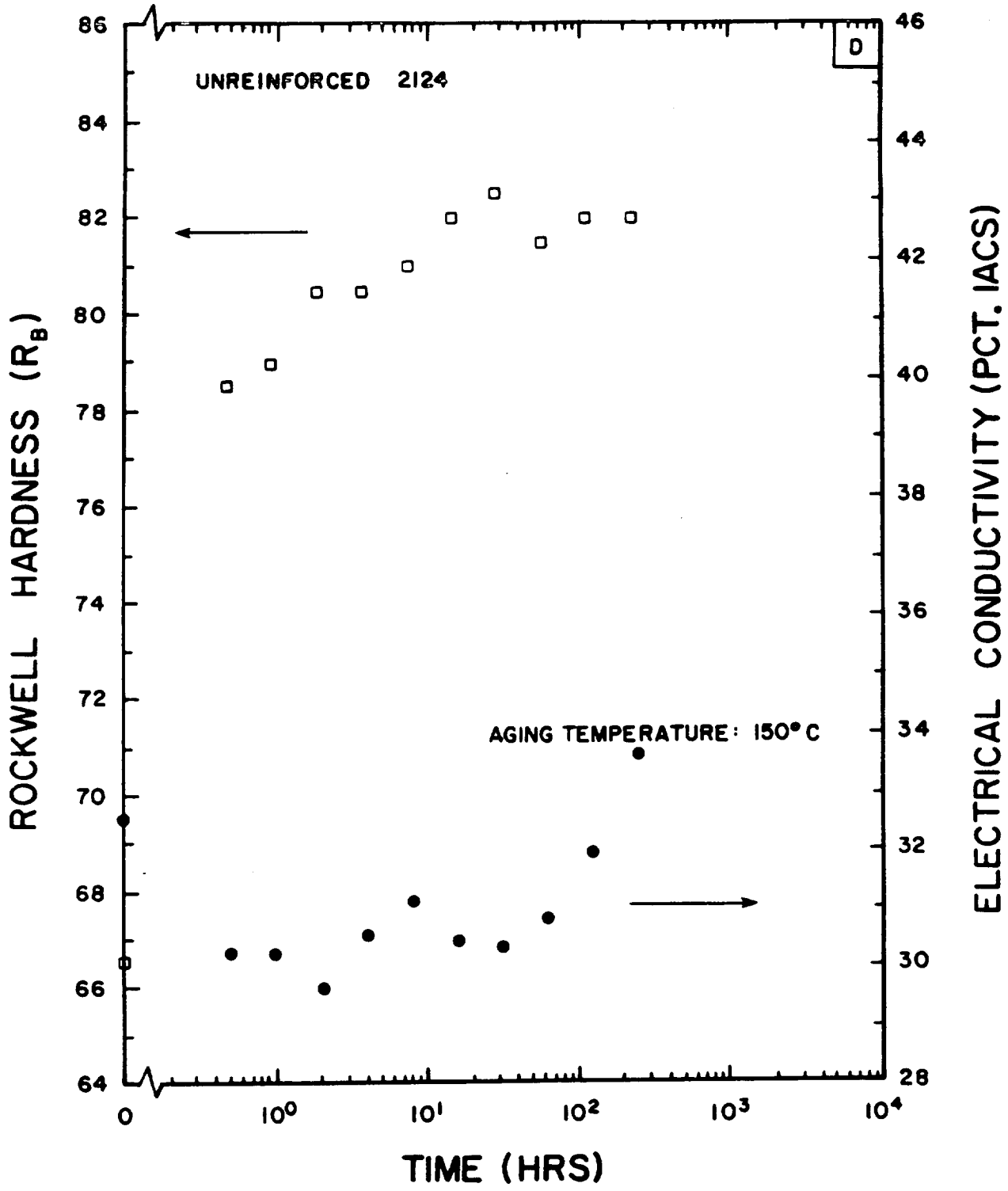

Figure 7 - Continued

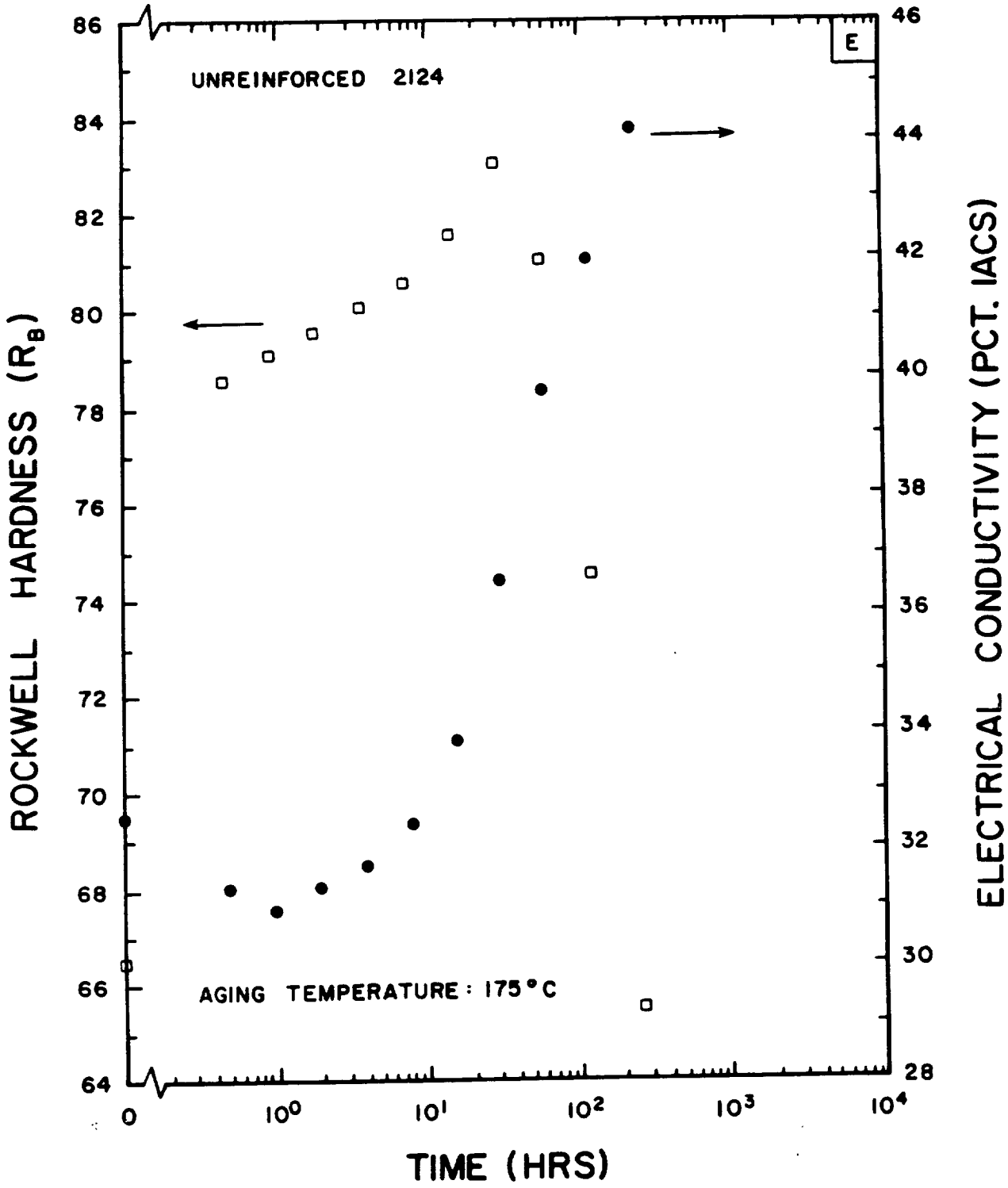

Figure 7 - Continued

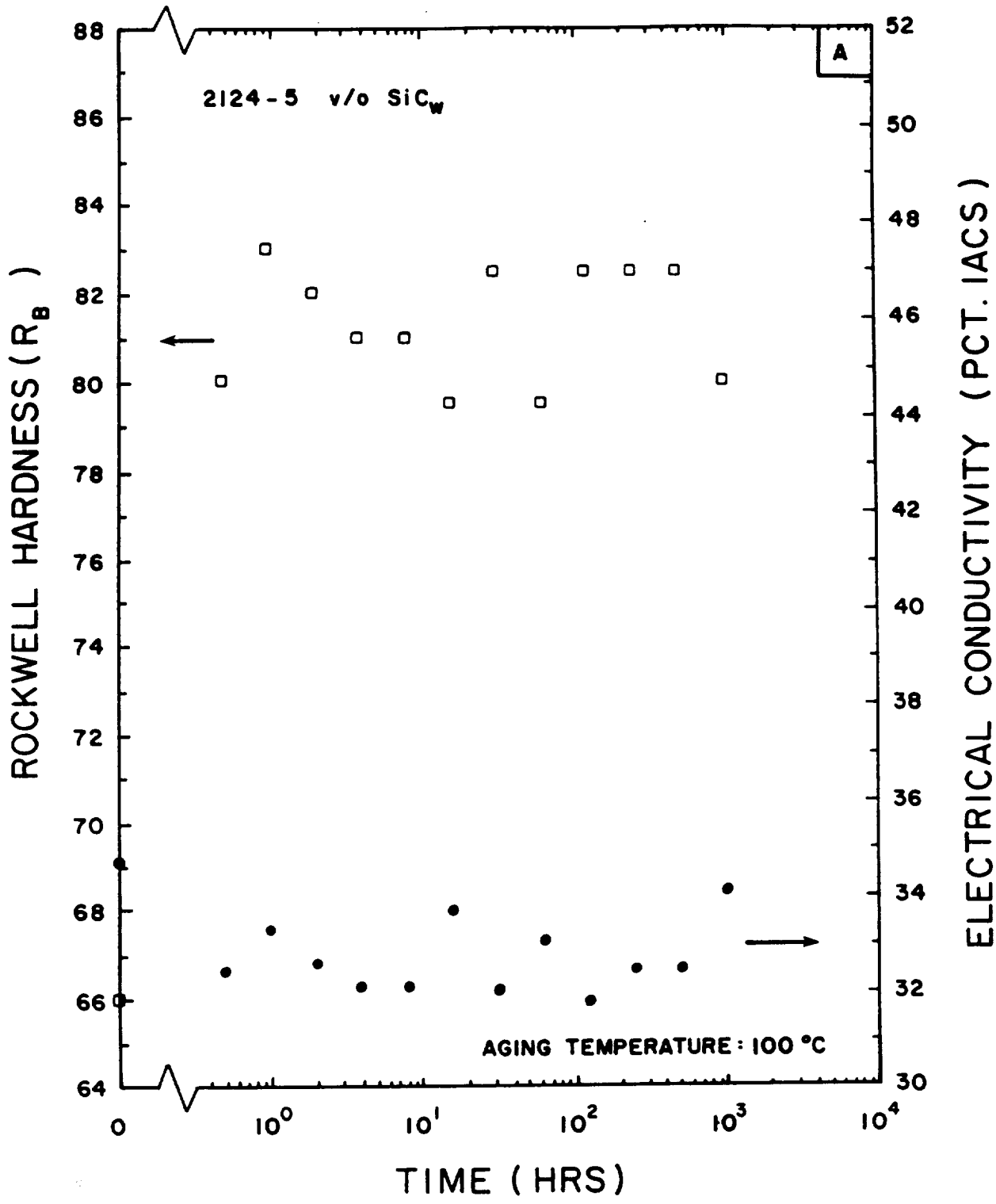

Figure 8 - Aging Response of 2124 Aluminum Reinforced With 5 Volume Percent SiC Whiskers Solution Treated at 495°C for 1 hour, Water Quenched and Aged at (a) 100°C, (b) 125°C, (c) 150°C and (d) 175°C.

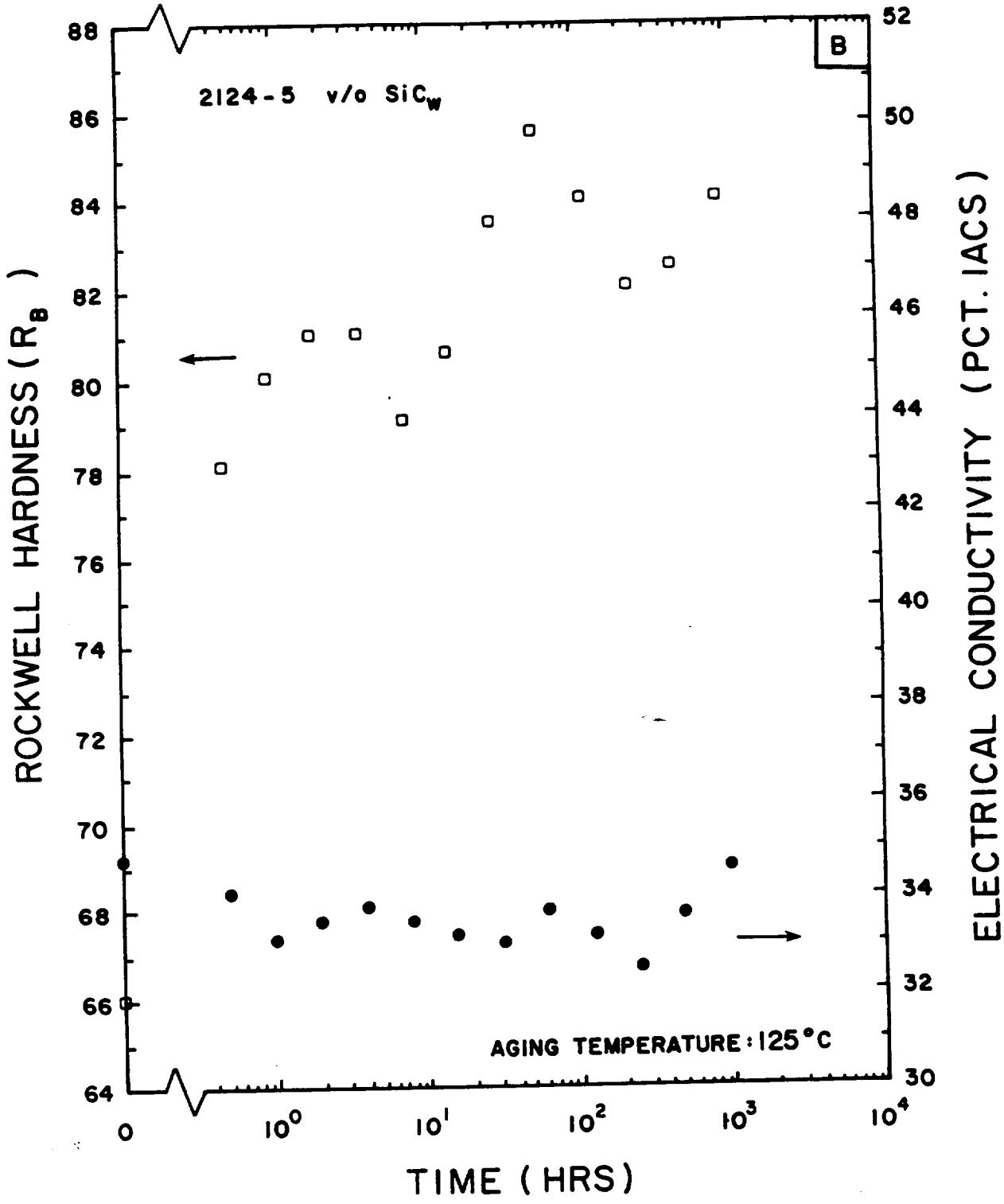

Figure 8 - Continued

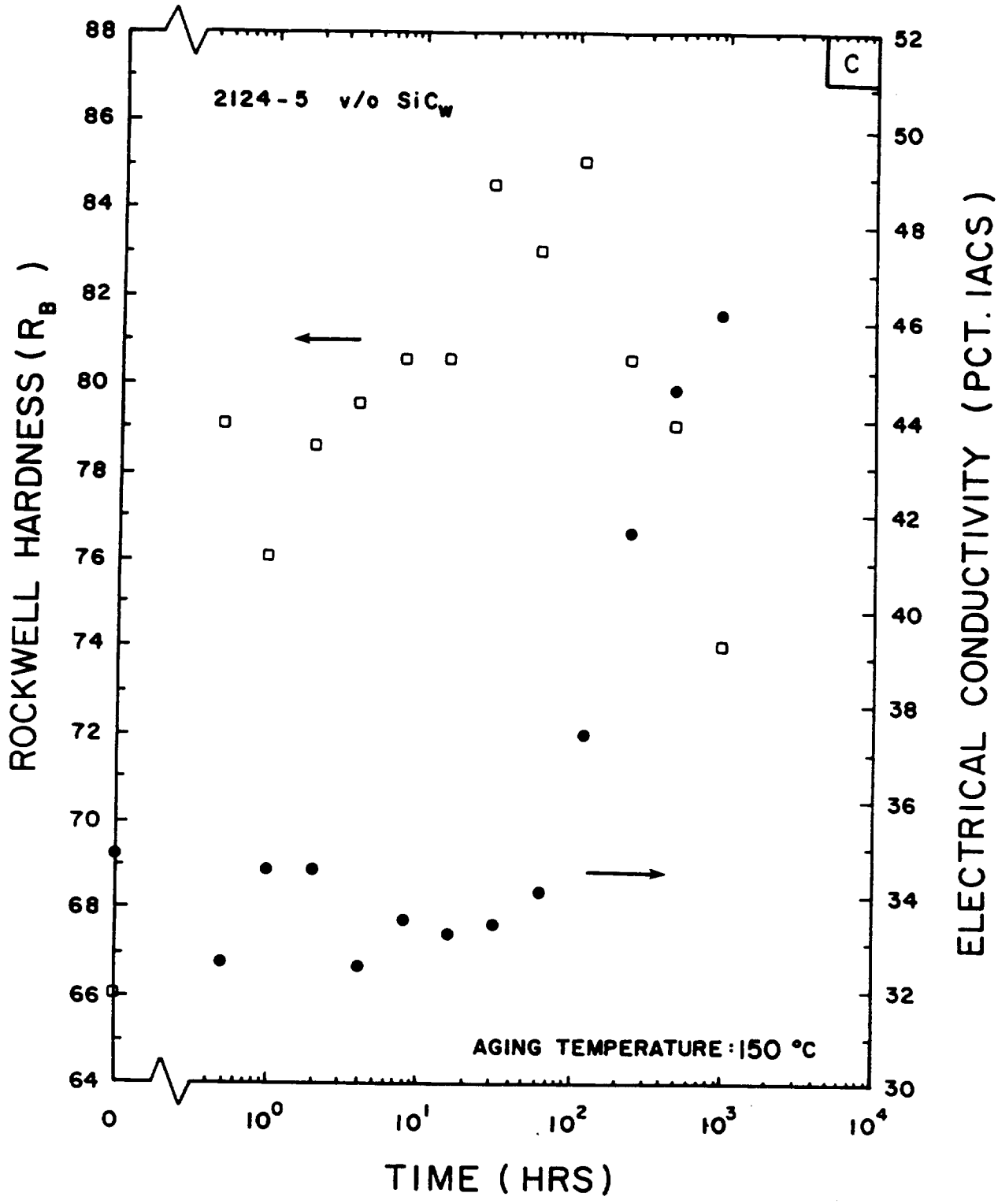

Figure 8 - Continued

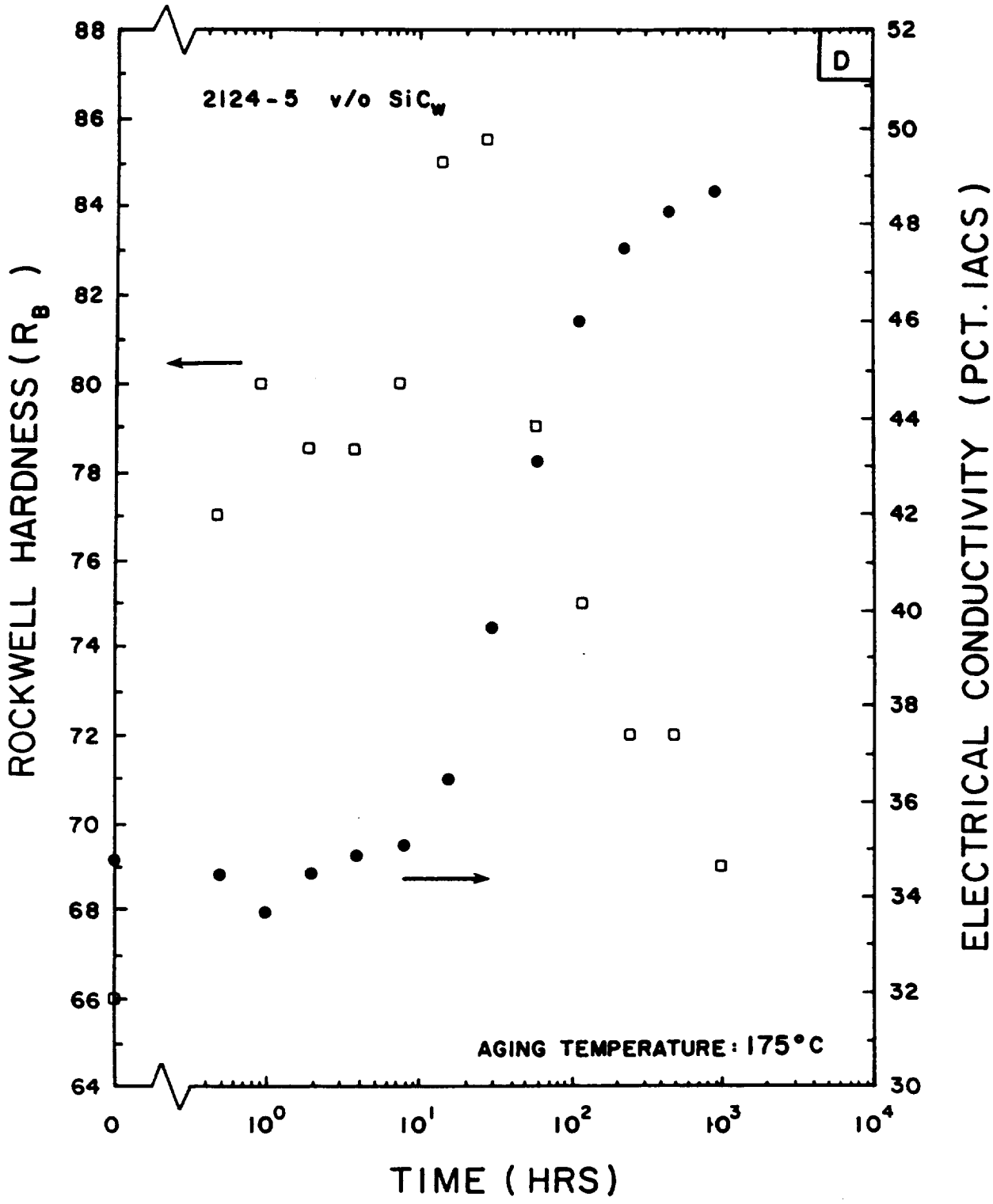

Figure 8 - Continued

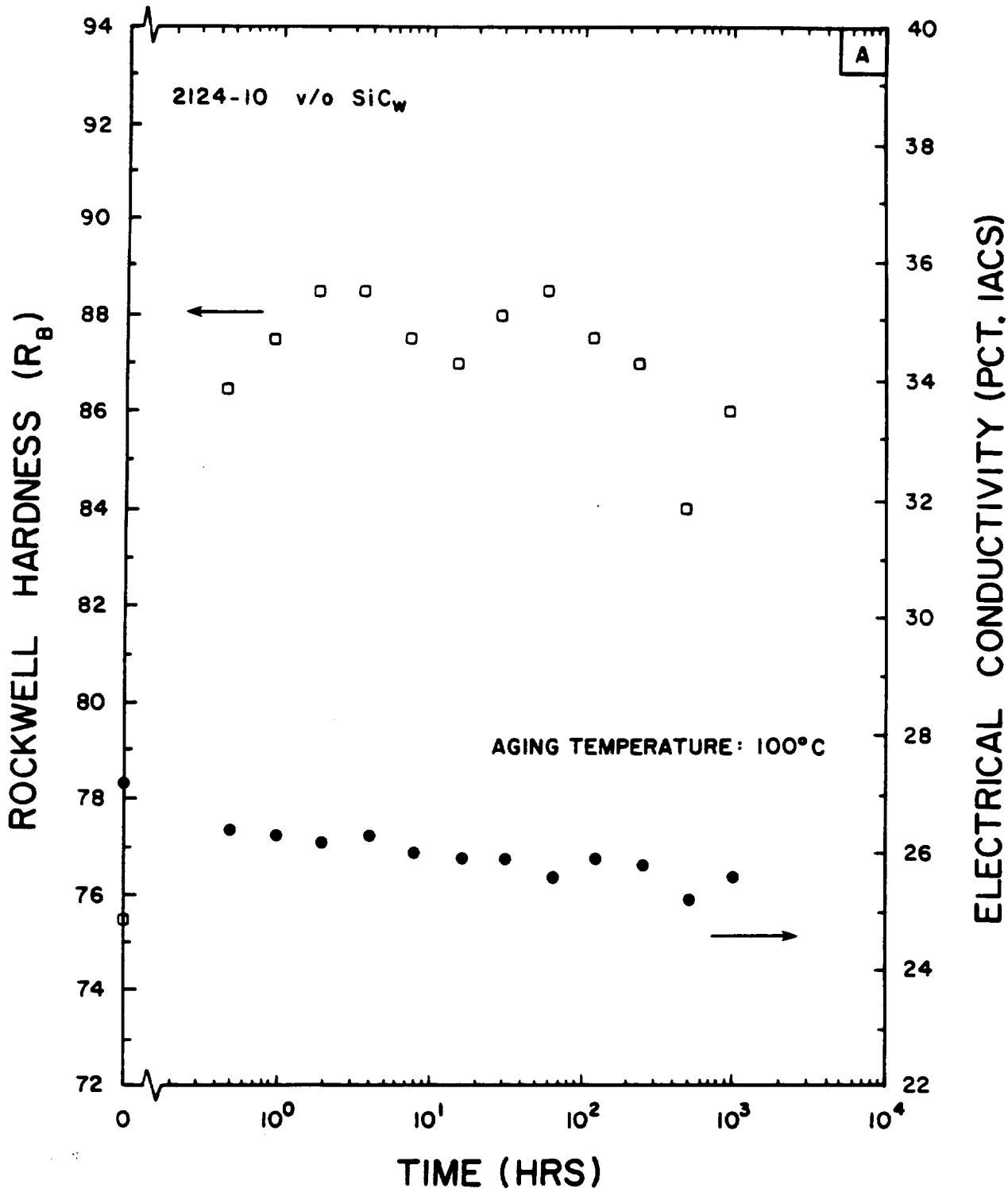

Figure 9 - Aging Response of 2124 Aluminum Reinforced With 10 Volume Percent SiC Whiskers Solution Treated at 495°C for 1 hour, Water Quenched and Aged at (a) 100°C, (b) 125°C, (c) 150°C and (d) 175°C.

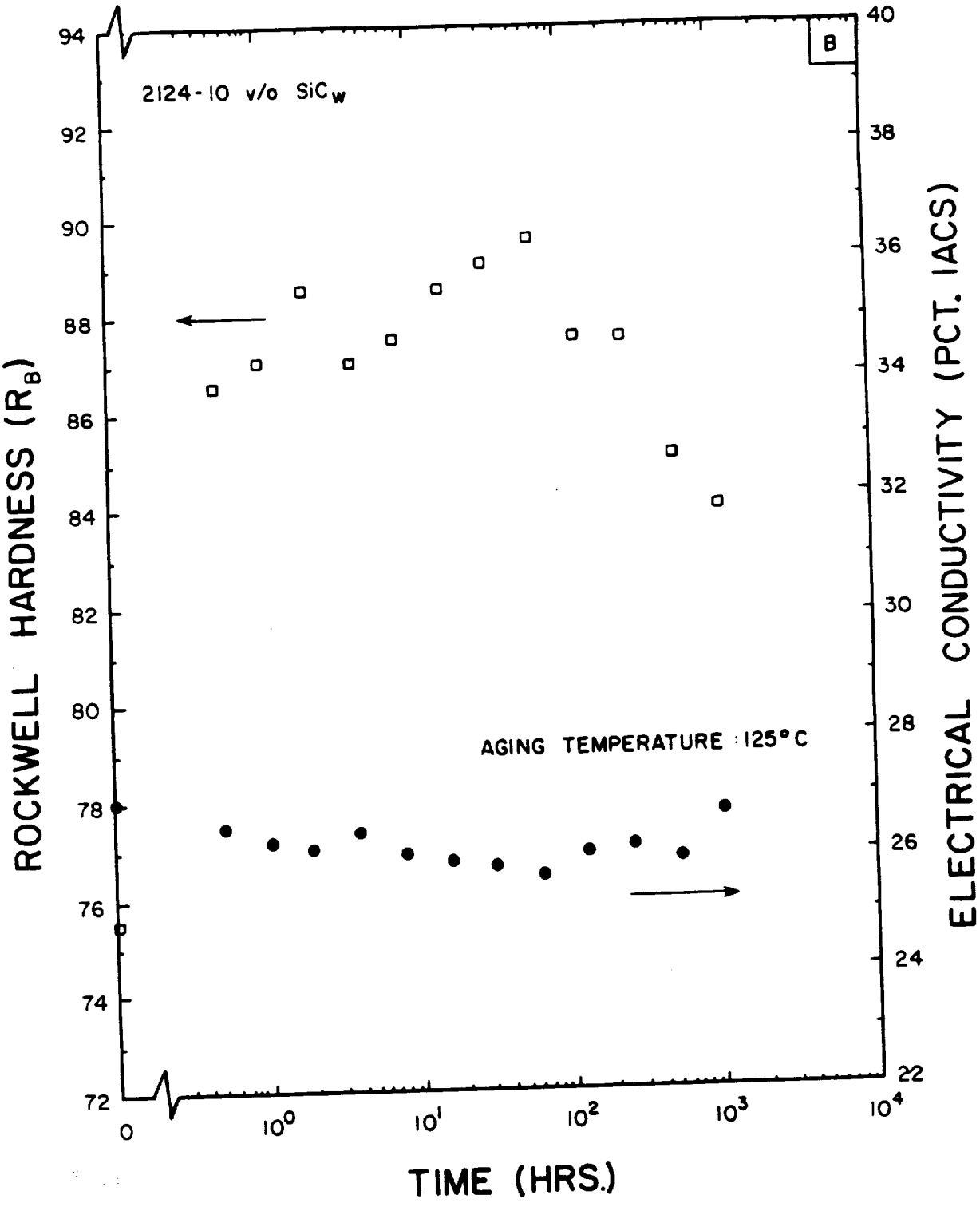

Figure 9 - Continued

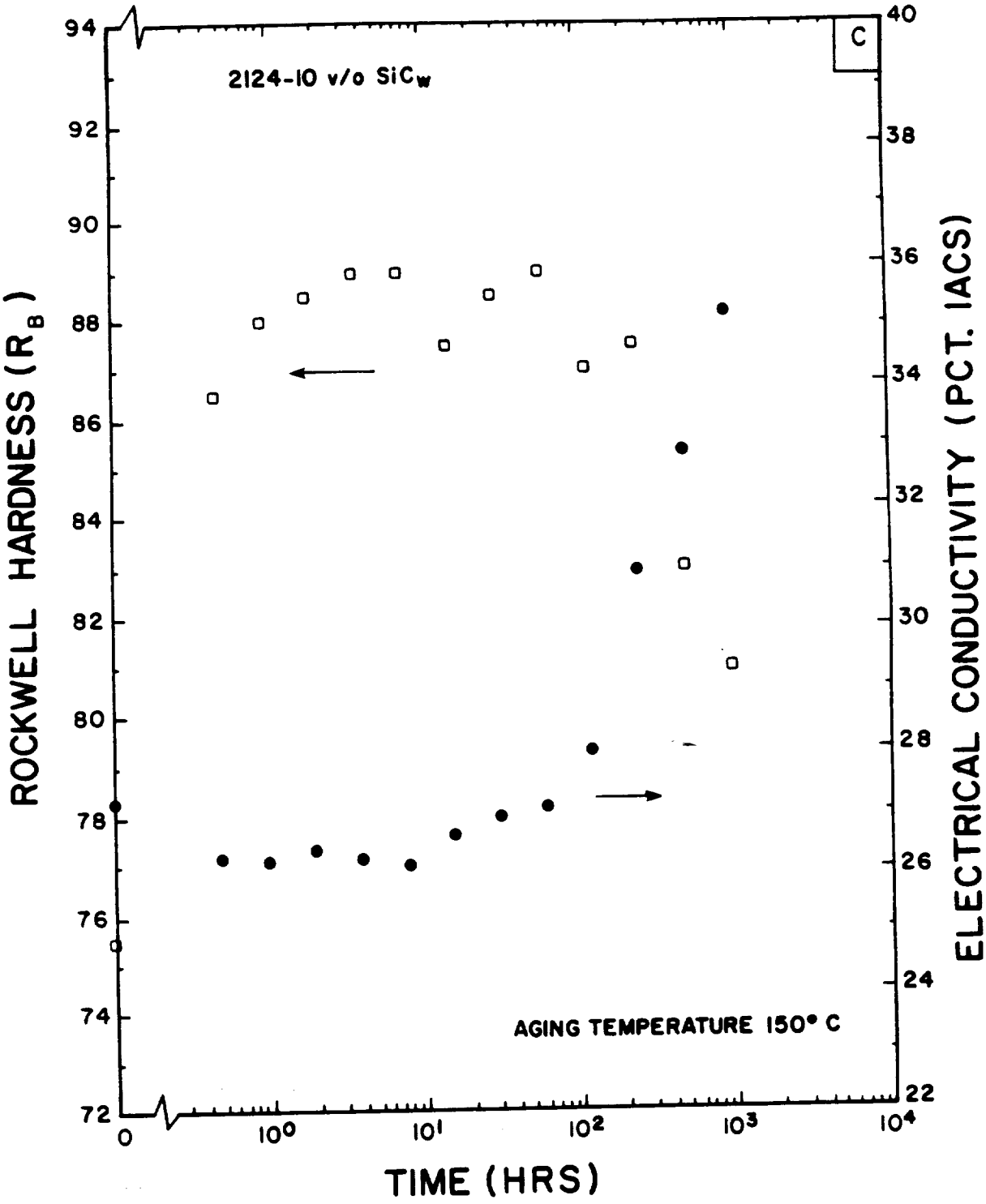

Figure 9 - Continued

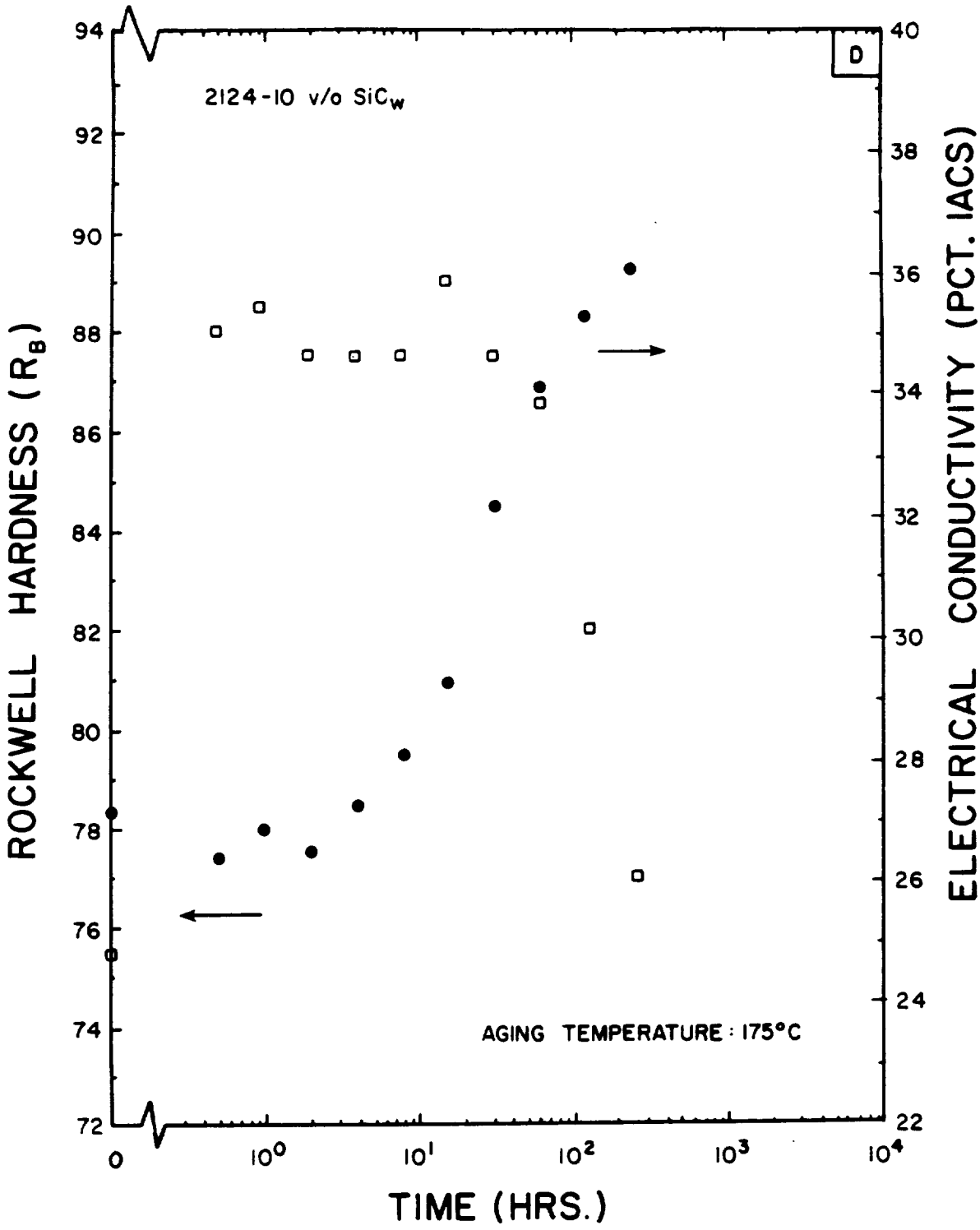

Figure 9 - Continued

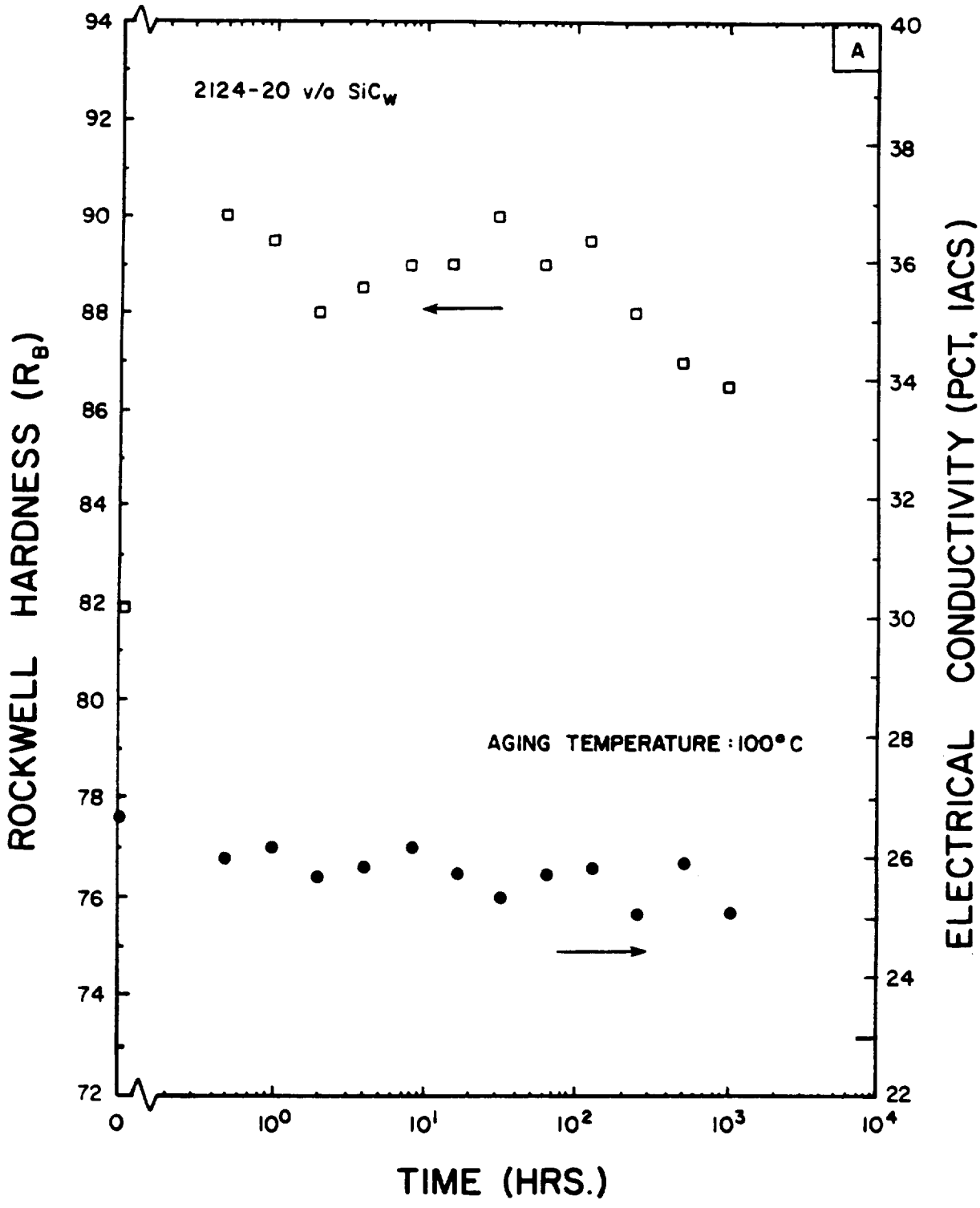

Figure 10 - Aging Response of 2124 Aluminum Reinforced With 20 Volume Percent SiC Whiskers Solution Treated at 495°C for 1 hour, Water Quenched and Aged at (a) 100°C, (b) 125°C, (c) 150°C and (d) 175°C.

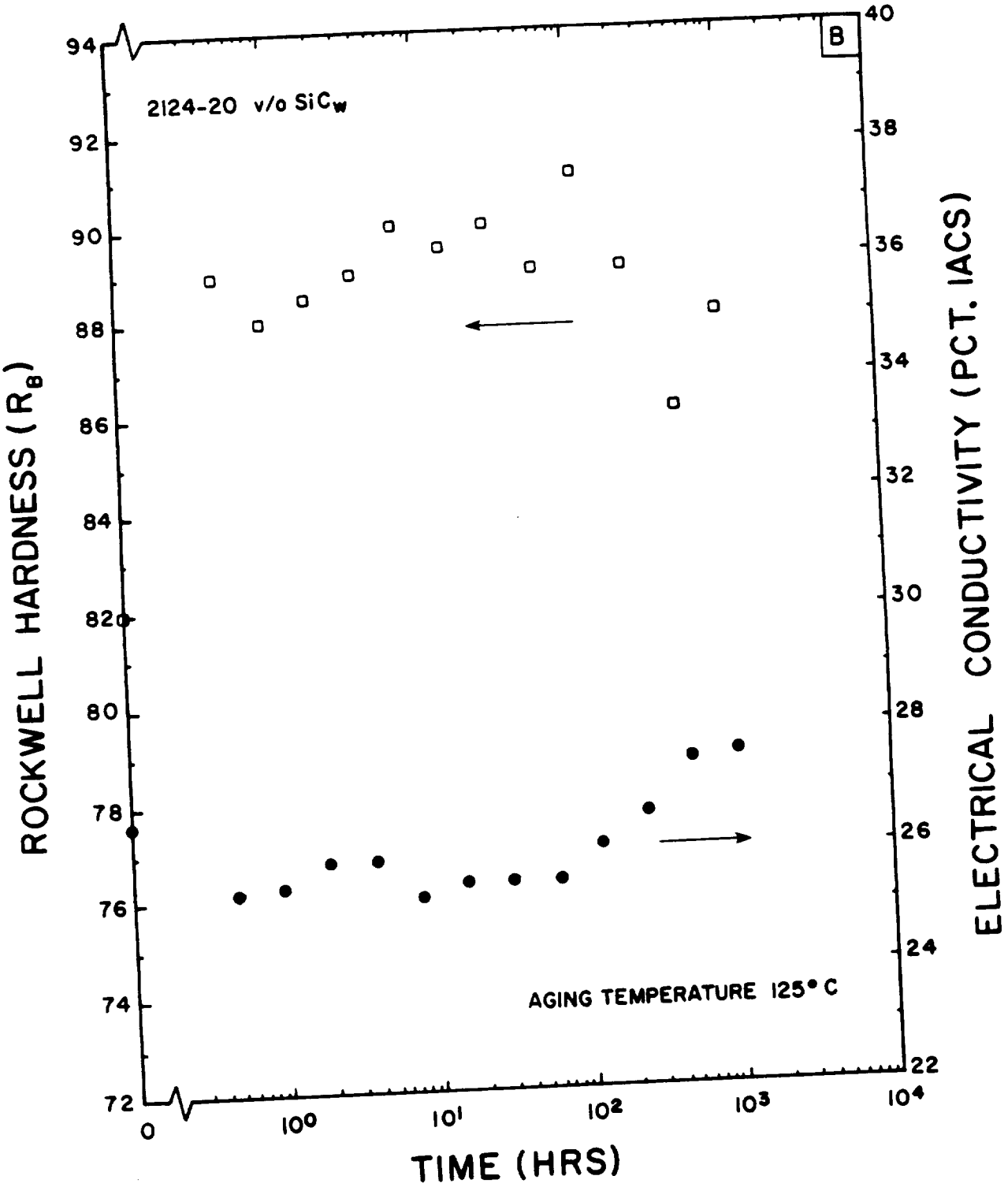

Figure 10 - Continued

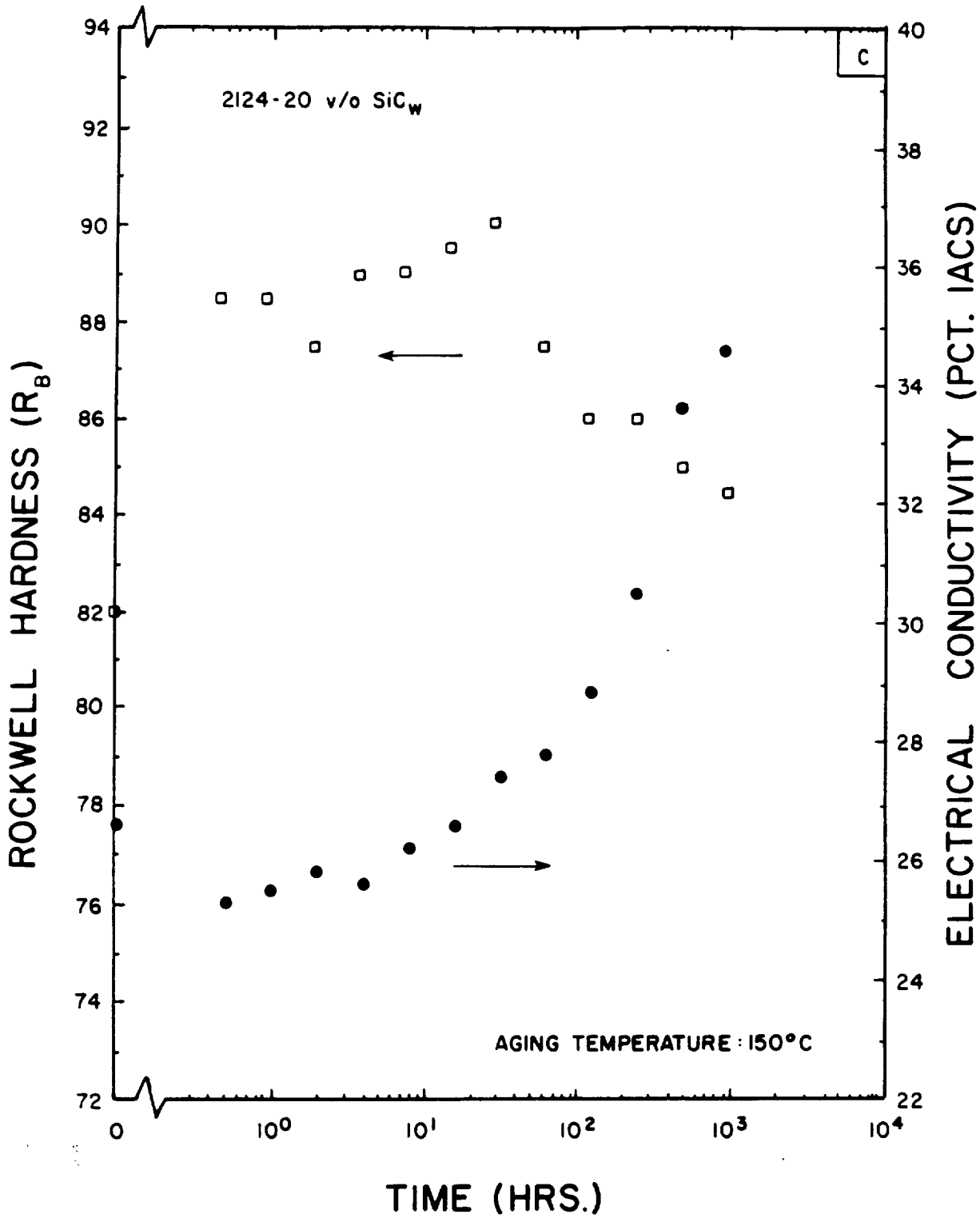

Figure 10 - Continued

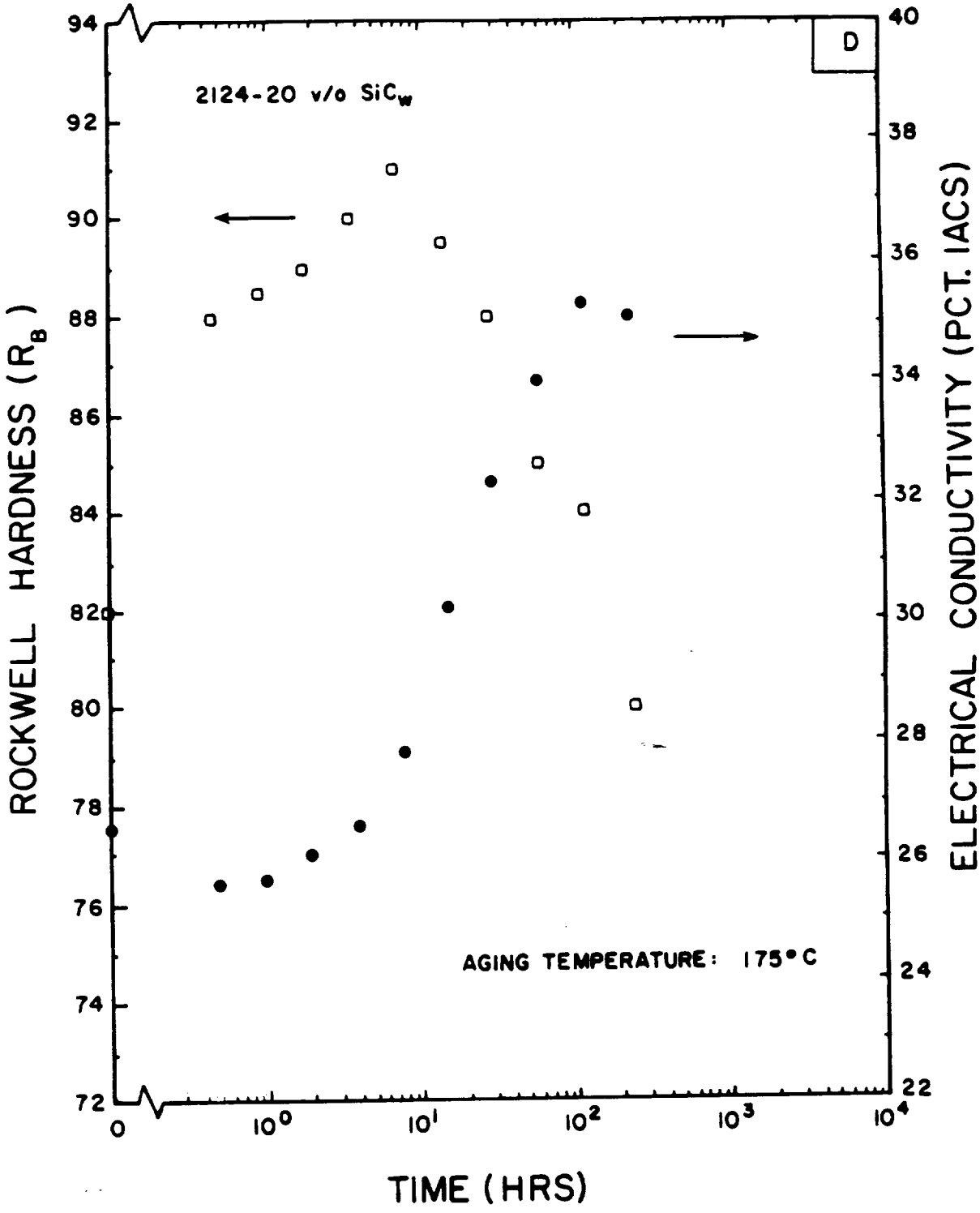

Figure 10 - Continued

(5 and 10 V/O reinforced), with the level of the second/single maxima increasing and the aging time required to achieve this maxima decreasing with increasing SiC whisker content. In contrast, the aging time required for the initial maxima observed in the 5 and 10 volume percent composite does not seem to be affected by the change in carbide content. Finally, at least at this aging temperature, it appears that there is no systematic influence of SiC whisker content on the aging time associated with initial S' formation, the latter being defined by the time necessary to achieve an increase in (%IACS) eddy current (11).

2. Aging at lower temperatures results in multiple hardness peaks for all materials examined. Once again, it appears that the hardness level increases, and the aging time required for the final peak decreases, as the SiC whisker content increases. In addition, at least at 150°C, eddy current results suggest that the time required for S' precipitation initiation may decrease slightly with increasing SiC whisker content, while at lower temperatures the results are complicated by overlapping reactions. Further analysis and interpretation of the low temperature aging response of SiC whisker reinforced 2124 will require completion of the X-ray and transmission electron microscopy studies currently underway.

The following heat treatments have been selected for detailed fracture toughness and plane strain tensile examination. These heat treatments were selected based on the aforementioned hardness and eddy current results and represent an attempt to allow examination of the broadest spectrum of microstructures on the plane strain plasticity and fracture behavior of SiC whisker reinforced 2124,

Heat Treatment		Anticipated Microstructure
Underaged	150°C - 1 hr	GPB zones
Peak Aged	150°C - 64 hr	GPB and S'
Overaged	150°C - 256 hr	S' and S

Mechanical Property Response

Appendix C summarizes the fracture toughness behavior of the 10 and 20 volume percent SiC whisker reinforced 2124-F extrusion. Probably the most important result obtained from this examination is that the fracture toughness of oriented, whisker reinforced aluminum is sensitive to sample configuration and stress state (plane strain versus plane stress). Testing of plane stress samples always involved self-similar crack growth, while plane strain compact tensile samples, taken such that initial crack growth should be perpendicular to the extrusion direction, did not exhibit self-similar crack growth.

At least part of this apparent anomaly can be explained by the scanning electron fractography results reported previously (9). The general fracture morphology in the plane strain T-L center cracked panels is quite smooth, while in the L-T orientation, the fracture is somewhat rougher and undulated. Fatigue crack growth and overload progresses either parallel (T-L) or perpendicular (L-T) to the SiC whiskers. In the former, whiskers lie within the plane of crack propagation, while in the latter, crack propagation occurs thru whiskers. Indeed, there appears to be little evidence, during self-similar crack propagation in the L-T orientation, for appreciable enhancement of the fracture toughness of whisker reinforced aluminum alloys by crack deflection along whisker/matrix interfaces during either fatigue crack propagation or final failure. These results strongly suggest that the bond strength between the SiC whiskers and the aluminum matrix far exceeds

the fracture strength of the SiC whiskers. This result is not surprising, given the faulted nature of the F-9 whiskers incorporated within these composites, see Appendix B.

This fracture morphology should also be contrasted with that observed in compact tension samples. Crack propagation in the T-L orientation is again quite smooth, with SiC whiskers once again lieing either within or near the fracture plane. Stable self-similar crack propagation was not observed in the 0.450 thick L-T oriented samples. Macroscopic self-similar crack propagation was observed in thin, 0.100 in. thick, samples. Micoscopic examination shows, Figure 11, that crack propagation in thin compact tension samples involved extensive localized crack deflection at appropriately oriented SiC whiskers.

The differences in macroscopic crack morphology observed between and among the various specimen configurations can be related to the differing contributions of bending in the two sample configurations. For the geometries utilized in this study the bending moment about the center-line of the net-section ligament is $P(25.4 + a)/2$ for the compact tensile geometry, while no bending moment exists in the center cracked panel. Clearly this important contribution of far-distance stress field violates one of the precepts of linear elastic fracture mechanics, wherein crack propagation is assumed to be controlled entirely by the near crack tip stress field. However, it is not nearly as clear as to why this same effect is not as prevalent in thin samples where, on a microscopic scale localized crack deflection has commenced, yet macroscopic crack growth maintains its self-similar character. This feature of the fracture process is under continuing study.

Figure 11 - Scanning Electron Fractographs of 0.1 inch Thick Compact Tension Sample of 20 Volume Percent SiC Whisker Renforced 2124-F, (a) T-L and (b) L-T orientation.

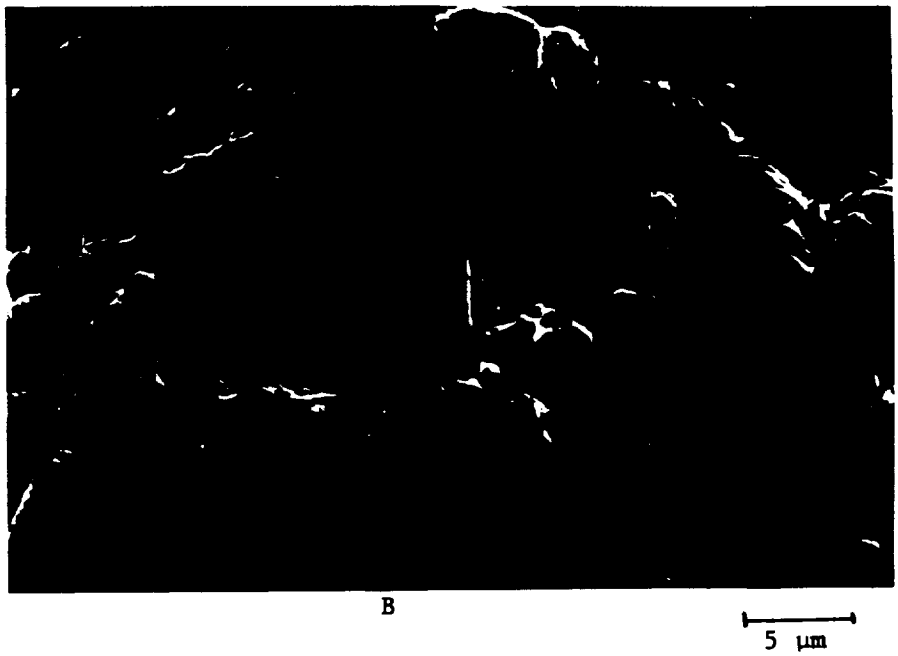

Figure 11 - Continued

CONCLUSIONS

1. The fracture toughness of SiC whisker reinforced 2124 aluminum is a function of whisker orientation, sample configuration and stress state.

2. Microscopic crack propagation is also a function of orientation and sample configuration, T-L orientations involving crack propagation parallel to SiC whiskers, L-T orientations involving whisker fracture or localized crack deflection at whisker/matrix interfaces, the latter due to the increased bending moment associated with a compact tensile specimen.

3. The influence of SiC whiskers on the aging response of 2124 is a sensitive function of whisker content, aging temperature and time. At aging temperatures and times where S' precipitaion predominates, SiC whisker reinforcement results in a decrease in time to maximum hardness, without influencing the time for initial S' formation.

FUTURE RESEARCH EFFORTS

1. Complete aging studies of 2124 reinforced with 0, 5, 10 and 20 volume percent SiC whiskers.

2. Initiate fracture toughness and plane strain testing of aged 5 v/o SiC whisker reinforced 2124 examining orientation and test temperature interactions.

3. Initiate micromechanical modeling of fracture phenomena in SiC whisker reinforced aluminum.

REFERENCES

1. Bates, Jr., W. F., "New Aluminum Structural Materials for the 1980's," Transportation Engineering Journal of the American Society of Civil Engineering, Proc. of the American Society of Civil Engineers, 106-TE6, 1980, pp. 845-853.

2. Schoutons, J. E., Particulate, Whisker and Fiber-Reinforced Metals: A Comparison and Discussion, Metal Matrix Composites Information Center Report, November 1981.

3. Reedy, E. D., "On the Specimen Dependence of Unidirectional Boron/Aluminum Fracture Toughness," Journal of Composite Materials Supplement, Vol. 14, 1980, pp. 118-131.

4. Crowe, C. R., Gray, R., and Hasson, D., "Microstructural Controlled Fracture Toughness of SiC/Al Metal Matrix Composites," Proceedings 5th International Conference on Composite Materials, W. C. Harrigan, Jr., J. R. Strife and A. K. Dhingra, eds., AIME, Warrendale, PA, 1985, pp. 843-866.

5. Nieh, T. G., Rainen, R. A., and Chellman, D. J., "Microstructure and Fracture in SiC Whisker Reinforced 2124 Aluminum Composite," Proceedings 5th International Conference on Composite Materials, W. C. Harrigan, Jr., J. R. Strife and A. K. Dhingra, eds., AIME, Warrendale, PA, 1985, pp. 825-842.

6. Rack, H. J., and Santner, J. E., ARCO Metals, unpublished Research, 1984.

7. Carroll, J. R., and Waitz, C. R., "Structural Advanced Material/Manufacturing Development," Proc. 5th Annual Metal Matrix Review Mtg., Evandale, Ohio, November, 1985.

8. Nardone, V. C., "Factors Affecting K_{IC} of Discontinuously Reinforced Composites," Proc. 9th Discontinuously Reinforced MMC Working Group, Park City, Utah, January, 1987.

9. Rack, H. J., Goree, J. G., Albritton, J., and Ratnaparkhi, P., "Fracture Criteria For Discontinuously Reinforced Metal Matrix Composites", Annual Report, NASA Grant NAG-1-724, November 17, 1987.

10. Scott, T. E., Mullins, J. W., and Rack, H. J., "Effects of Composition and Process Variables on the Properties of Discontinuously Reinforced Aluminum Metal Matrix Composite Materials", Report AFWAL-TR in press.

11. Rosen, M., Horowitz, E., Swartzendruber, L., Fick, S., and Mehrabian, R., "The Aging Process in Aluminum Alloy 2024 Studied by Means of Eddy Current", Materials Science and Engineering, Vol. 53, 1982, pp. 191-198.

12. Silcock, J. M., Journal of the Institute of Metals, Vol. 89, 1960-61, pp. 203-210.

APPENDIX A

Damage Tolerance of Discontinuously Reinforced Metal Matrix Composites

H. J. Rack

and

P. Ratnaparkhi

To be Published

Journal of Metals

November, 1988

DAMAGE TOLERANCE OF DISCONTINUOUS REINFORCED METAL MATRIX COMPOSITES

H. J. Rack and P. Ratnaparkhi

Department of Mechanical Engineering

Clemson University

Clemson, South Carolina 29634-0921

Much recent interest has been shown in the use of discontinuously reinforced metal matrix composites for primary structural application(1,2). These composites can offer distinct cost and technological advantages over continuously metal matrix composites. Cost advantages result from both lower fiber costs, e.g., $2-3 per lb for SiC_p, and the ability of discontinuously reinforced metal matrix composites to be fabricated utilizing standard metal working practices. In addition, properly prepared discontinuous reinforced metal matrix composites can be competitive, both on a cost and performance basis, with cross-plied graphite fiber reinforced polymers, particularly for high temperature applications.

Discontinuously reinforced metal matrix composite billets may be fabricated utilizing powder blending, direct spraying or casting techniques. All three approaches have produced acceptable composites, with short fibers, whiskers and particulates serving as reinforcements. This paper will present a short review of the damage tolerance behavior of discontinuously reinforced metal matrix composites, a more detailed description of the procedures utilized in fabricating these materials may be found elsewhere(3-7).

Damage Tolerance Behavior

Extreme care must be taken in assessing the mechanical response of any new and developing material. This is particularly true for discontinuously reinforced metal matrix composites, where, prior to 1985, the quantity of material available for testing was extremely limited and quite variable. For example, Williams and Fine(8) reported that fatigue crack initiation in SiC_w reinforced 2124 fabricated during 1983 was associated with either whisker clumping or large inclusions. Similar conclusions with respect to those factors controlling the fracture toughness of whisker and particulate reinforced aluminum metal matrix composites have been reported by Crowe et. al.(9). Subsequent alloy and processing modifications have however virtually eliminated these imperfections as factors limiting the damage tolerance behavior of discontinuously reinforced aluminum alloys.

Indeed, several studies have shown that the long life fatigue behavior of whisker reinforced metal matrix composites is superior to that of the unreinforced matrix, while that of particulate reinforced aluminum metal matrix composites is at least equivalent to the unreinforced alloy, Figure 1. Accompanying detailed microstructural examination suggests that the principal benefits of the whisker reinforcement, vis a vis particulate reinforcements, on long life fatigue, can be attributed to the increase in the number of cycles required for fatigue crack growth initiation, the number of cycles involved in fatigue crack growth still being limited by the decreased fracture toughness of the metal matrix composite.

Historically, the damage tolerance behavior of metallic materials, including discontinuously reinforced metal matrix composites, has utilized the principals of linear elastic fracture mechanics(LEFM). This approach assumes that K, the linear elastic stress intensity factor, gives an accurate representative of the stress field at the tip of an atomically sharp crack in either an unreinforced or a discontinuously reinforced metal matrix composite. Based on this assumption, methodologies previously developed for unreinforced materials have been applied to determine K_{Ic}, the mode I plane strain fracture toughness, $K_{threshold}$, the threshold for fatigue crack growth and da/dN, the fatigue crack growth rate, the latter as a function of the stress intensity range, ΔK, for a number of composite systems.

An illustration of this approach for a particulate reinforced aluminum metal matrix composite is shown in Figure 2. This data indicates that $K_{threshold}$ for 6.4 mm thick peak-aged SiC_p particulate reinforced MB 78, a 7000 series aluminum alloy, is a function of the reinforcement size. For fine SiC_p reinforced MB 78, the threshold is below that of the unreinforced matrix, that is the initial fatigue crack growth resistance is inferior to that of the unreinforced material. If however, coarser SiC_p is utilized as the reinforcement, the threshold appears to be equivalent to the unreinforced matrix. Furthermore, at higher ΔK, within stage II, the fatigue crack growth resistance of both fine and coarse SiC_p reinforced MB 78 appears to be superior to that of the unreinforced matrix, until a ΔK level is reached where the lower fracture toughness resistance of the discontinuously reinforced metal matrix composite once again predominates. Shiang and Ritchie(11) have ascribed this beneficial

effect of particulate reinforcement during Stage II fatigue crack growth to an increase in crack tortuousity, while the decrease in fracture toughness is due to particle cracking and particle-matrix decohesion(12).

The importance of proper particulate reinforcement size selection for enhanced fracture toughness has been extensively investigated by Hunt and his co-workers at ALCOA(12,13). Their data, as illustrated in Figure 3, indicates that an optimum discontinuous reinforcement particle size exists, finer sizes leading to clumping, a characteristic of non-uniform reinforcement distribution, a coarser size to particulate cracking and early fracture. Figure 3 also shows that overaging, an approach conventionally used in unreinforced 7000 series aluminium alloys for enhancing the fracture toughness of this alloy system, without unduly sacrificing tensile yield and ultimate properties, is not applicable to particulate reinforced aluminum metal matrix composites. Similar results have also been reported in overaged whisker reinforced aluminum alloys where the results have been ascribed to the deleterious effects arising from heterogeneous precipitation of equilibrium phases at reinforcement/matrix interfaces(3,14).

Studies of the fatigue crack growth and fracture toughness behavior of whisker reinforced metal matrix composites have also been reported. Suresh and Lewis(15) have shown that $K_{threshold}$ for 6.3 mm. thick whisker reinforced 2124 aluminum is superior to that of the unreinforced alloy. Once again the fatigue crack growth rate in Stage II is lower for the

reinforced alloy vis a vis the unreinforced matrix until Stage III, unstable crack propagation occurs, Figure 4.

Recent observation by the authors and their co-workers(17,18) suggests however that the general applicability of linear elastic fracture mechanics to short fiber/whisker reinforced metal matrix composites may not be warranted. If linear elastic fracture mechanics is to be considered as an appropriate design criteria, then the stress field in the very near vicinity of the crack tip should control the fracture behavior of the composite and the determination of the critial K value should not be sample dependent. Figure 5 shows the macroscopic fracture appearance of identically oriented 12 mm. thick compact tensile and center cracked panels. These specimens were machined from a 11.5:1 extrusion oriented so that the subsequent crack propagation direction was perpendicular to both the whisker orientation and extrusion direction. Clearly, any results obtained from the compact tension sample are invalid, extension crack deflection having occurred. This conclusion has been substantiated by the following experiment. A center cracked panel, oriented as above, was precracked, compact tension samples machined from the panel and loaded either in fatique or directly to failure. In both instances the self-similar crack previously introduced during precracking of the center cracked panel immediately turned, rendering both compact tension tests invalid.

A final complicating factor must also be considered in whisker

reinforced metal matrix composites: stress state. A 3 mm. thick, plane stress, compact tensile sample, prepared from the mid-section of the aforementioned extrusion and pre-cracked according to accepted ASTM procedure, in contrast to the 12 mm. thick sample, exhibited self-similar fatigue crack growth. Further, scanning electron microscopy showed that self-similar crack growth in plane strain center cracked panels did not exhibit any localized crack deflection at whisker/matrix interfaces, while large amounts of localized crack deflection was observed during self-similar crack growth in thin compact tensile samples, Figure 6.

Conclusions

Renewed interest in discontinuously reinforced metal matrix composites for primary structural applications has prompted further attention to their damage tolerance behavior. In general it has been shown that the fatigue and fracture toughness behavior of particulate reinforced metal matrix composites can be described utilizing LEFM. However, the generalized use of this methodology for whisker or short fiber reinforced metal matrix composites, where reinforcement orientation effects may be paramount, must be approached with caution

Acknowledgements

The author wishes to acknowledge the continued support of NASA-Langley under NASA Grant NAG-1-724, W. Brewer contract monitor AFOSR under contract F49620-80-C-0017, A. Rosenstein contract monito

REFERENCES

1. A. P. Divecha and S. G. Fishman in K. J. Millers and R. Smith, eds., Proceedings Third International Conference on Composite Materials, Vol. 3, 1980, pp. 351-361.

2. T. E. Steelman, A. D. Dakalyar and L. Konopka, Aluminum Matrix Composite Structural Design Development, AFWAL-TR-86-3087, March, 1987.

3. T. E. Scott, J. W. Mullins and H. J. Rack, Effects of Composition and Process Variables on the Properties of Discontinuous Silicon Carbide Reinforced Aluminum Metal Matrix Composite Materials, Report AFWAL-TR, in press.

4. H. J. Rack, in P. Kumar, K. Vedula and A. Ritter, eds., Powder Metallurgy Composites, The Metallurgical Society, Warrendale, Pa., 1988, pp. 155-168.

5. H. J. Rack, in Y. W. Kim, ed., Dispersion Strengthened Aluminum Alloys, The Metallurgical Society, Warrendale, Pa., 1988, in press.

6. H. J. Rack, Advanced Materials and Manufacturing Processes, 3, (1988) in press.

7. H. J. Rack and P. Ratnaparki, Encyclopedia of Composites, VCH Publishers, New York, 1988, in press.

8. D. R. Williams and M. E. Fine, Proceedings Fifth International Conference on Composite Materials, AIME, Warrendale, PA, 1985, pp. 639 - 669.

9. C. R. Crowe, R. A. Gray and D. F. Hasson, Proceedings Fifth International Conference on Composite Materials, AIME, Warrendale, PA, 1985, pp. 843 - 866.

10. C. R. Crowe and D. F. Hasson, in R. C. Grifkins, ed., Strength of Metals and Alloys, Pergamon Press, New York, 1983, pp. 859-865.

11. J. K. Shiang and R. O. Ritchie, Materials Science and Engineering, Vol 102-A,1988,pp.181-192

12. W. H. Hunt, Jr. C. R. Cook, K. P. Armanie and T. B. Gargenus, in P. Kumar, A. Ritter and K. Vedula (in ref.4), pp. 117 - 137.

13. W. H. Hunt, Jr., O. Richmond and R. D. Young in F. L. Matthews, N. C. R. Buskell, J. M. Hodgkinson and J. Morton, eds. Proceedings Sixth International Conference on Composite Materials, Elsevier Applied Science, London, U.K., 1987, pp. 2.209 - 2.223.

14. H. J. Rack and J. W. Mullins, in G. Hildeman and H. Kosak, eds., High-Performance Powder Aluminum Alloys-II, The Metallurgical Society, Warrendale, Pa., 1986, pp. 155 - 171.

15. S. Suresh and R. E. Lewis, in W. C. Harrigan, Jr., J. Strife and A. Dhingra, eds., Proceedings Fifth International Conference on Composite Materials, The Metallurgical Society, Warrendale, Pa. 1985, pp. 825 - 842.

16. F. [redacted]man and S. Suresh, Materials Science and Engineering, in press.

17. H. J. Rack, J. G. Goree, J. Albritton and P. Ratnaparkhi, Annual Progress Report, NASA Grant NAG-1-724, November, 1987.

18. J. R. Albritton and J. G. Goree, Proceedings Seventh International Conf. on Fracture 1989 (ICF 7), Houston, Texas, March, 1989, to be published.

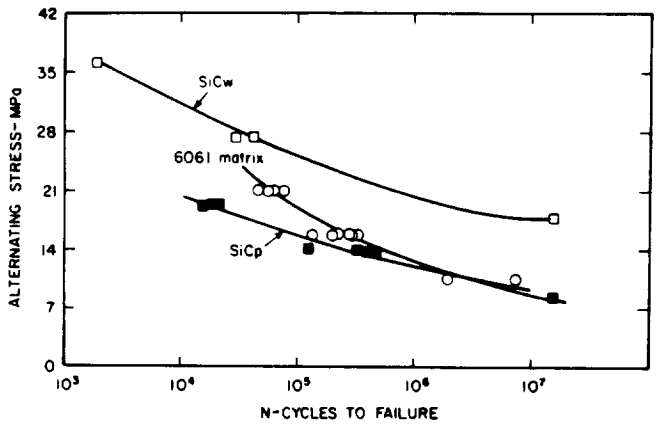

FIGURE 1 : S-N Curves for SiC Reinforced 6061 Aluminium(10)

ORIGINAL PAGE IS
OF POOR QUALITY

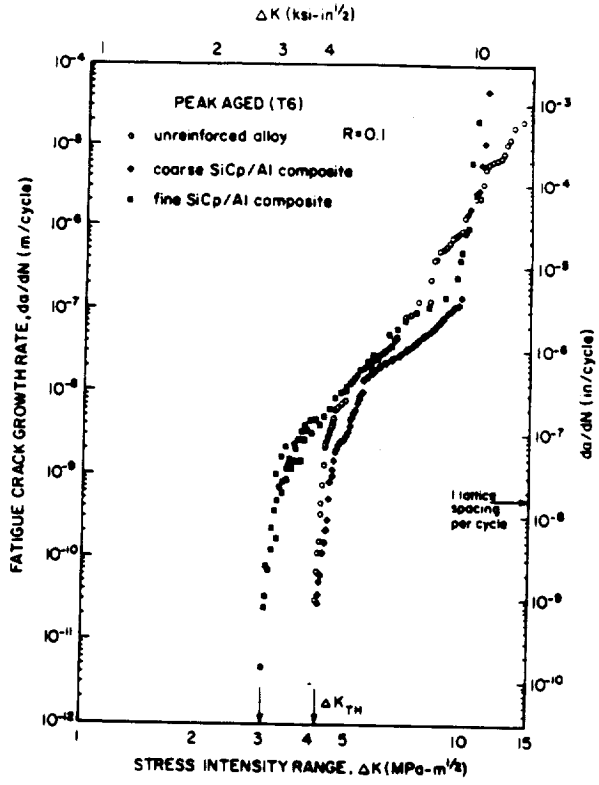

FIGURE 2: Variation in Fatigue Crack Growth Rates (da/dN) with Nominal Stress Intensity Range (ΔK) at R = 0.1 for SiC Particulate Reinforced Peak-Aged MB 78(11).

ORIGINAL PAGE IS
OF POOR QUALITY

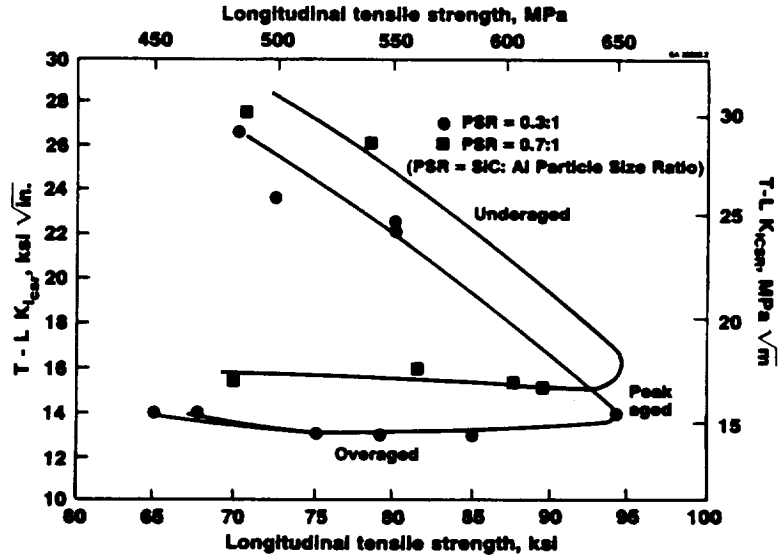

FIGURE 3: Fracture Toughness-Strength Relationships for MB 78 + 2
v/o SiC Particulate Composites(12).

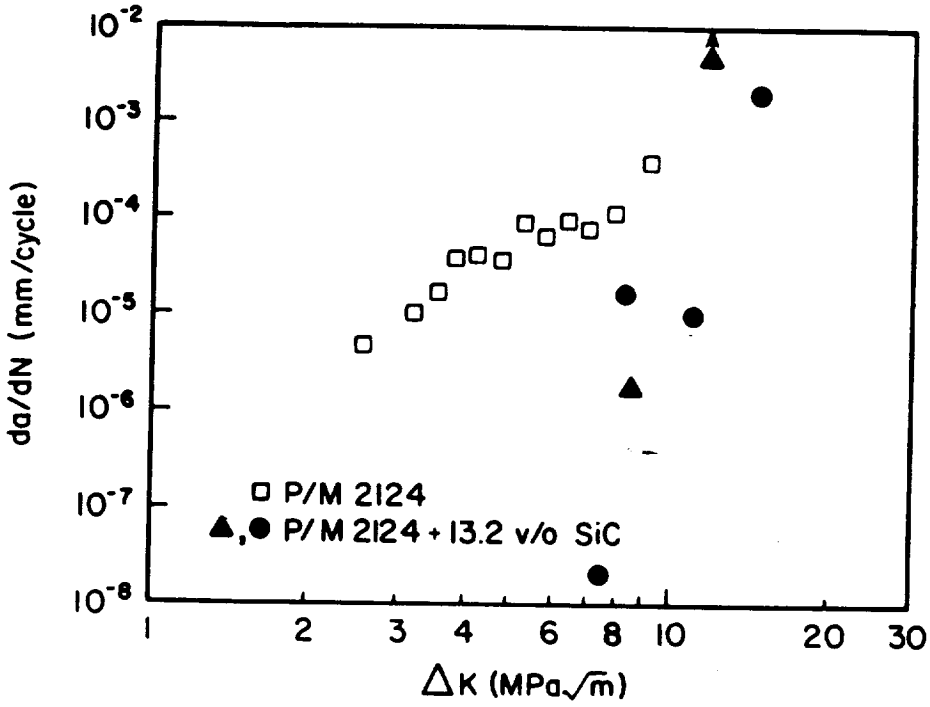

FIGURE 4: Variation in Fatigue Crack Growth Rates (da/dN) with Nominal Stress Intensity Range (ΔK) at R = 0.1 for SiC Whisker Reinforced 2124 (1a).

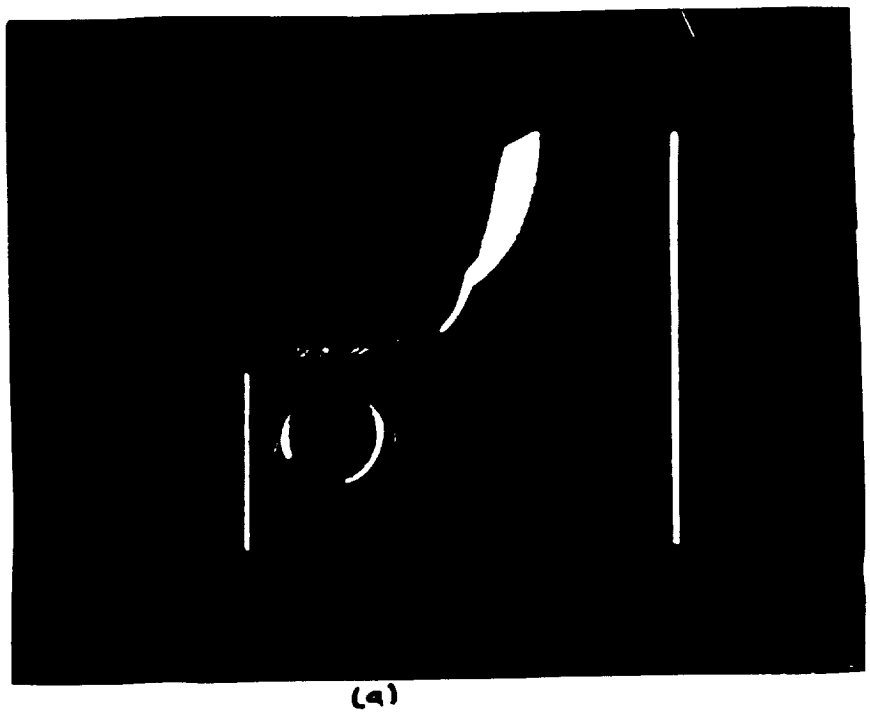

(a)

(b)

FIGURE 5: Macro-photographs of 12 mm. Thick 20 v/o SiC Whisker Reinforced 2124-F, (a) Compact Tension and (b) Center Cracked Panel

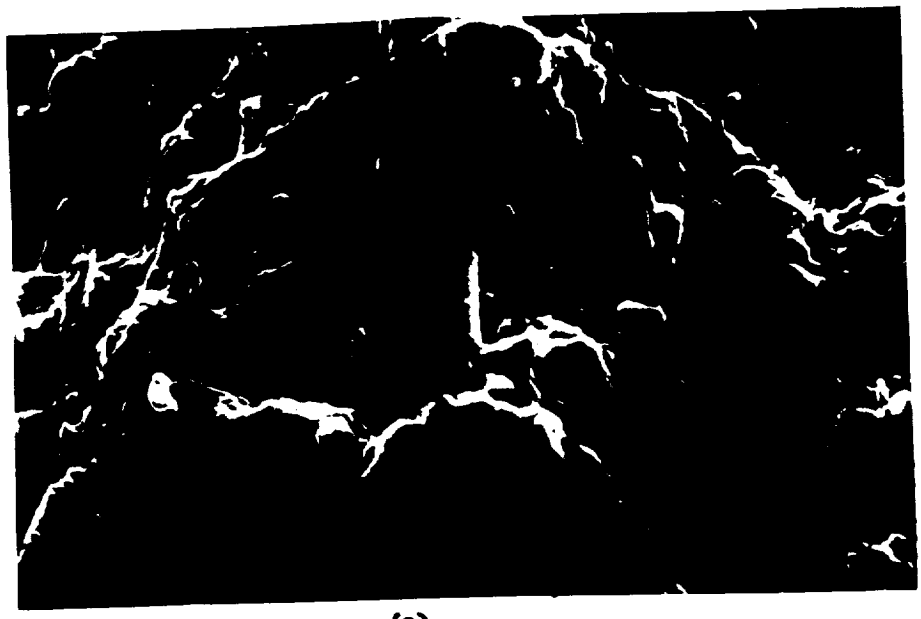

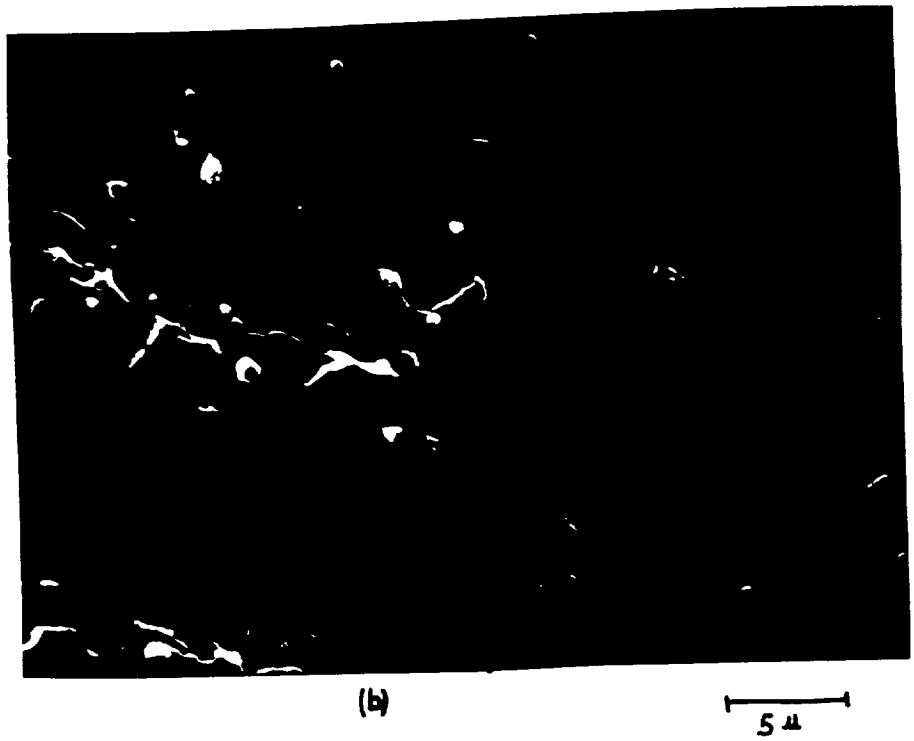

FIGURE 6: Scanning Electron Micrographs of Fatigue Crack Growth Region in L-T Oriented (a) 3 mm. Thick Compact Tension and (b) 12 mm. Thick Center Cracked Panel 2124-F Reinforced with 20 v/o SiC Whiskers.

APPENDIX B

Powder Metal Composites

H. J. Rack

and

P. Ratnaparkhi

To be Published

Encyclopedia of Composites

VCH Publishers

New York

1988

POWDER METAL COMPOSITES

H. J. Rack* and P. Ratnaparkhi*

Materials Engineering Activity

Department of Mechanical Engineering

Clemson University

Clemson, South Carolina 29634-0921

ABSTRACT

This chapter reviews the fabrication, age hardening and mechanical response of powder metallurgy based discontinuously reinforced metal matrix composites. Principal emphasis is placed on SiC reinforced aluminum metal matrix composite materials. Fabrication includes criteria for matrix and reinforcement selection, blending, compaction, primary processing(rolling, extrusion and forging) and secondary processing(sheet forming, spinning and joining). The age hardening response of aluminum metal matrix composites is contrasted with unreinforced alloys, utilizing Al-Mg-Si and Al-Cu-Mg matrices for illustrative purposes. It is shown that the presence of the discontinuous reinforcement may alter the kinetics of matrix age hardening thru an acceleration of second phase nucleation and an increase in precipitate diffusional growth. Finally, the current understanding of those intrinsic and extrinsic factors which appear to control, and limit, the tensile ductility and fracture toughness of discontinuously reinforced aluminum metal matrix composites are discussed.

---

* Respectively, Professor of Mechanical Engineering and Metallurgy, and Graduate Student.

INTRODUCTION

Modern design procedures continually strive to increase structural efficiencies through reductions in either absolute weight or increases in the strength-to-weight ratio. Figure 1 illustrates how, for a cargo-bomber aircraft application (1), reductions in material density, or increases in modulus(stiffness), yield strength and/or ultimate tensile strength, can be directly translated to reductions in structural weight. For example, a 10 percent reduction in alloy density, which can be achieved through substitution of Al-Li alloys for 2000 series aluminum alloys, will result in a 10 percent reduction in structural weight. Alternatively, a 50 percent increase in modulus, which can be achieved through substitution of a discontinuous silicon carbide(SiC) reinforced alloy for an unreinforced wrought aluminum alloy, will also result in a 10 percent reduction in structural weight(2). Indeed, it is possible to envision combining these effects thru the development of a reinforced Al-Li alloy(3-7).

System trade-studies, such as outlined above, have been the primary motivating factor in the reneved interest shown in metal matrix composites. Initially, these investigations focused on continuous fiber reinforced materials emphasizing C, SiC, B, B_4C or Al_2O_3 filaments or toves(8-11). Matrices of interest have included Al, Mg, and most recently Ti. Continuous fiber reinforced metal matrix composite fabrication has utilized plasma spraying, hot molding/superplastic diffusion bonding of foil/fibers laminates and pressure infiltration of woven preforms. Widespread industrial

application of these composites has however been limited by the high costs of both the reinforcement fiber, e.g., $300/lb for B, and the metal matrix component fabrication process.

These cost-performance considerations have focused current commercial attention on discontinuously reinforced metal matrix composites, for example, silicon carbide whisker(SiC_w), particulate(SiC_p) and alumina/alumina-silica(Al_2O_3-SiO_2) reinforced aluminum(12-16). Discontinuously reinforced metal matrix composites benefit from substantially lower fiber costs, for example, $2-3 per lb. for SiC_p. In addition, discontinuously reinforced aluminum matrix composites can be fabricated utilizing standard or near-standard metal fabrication procedures, e.g.,rolling, sheet forming, spinnning, brazing, welding, investment casting, etc., to yield materials with near isotropic properties(17-24). Finally, several studies have shown that when careful attention is paid to processing detail, an extremely attractive combination of mechanical properties can be obtained, for example, a 50 percent increase in stiffness can be achieved in SiC reinforced aluminum while maintaining adequate levels of strength, ductility and fracture toughness(25,26).

Discontinuously reinforced metal matrix composites may be fabricated utilizing either ingot or powder metallurgy techniques. This chapter will examine powder metallurgy, P/M, based discontinuously reinforced metal matrix composites. While emphasize will be placed on SiC_w and SiC_p reinforced aluminum matrix composites, it should be recognized that the principles presented herein are applicable to a

wide range of discontinuously reinforced metal matrix composite systems. The chapter will initially review the general fabrication utilized in the manufacture of these composites, and then consider how the age hardening response and mechanical properties of discontinuously reinforced powder metallurgy metal matrix composites differ from those of unreinforced alloys.

FABRICATION

Figure 2 shows a generalized flow chart depicting the principal steps involved in the production of powder metallurgy, discontinuously reinforced metal matrix composites. These procedures, as briefly outlined below, are being routinely applied to the manufacture of 13 inch diameter, 250 lb. SiC reinforced aluminum metal matrix billets with scaleability to 1000+ lb. billets having been demonstrated(19).

Billet Fabrication

Reinforcement-Matrix Selection

The initial step in the manufacturing sequence involves proper selection of the discontinuous ceramic reinforcement and the matrix alloy. Various selection criteria for the ceramic reinforcement may be envisioned, the most important being:

- elastic modulus
- tensile strength
- density
- melting temperature
- thermal stability
- compatibility with matrix
- thermal coefficient of expansion
- size and shape
- cost

While mechanical and physical property requirements may often limit the reinforcement choices, the chemical reactivity of the ceramic reinforcement, during either fabrication or service, will oftentimes establish the final reinforcement-matrix combination. Recent

investigations by Spencer(27) and Ahn(28) suggest however that it may be possible to tailor matrix-reinforcement interfaces. For example, SiC, while possessing excellent mechanical strengths and moduli, is thermodynamically unstable in aluminum alloys at high temperature. Selective coatings, applied utilizing sol-gel procedures, may offer a cost effective method for combining these high strength reinforcements with matrices intended for long term exposure at elevated temperature.

If the composite is to be subjected to repeated thermal cycling, for example, as might occur in an internal combustion engine it is imperative that the thermal mismatch between the proposed reinforcement and matrix be minimized. The importance of this mismatch criteria can be appreciated by recognizing that, to a first approximation, the strain, $\delta\epsilon$, developed at the interface of a discontinuously reinforced metal matrix composite due to a single thermal cycle is:

$$\delta\epsilon = \delta\alpha\ \delta T$$

where $\delta\alpha$ is the difference between the thermal coefficients of expansion for the reinforcement and the matrix, and δT is the range of temperature experienced during a thermal excursion. Naturally if $\delta\epsilon$ exceeds the yield strain, localized plastic flow at the reinforcement-matrix interface will occur, and damage will accumulate. Therefore, in order to minimize strain accumulation, differences in expansion coefficients between reinforcement and matrix should be minimized.

Reinforcement

Currently, SiC is the most widely utilized discontinuous ceramic

reinforcement. This reinforcement is available in a range of sizes and morphologies as illustrated in Figures 3 and 4. The various morhologies may contain α(hcp), β(bcc) or a mixture of α and β polymorphs. Transmission electron microscopy has also shown that these reinforcements are heavily faulted, the degree of faulting varying as a function of reinforcement manufacturing method(29,30). Figure 5 illustrates this heavily faulted substructure in a SiC whisker viewed perpendicular to its length. Detailed analysis indicates that, in this instance, the whisker has a zinc-blend structure with a high density of microtwins on (111) planes. Possibly most important, particularly from the viewpoint of ultimate mechanical behavior, is that this high density of microtwins or faults results in an uneven or serrated reinforcement surface, as shown along A in Figure 5.

Variations can also be observed in chemical composition, both within and between SiC morphological types, see Table 1. In one instance, that is for ACMC whiskers, the high Ca content has been traced to extremely fine Ca riched inclusions within the as-manufactured whisker(31).

Matrix

Table 2 summarizes the wide range of alloys that have been, or are being examined, as possible aluminum matrices. Historically, wrought alloy compositions, e.g., 6061, were selected as matrix materials(32-34). These alloys were initially prepared as either elemental or pre-alloyed air/helium inert gas atomized powders. Currently however all suppliers of powder metallurgy discontinuously reinforced aluminum matrix composites utilize pre-alloyed powders.

Typically, powders utilized in the fabrication of discontinuously reinforced aluminum metal matrix composites have a mean size of 15μm, nominally -325 mesh, Figure 6, and are either air or helium inert gas atomized.

Numerous investigations(14,35-38) have concluded that the minor alloying elements, Mn and Cr, commonly included in wrought alloys are detrimental to the composites' mechanical properties. This deleterious effect has been related to the formation of large (Mn,Cr) containing intermetallic compounds during consolidation and subsequent processing. Such observations have resulted in the elimination of Mn and Cr in high strength metal matrix composites, Zr being substituted in many instances to insure adequate grain size control and deep hardenability. Further study(39) has also shown that leaner alloy compositions, that is alloys whose compositions lie on the lower end of what might be considered to be the standard alloy specifications, develop a better combination of strength, ductility and fracture toughness.

More recently, matrix compositions which take full benefit of rapid solidification technology have begun to be examined. These include 7090(14,33), 7091(14,33), MR87(40,41), Al-Fe-Ce(14,42) and Al-Cu-Mg-Li(4). Unfortunately, early data indicates that the 7000 series alloys do not appear to be promising candidates for aluminum composite matrices. For example, overaging heat treatments, which has classically been used to enhance strength-fracture toughness trade-offs in 7000 series alloys, do not appear to be effective in composite systems.

Blending

A dry or wet blending operation normally follows selection of the reinforcement and matrix powder. While conceptually simple, the blending step ultimately controls many of the important properties metal matrix composites are intended to achieve. If whiskers or short fibers are to be included in the composite this blending step must be preceeded by deagglomeration of the reinforcement. Skovronek et.al.(33) have described one method for deagglomeration which involves ultrasonic agitation of alcohol fiber suspensions.

An important characteristic of reinforcement/powder blends is shown in Figure 7. This figure shows a typical SiC whisker/aluminum powder blend; note the large size difference between the whisker reinforcement and the matrix powder. This difference makes it impossible to achieve uniformly high properties in whisker reinforced composites that have not undergone an extensive amount of deformation processing. If the degree of deformation is inadequate, whisker reinforced powder metallurgy composites will always exhibit some degree of non-uniformity; indeed if blending and processing are not optimized whisker clumping, early crack initiation and non-uniform precipitation will be observed(44-48).

The importance of reinforcement-powder size selection has also been extensively investigated by Hunt and co-workers at ALCOA(40,41). These investigators have shown that, in particulate reinforced aluminum metal matrix composites, optimal mechanical response requires selection of a specific ratio of particulate to powder size, see Figure 8. Fortunately this ratio, once determined, can easily be specified in

particulate reinforced aluminum metal matrix composites. However, the same approach cannot be utilized in whisker metal matrix composites. In the latter, the whisker diameters are generally fixed within a rather narrow size range(14). In the latter composites, mechanical working procedures offers the only potential for minimizing the detrimental effects of dissimilar powder and reinforcement sizes.

Consolidation

Final billet fabrication involves cold compaction, outgassing and hot isostactic or vacuum hot pressing, Figure 9. While the principal function of the cold compaction step is to provide a compact having some green strength, it is essential that the cold compaction densities be controlled to insure an open interconnecting pore structure. The latter is extremely important since it is these channels which allow for the egress of the various gaseous products that will be liberated during subsequent heating and outgassing.

Normally the details of the reinforcement-powder blend outgassing procedures are considered proprietary by the composite manufacturer, however they all involve, at a minimum, the removal, through the combined action of heat, vacuum and inert gas flushing, of adsorbed or chemically bound water and other volatile species. Outgassing of SiC reinforced aluminum metal matrix composites involves removal of adsorbed water from both SiC and aluminum, as well as chemically bound water from the aluminum alloy. The principal reactions occurring during the outgassing process are given in Table 3, where H_2 and H_2O are the primary gaseous reaction products and Al_2O_3 is the primary solid

product(20, 49).

The extent of the reactions which occur during outgassing of SiC_p and SiC_w reinforced 6061 Al blends is depicted in Figure 10. These data indicate that the observed reactions are strongly dependent upon reinforcement surface chemistry. Other investigators have also shown that the details of the reactions listed in Table 3 will be sensitive to the Al alloy chemistry(50).

Once the desired isothermal temperature is reached, final consolidation is accomplished by pressure application. Selection of the consolidation temperature is typically based on the need to minimize the pressures necessary for complete consolidation without degrading the powder matrix. Preliminary data also suggest that dynamic compaction may be an attractive alternative when dealing with highly unstable rapidly solidified aluminum alloys(51). Finally, while both solid state and mushy zone consolidation temperatures have been employed, growing evidence suggests that higher tensile ductilities can be achieved following solid state pressing(52).

After consolidation metal matrix composite billets are homogenized, scalped and inspected. Typical inspection criteria assure 98 percent theoretical density prior to subsequent processing.

Primary Processing

Consolidated billets, generally 98+ percent theoretical density, can now be fabricated into a wide variety of shapes utilizing semi-standard metal working equipment. Because these

materials are based upon powders, discontinuously reinforced metal matrix composites must be worked in order to develop optimal properties. Primary working operations involving rolling, extrusion and forging have all been demonstrated. Figure 11 illustrates the extremely uniform distribution of SiC that can be achieved in aluminum matrix composites when proper processing procedures are utilized. These procedures must however be adjusted, recognizing the forming temperatures, deformation rates and flow conditions are uniquely identified with each composite system(53).

Several methods of selecting the appropriate strain rates and deformation temperatures for discontinuously reinforced metal matrix composites have been suggested(15, 18, 19, 53-56). Most are based on experience or trial and error. One approach which appears to warrant further consideration utilizes the material's true stress-true strain rate constitutive behavior as a function of strain rate and temperature(56). If the dynamic constitutive behavior is represented by a relationship of the form,

$$\sigma = A \dot{\epsilon}^m$$

where m is the strain rate sensitivity, then the deformation efficiency, that is the amount of energy transformed into shape change without recourse to damage accumulation within the material, can be defined by

$$\eta = \frac{2m}{m + 1}$$

noting that m, is a function of both temperature and strain rate.

Optimal processing conditions of strain rate and temperature can then be defined, at least to a first approximation where η is maximized.

Figure 12 illustrates the application of this principle to 2124 reinforced with 20 volume percent silicon carbide whiskers(57). This data suggests that the optimal deformation temperature and strain rate conditions for this composite system are 485°C and 10^{-4} sec^{-1}.

The attainment of maximum useful work, as defined above, should be considered to be a necessary but not sufficient condition for establishing optimum deformation parameters. For example, Gegel et. al.(57) have also shown that this maxima in 2124 reinforced with 20 volume percent SiC whiskers, is associated with nearly complete dynamic recovery, higher temperatures and rates leading to incipient melting, lower temperatures and rates to dislocation accumulation. In contrast, it is well known that maximum toughness in wrought aluminum alloys is generally associated with an unrecrystallized grain structure. Indeed, further experimental examination of the microstructural conditions associated with optimized processing of SiC reinforced 2124 has reconfirmed the latter concepts and have resulted in the deformation temperatures being lowered to 400°C(25).

In addition to appropriate selection of deformation temperature and strain rate, optimal thermomechanical treatment of aluminum metal matrix composites requires control, particularly during extrusion and forging, of metal flow conditions. While initial attention in this area was focused on whisker and short fiber composites, the aim being to minimize whisker/fiber breakage while controlling orientation,

Greenfield(58) has recently demonstrated that particulate sizes and orientations are also affected by deformation processing.

Figure 13 schematically compares two extrusion die geometries currently employed for discontinuously reinforced aluminum metal matrix composites(54). Figure 13(a) shows the flow fields associated with a shear faced die, while Figure 13(b) shows those of "stream-line" flow die. The latter die configuration has been designed to simulate hydrostatic flow conditions, eliminating the re-entrant corners and "dead" zones where reinforcement in shear faced dies are forced to undergo sharp velocity discontinuities. While it may be argued that normally all required shapes can be extruded utilizing shear faced dies, Table 4 shows the potential benefits that can be achieved when the stream-lined die design approach, as combined with the deformation mapping approach described previously, is applied to the extrusion of 2124 containing 20 volume percent SiC whiskers. Minimum whisker damage occurs.

Finally, measurements of whisker orientation further suggest that only moderate extrusion ratio's will be required for essentially complete alignment of SiC reinforcements, Figure 14. While this alignment can be beneficial, for example, near rule-of-mixture elastic moduli can be attained in properly processed extruded whisker reinforced aluminum alloys, Figure 15, its presence can result, at least in whisker and short fiber discontinuously reinforced composites, in a highly anisotropic fracture behavior(60).

Secondary Processing

Secondary processing procedures which have been successfully

applied to discontinuously reinforced aluminummetal matrix composites include shear spinning(22), superplastic forming(61-65) and joining(23,24). For example, Figure 16 illustrates that elongations in excess of 300 percent can be achieved in SiC whisker reinforced 2124 thru proper selection of temperature and strain rate. Of particular technological interest is the fact that the strain rates associated with superplastic behavior in these materials are rather high when compared to those reported in other structural materials.

Reinforced aluminum composites may also be welded using a variety of processes. However, two precautions should be observed. First, since they are powder products, it is essential that the composites be thoroughly outgassed, for example by vaccum annealing, prior to welding. This procedure will assist in minimizing subsequent porosity in the weld fusion zone. Secondly, the weld energy input should be carefully controlled to prevent or minimize the reaction between SiC and aluminum, this reaction leading to the unwanted formation of Al_4C_3.

AGING RESPONSE

Several comparisons of the age hardening response of unreinforced and reinforced powder metallurgy discontinuously reinforced aluminum metal matrix composites have been reported(12, 14, 15, 18, 66-70). In general these studies, relying principally upon hardness data, have indicated that the introduction of a discontinuous reinforcement results in an increase in the maximum hardness attained during aging and a decrease in the time necessary for achieving this hardness.

Al-Mg-Si Matrix Alloys

Figure 17 summarizes the artificial aging response of a direct quenched and aged unreinforced and reinforced Al-Mg-Si alloy. In both materials the hardness increases with increasing aging time, with overaging being observed after aging at either 155° or 170°C. Times to attain maximum hardness are shorter for the reinforced alloy, with overaging being more rapid. Further, higher hardness levels may, for both unreinforced and reinforced materials, be achieved by aging longer times at lover temperatures. Finally, the degree of age hardening is less and hardness levels obtainable higher in the reinforced Al-Mg-Si alloy when compared to the unreinforced.

Transmission electron microscopy has shown that the aging sequence observed in unreinforced and reinforced Al-Mg-Si composites is essentially that previously reported in ingot alloys(66, 70-71), i.e.,

$$SSS \longrightarrow GPZ \longrightarrow \beta'' \longrightarrow \beta' \longrightarrow \beta(Mg_2Si)$$

where SSS = supersaturated solid solution, GPZ = vacancy rich

Guinier-Preston zones, β'' a needle shaped semi-coherent phase, β' = a rod shaped transition phase and β = incoherent equilbrium Mg_2Si. However, the details clearly dependent upon the presence of the reinforcement phase. For example, Figure 18 shows the morphology and distribution of precipitates observed in a peak aged (12 hours at 160°C) unreinforced alloy. Matrix preciptates include semi-coherent β'' and β' needles and lathes, with β(Mg_2Si) precipitation at prior powder boundaries. This microstructure should be contrasted with that shown in Figure 19 for peak aged SiC_w reinforced 6061. In the latter, no identifiable β'', β' or β precipitates are observed, rather maximum age hardening appears to be related with the presence of extremely fine particles(< 10 μm).

Al-Cu-Mg Matrix Alloy

The artificial aging response of a typical unreinforced and reinforced Al-Cu-Mg alloy is shown in Figures 20 and 21. Once again, the results indicate that artificial aging is enhanced in the SiC reinforced alloy, relative to that observed in the unreinforced material. Maximum hardness obtainable in the direct quenched and aged reinforced composite is higher and the time required for attaining this hardness is shortened. It should be noted however that the aging response of reinforced Al-Cu-Mg alloys appears to be quite sensitive to experimental detail, that is section size, quench rates, delays. For example, Christian and Suresh(67) have reported that the hardness of unreinforced and reinforced 2124 is nearly identical.

In addition, the detailed comparison of aging in unreinforced and reinforced Al-Cu-Mg is quite complex. For example, aging below

150°C results in a number of hardness minima, the times for attaining these minima decreasing with the introduction of the SiC reinforcement. However, the time at constant aging temperature for initial S' formation, as determined by the time for the initial increase in the electrical conductivity(71), is <u>not</u> altered by the introduction of the SiC reinforcement.

Continuing transmission electron microscopy and X-ray analysis has shown that the aging sequence observed in unreinforced and reinforced Al-Cu-Mg matrix composites is essentially that previously reported in ingot alloys(72,73), i.e.,

$$SSS \longrightarrow GPB \longrightarrow S'(Al_2CuMg) \longrightarrow S(Al_2CuMg)$$

where SSS = supersaturated solid solution, GPB = Guinier-Preston zone, S' = semi-coherent intermediate phase, S = incoherent equilibrium phase. Again, the details are dependent upon the presence of the reinforcement and, as noted above, on the aging procedures. Figure 22 shows that the rate of S' growth is higher in direct quenched and aged whisker reinforced 2124 than in unreinforced 2124. If aging is delayed, for example by holding at room temperature prior to artificial aging, a reverse impression of the influence of reinforcement on the size of S' may be obtained, Figures 23 and 24. Figure 23, taken from earlier studies of natural plus artificially aged unreinforced 2124 shows both S' and S phases present in the matrix, with the S phase also heterogeneously precipitated at prior powder particle boundaries. This micrograph should be contrasted with the refined S' and S phase distribution shown in Figure 24 for natural plus overaged reinforced 2124.

These differences in age hardening response between unreinforced and reinforced powder metallurgy aluminum composites have been attributed by several to the presence of a dislocation substructure in the reinforced material. This substructure is introduced into the reinforced composite during cooling from the solution treatment temperature through plastic relaxation of the reinforcement-matrix thermal expansion mismatch strains. Various authors(45,66,70,74) have reported that the dislocation density of the reinforced aluminum matrix, in contrast to unreinforced alloys(78), is both high and non-uniform. For example, Vogelsang et.al.(75) have shown that the dislocation density at the reinforcement-matrix interface in as-quenched 6061 reinforced with 20 volume percent SiC$_p$ is high, $10^{13}/cm^2$, and decreases with increasing distance from this interface. Similar results have also been obtained in Cu-W composites(76,77).

It is possible that this dislocation substructure may have two separate, but interrelated effects, on age response in reinforced aluminum composites. The first, would be an increase in the nucleation rate of certain phases, to the possible exclusion of others, the second, an increase in precipiate growth rates through enhanced dislocation assisted diffusion. The former instance may be rationalized by considering the effect of the presence of a dislocation substructure on the steady state precipitate nucleation rate, J, as represented by(76):

$$J = Z \beta^* N \exp(-\Delta G^*/kT)$$

where Z is the Zeldovich non-equilibrium factor, β^* the rate at which solute atoms are added to the critical nucleus, N the number of nucleation sites per unit volume, ΔG^* the Gibbs free energy for the formation of a critical nucleus, k is Boltzmann's constant, and T is the absolute temperature. The volumetic nucleation site density, N, in the presence of a dislocation field, is expected to be proportional to the dislocation density, ρ_d, times the number of sites per unit line length, i.e.,

$$N = \rho_d / a$$

where a is the lattice constant. Therefore the nucleation rate should increase with increasing dislocation density. In addition, the presence of the dislocation substructure will tend to reduce the free energy barrier to nucleation, ΔG^*. This decrease is due to the effective decrease in the volume strain energy accompanying the formation of a critical nucleus when the latter event occurs in the presence of a dislocation line.

A schematic illustration of the possible combined effects of dislocation density strain and aging temperature on the steady state nucleation rate is shown in Figure 25. If the aging temperature is low, for example, below T_s in Figure 24, where formation of homogeneously nucleated phases, e.g., GP zones, predominate, the presence of a dislocation substructure will have little effect on the nucleation rate. In contrast, at temperatures above T_s, where nucleation of phases, e.g., semi-coherent transition phases, can be enhanced by the presence of additional heterogeneous nucleation sites, preciptation rates in reinforced alloys should be higher than in unreinforced materials. Further, as depicted in

Figure 25, the temperature regime over which the transition phase is preferentially nucleated may be altered by the introduction of the dislocation substructure. Currently available results(66,70) indicate that this analysis can explain the variations in aging response between unreinforced and SiC reinforced Al-Mg-Si alloys.

However, this analysis does not appear to be consistent with the present data on direct aged SiC reinforced Al-Cu-Mg composites. Available information indicates that the dislocation substructure observed in SiC reinforced Al-Cu-Mg alloys does not influence the time for initial S' formation. In addition, the size and growth rate of S' in direct aged composites are larger than in unreinforced alloys. These observations suggest that the primary role of the dislocation substructure in Al-Cu-Mg composites is to provide a short-circuit path for enhanced diffusion.

MECHANICAL BEHAVIOR

The mechanical behavior of discontinuously reinforced aluminum matrix composites has been examined by numerous investigators(80-100). Figure 26 shows that in an 1100 aluminum matrix, where the complicating effect of precipitation has been eliminated, increasing the volume fraction of reinforcement results in an increase in elastic modulus, yield and ultimate tensile strength and a decrease in tensile elongation. This data further demonstrates that, at constant volume percent reinforcement, whisker reinforced aluminum composites exhibit higher stiffness', higher yield and ultimate tensile strengths, and lower tensile elongations. Similarly, the fracture toughness of particulate reinforced aluminum metal matrix composites tends, again at constant volume percent reinforcement, to exceed that of whisker reinforced aluminum composites, Figure 27. The latter figure also demonstrates that the toughness of aluminum metal matrix composites is a distinct function of thickness, increasing with decreasing thickness.

These, and other studies, suggest that differing factors may control the tensile ductility and fracture toughness of discontinuously reinforced aluminum alloys. Void initiation during tensile loading has been variously associated with pre-existing matrix voids(99), cracked reinforcements(89,90), large intermetallic($Al_{20}Cu_2(Cr,Fe)_3$) particles, SiO_2 inclusions and large SiC particulate particles(35,36,38), small solute rich constituent particles(14,38), whisker and particulate clusters(40,41,44,46,84,92,95) and whisker-matrix interfaces(87,88,97). Void initiation associated with large SiC particles and Al,Cu rich

constituent particles are illustrated in Figure 28.

Recent improvements in particulate/powder sizing, blending and deformation processing have largely eliminated premature tensile failure due to pre-existing voids and reinforcement clustering(40). Large intermetallic particles, SiO_2 inclusions and SiC particulates can be eliminated by minimizing Cr, Fe and Mn additions to the matrix alloy, consolidating below the alloy solidus and careful selection/screening of the whisker and particulate reinforcements, respectively. Finally, the presence of small undissolved solute rich constituent particles can be minimized by rebalancing the matrix chemistry(14). These steps, when taken together, have resulted in the fabrication of discontinuosly reinforced aluminum metal matrix composites having tensile elongations consistently above 5 percent(25,40).

Ultimately, the attainment of higher tensile ductility of SiC reinforced aluminum composites will be limited by the intrinsic properties of the matrix and reinforcement. For example, several studies (14,40,41) indicate that in 7000 series alloys heterogeneous precipitation of $MgZn_2$ occurs at the reinforcement-matrix interface. Subsequent tensile deformation of these composites will result in low elongations due to early void initiation at the precipitate-reinforcement interface.

Others, Nutt et al(87,88,97), have observed void initiation at a presumably precipitate free whisker end-matrix interface in SiC whisker reinforced aluminum alloys. Here void initiation occurs by strain localization at the end of the whisker, as depicted schematically in Figure 29. Void formation initially occurs at the interface between the whisker end and the matrix, with void growth progressing across the whisker end. A similar void initiation mechanism can be envisioned for particulate

reinforced metal matrix composites where void initiation could occur at sharp corner particulate stress concentrations.

Alternatively, the reinforcement may fracture under the action of the tensile stress and a void form at the intersection of the fractured reinforcement and the matrix. While no direct experimental evidence has been yet been presented to support this hypothesis, it is well known that reinforcement, both whiskers and particulates, do crack during mechanical processing. In addition, both particulate and whisker reinforcements have a heavily faulted substructure, which Wawner(102) has shown, during in-situ straining within the electron microscope, to be preferred paths for crack propagation.

Finally, theoretical studies(101) indicate that at high volume fractions, or small spacings, direct matrix void initiation may occur. For example, for two cylindrical inclusions, when widely separated, the location of maximum elastic stress concentration will be at the inclusion-matrix interface. However, as the spacing between the cylindrical inclusions approaches the inclusion size, the location of the maximum stress, and presummably the maximum strain concentration, shifts to the midpoint between the two particles. This analysis, when applied to discontinuosly reinforced aluminum metal matrix composites, predicts that, as the volume fraction of constant sized reinforcement increases, the void initiation path should change from one which favors the reinforcement-matrix interface to one which favors matrix fracture. Some support for this hypothesis is given by the fractographic results of You et al(98) who found that tensile failure of 20 volume percent α-SiC particulate reinforced 2124 occurs in a random fashion through

the composite, rather than seeking out SiC particulates.

Much less is known about the factors controlling the fatigue and fracture toughness behavior of discontinuous metal matrix composites. Figure 30 shows that the long life fatigue behavior of whisker reinforced aluminum composites is far superior to the unreinforced alloy, while that of particulate reinforced composites is similar to the unreinforced matrix. Detailed microstrucural studies(47,102) indicate that the benefits of the reinforcement can be attributed to an increase in the number of cycles required for fatigue crack initiation, the number of cycles in the fatigue crack growth regime being limited. This conclusion appears to be substantiated by the available data on the fatigue crack growth resistance of reinforced aluminum alloys. Figure 31 shows that K threshold for 6.4 mm thick particulate reinforced 7000 series, MB78, aluminum alloy is similar, or inferior, to the unreinforced matrix. At higher delta K, that is within Stage II, the crack growth rates of peak-aged reinforced MB78 are slower than the unreinforced matrix alloy, until at rather low delta K's unstable crack propagation occurs. Others(95) have shown that K threshold for 6.3 mm thick whisker reinforced 2124 aluminum is generally superior to the unreinforced alloy, see Figure 32. Once again the fatigue crack growth rate in Stage II is lower for the reinforced alloy vis a vis the unreinforced matrix until Stage III, unstable crack propagation, occurs.

Further study(94) has also shown that K_{th}, at least in 5.3 mm thick whisker reinforced 2124, may be sensitive to heat treatment, over-aging resulting in an increase in K_{th}, see Figure 33. That this is a matrix effect is clearly demonstrated by the similar response, i.e., an

increase in K_{th}, observed in unreinforced 2124.

Interpretation of at least the whisker results are further complicated by recent studies(60) which indicate that the details of fatigu crack growth and unstable crack propagation in whisker reinforced aluminum alloy composites are extremely sensitive to both sample thickness and far-field stresses. Figure 34 shows scanning electron micrographs of the fatigue pre-crack regions in thin(3 mm) compact tension an thick(12 mm) center cracked fracture toughness samples, both having been prepared from a 12.5 mm thick, 20 volume percent reinforced 2124 extrusion in the L-T orientation. Clearly, Figure 34(a) shows the large amount of local, whisker associated crack deflection, which might be expected in oriented short fiber discontinuously reinforced composites. However, fractographic examination of the center cracked 12 mm thick samples did not show any evidence of localized crack deflection, Figure 34(b).

Not only is the fracture toughness of aluminum metal matrix composites a function of reinforcement content, thickness and far-field stresses it is influenced by both thermal and mechanical processing (14, 25, 35, 41). These observations suggest that the fracture toughness of these materials can best be understood by separating possible toughening mechanisms into their intrinsic and extrinsic components(103 Intrinsic components which are expected to contribute to the toughness of discontinuously reinforced metal matrix composites include matrix heat treatment and the volume fraction, size and spacing of small constituent inclusions(typically less than 0.1 μm in size).

The former will influence the ability of the matrix to relieve the stress concentration associated with the propagation of a sharp crack by localized plastic deformation, while the latter will influence the composites' propensity towards void sheet formation.

Extrinsic components which are expected to contibute to the fracture toughness of discontinuously reinforced metal matrix composites include fiber size, spacing, uniformity of spacing and alignment. For example, recent investigations have shown that the fracture toughness of whisker reinforced sheet can be materially enhance thru proper control of thermo-mechanical processing procedures, see Figure 35. Thin sheet fracture toughness values reported in this figure are equivalent to those that would be expected from unreinforced 2000 aluminum alloys heat treated to the higher strength levels obtainable in SiC reinforced alloys.

REFERENCES

1. "Application of Reinforced Metals to Cargo-Bomber Aircraft" (AFWAL-TR-3061, U. S. Air Force Wright Aeronautical Laboratory, June 1981).

2. A. P. Divecha and S. G. Fishman in K. J. Millers and R. Smith, eds., Proceedings Third International Conference on Composite Materials, Vol. 3, 1980, pp. 351-361.

3. D. Webster, Metallurgical Transactions, 13A, 1511 (1982).

4. G. Piper and H. J. Rack, Clemson University, Clemson, South Carolina, Unpublished Research, 1988.

5. J. White, I. R. Hughes, T. C. Willis and R. M. Jordan, Aluminum-Lithium III, in press.

6. T. C. Willis and R. M. Jordan, ALCAN International Ltd, Banbury, U. K., Private Communication, July, 1987.

7. J. White, T. C. Willis, I. R. Hughes, I. G. Palmer and R. M. Jordan, in Y. W. Kim, ed., Dispersion Strengthened Aluminum Alloys, The Metallurgical Society, Warrendale, Pa., 1988, in press.

8. M. E. Buck and R. J. Suplinskas in C.A. Dostal, ed., Engineered Materials Handbook, Volume 1, Composites, ASM International, Metals Park, Ohio, 1987, pp. 851-857.

9. J. A. McElman in C. A. Dostal (in ref. 8), pp. 858-866.

10. D. A. Goddard, P. A. Burke, D. E. Kizer, R. Bacon and W. C. Harrigan, Jr., in C. A. Dostal (in ref. 8), pp. 867-873.

11. J. C. Rommie in C. A. Dostal (in ref. 8), pp. 874-877.

12. H. J. Rack in Y. W. Kim (in ref. 7), in press.

13. H. J. Rack, in P. Kumar, K. Vedula and A. Ritter, eds., Powder Metallurgy Composites, The Metallurgical Society, Warrendale, Pa., 1988, in press.

14. T. E. Scott, J. W. Mullins and H. J. Rack, Effects of Composition and Process Variables on the Properties of Discontinuous Silicon Carbide Reinforced Aluminum Metal Matrix Composite Materials, Report AFWAL-TR, in press.

15. T. E. Steelman, A. D. Bakalyar and L. Konopka, Aluminum Matrix Composite Structural Design Development, AFWAL-TR-86-3087, March, 1987.

16. H. J. Rack, Advanced Materials and Manufacturing Processes, 3, (1988) in press.

17. A. P. Divecha, S. G. Fishman and S. K. Karmaker, Journal of Metals, 33, 12 (1981).

18. P. Hood, Baseline Property and Fabrication Data for Silicon Carbide Whisker Reinforced Aluminum Alloy, Final Report N60921-81-A328, NSWC, White Oak, Md., October, 1982.

19. H. J. Rack, P. Hood, P. Nishanen and J. L. Cook in, Proceedings Third Discontinuous Metal Matrix Working Group, Metal Matrix Comp. Infor. Center, Santa Barbara, Cal., 1983.

20. W. R. Mohn, Manufacturing Technology Development of Extrusion Billet Stock, Final Report NSWC Contract N60921-83-C-0120, January, 1985.

21. W. R. Mohn and G. A. Gegel, in Advanced Composites: The Latest Developments, ASM International, Metals Park, Ohio, 1986, pp.69-73.

22. C. Standard, LTV-Vought Corporation, Grand Prairie, Texas, Private Communication, January, 1987.

23. J. Ahern, C. Cooke and S. G. Fishman, Metal Construction, 14, 192 (1982).

24. T. S. Luhman, R. L. Williams and K. B. Das, Development of Joint and Joint Techniques for Metal-Matrix Composites, AMMRC-TR 84-35, August, 1984.

25. J. R. Carroll, Jr. in Y. W. Kim (in ref. 7), in press.

26. W. S. Cebulak, in Advanced Metallic Structures Review, AFWAL-TR-87-3042, October, 1986.

27. H. G. Spencer, J. P. Clement and H. J. Rack, Clemson University, Clemson, South Carolina, Unpublished Research, 1988.

28. P. Ahn in Y. W. Kim (in ref. 7), in press.

29. S.R. Nutt, Journal of the American Ceramic Society, 67, 428 (1984).

30. J. Hove, Carnegie-Mellon University, Pittsburgh, Pa., Private Communication, March, 1988.

31. R. A. Crooks, ARCO Metals Corporation, Arlinton Heights, Ill., Unpublished Research, 1985.

32. H. J. Rack, T. R. Baruch and J. L. Cook in T. Hayashi, K. Kawata and S. Umekawa, eds., Progress in the Science and Engineering of Composites, Japan Society for Composite Materials, Tokyo, 1982, pp. 1465 - 1472.

33. W. C. Harrigan, in C. A. Dostal (in ref. 8), pp. 889-895.

34. J. L. Cook and W. R. Mohn, in C. A. Dostal (in ref. 8), pp. 896-902.

35. H. J. Rack and J. W. Mullins, in G. Hildeman and M. Koczak, eds., High-Performance Powder Aluminum Alloys-II, The Metallurgical Society, Warrendale, Pa., 1986, pp. 155 - 171.

36. F. Wawner, A. T. Chueng and S. Bettadapur, in J. D. Buckley, ed., Metal Matrix, Carbon, and Ceramic Composites, NASA Technical Conference Report No. 2357, NASA, Langley, Va., 1984, pp. 97 - 118.

37. T. G. Nieh, R. A. Rainen and D. J. Chellman in W. C. Harrigan, Jr., J. Strife and A. K. Dhingra, Proceedings Fifth International Conference on Composite Materials, The Metallurgical Society, Warrendale, Pa., 1985, pp. 825 - 842.

38. W. A. Johnson, Baseline Property and Fabrication Data for Silicon Carbide Whisker Reinforced Aluminum Alloy(Final Report, Contract N60921-81-C-A328, 1984).

39. H. J. Rack, Clemson University, Clemson, South Carolina, Unpublished Research, 1987.

40. W. H. Hunt, Jr. C. R. Cook, K. P. Armanie and T. B. Garganus, in P. Kumar, A. Ritter and K. Vedula (in ref.13) in press.

41. W. H. Hunt, Jr., O. Richmond and R. D. Young in F. L. Matthews, N. C. R. Buskell, J. M. Hodgkinson and J. Morton, eds. Proceedings Sixth International Conference on Composite Materials, Elsevier Applied Science, London, U.K., 1987, pp. 2.209 - 2.223.

42. F. Wawner, University of Virginia, Charlottesvile, Va., Private Communication, April, 1988.

43. C. J. Skovronek, A. Pattnaik and R. K. Everett, Dispersion and Blending of SiC Whiskers in RSP Aluminum Powders, Naval Research Laboratory Memorandum Report 5750, Naval Research Laboratory, 1986.

44. M. McKimpson and T. E. Scott, Michigan Technological University, Houghton, Michigan, Private Communication, September, 1986.

45. S. R. Nutt and R. W. Carpenter, Materials Science and Engineering, 75, 169 (1985).

46. G. Mott and P. K. Liaw, Westinghouse Research Laboratories, Pittsbugh PA., Unpublished Research, September, 1986.

47. D. R. Williams, Ph.D. Thesis, Northwestern University, Evanston, Ill. 1985.

48. P. K. Liaw, J. G. Greggi and W. A. Logsdon, Journal of Materials Science, accepted for publ.

49. P. P. Pronka, R. S. Bhattacharga, J. J., Kleek and F. H. Froes, Metallurgical Transactions, 19A, 372 (1988).

50. L. Ackerman, I. Guillemin, R. Lalauze and C. Pijolat in M. Koczak and G. Hildeman (in ref. 35), pp.175 - 191.

51. M. A. Meyers, New Mexico Institute of Mining and Technology, Socorro, New Mexico, Private Communication, January, 1987.

52. D. Chellman, Lockheed-California Company, Burbank, Cal., Private Communication, October, 1985.

53. H. J. Rack and P. N. Nishanen, Light Metal Age, Feb. 1984, pp. 9 -12.

54. J. R. Pickens, T. J. Langan R. O. England and M. Liebson, Metallurgical Transactions, 18A, 303 (1987).

55. Ph. Jarry, W. Loue and J. Bouvaist in F. L. Matthews, N. C. R. Buskell, J. M. Hodgkinson and J. Morton (in ref. 41), pp. 2.350 - 2.361.

56. Y. V. R. K. Prasad, H. L. Gegel, S. M. Doraivelu, J. C. Malas, J. T. Morgan, K. A. Lark and D. R. Barker, Metallurgical Transactions, 15A, 1883 (1984).

57. H. L. Gegel, J. C. Malas and Y. Prasad in J. Bailey, S. Fishman and P. Parrish, eds., Proceedings Tri-service Workshop on Dynamic Mechanical Properties, Characterization and Processing of Lightweight Metal Matrix Composites, U. S. Army Research Office, Durham, N. C., 1984.

58. J. Sun and I. Greenfield in F. L. Matthews, N. C. R. Buskell, J. M. Hodgkinson and J. Morton (in ref. 41), pp. 2.287 - 2.296.

59. H. L. Gegel, U. S. Air Force Wright Aeronautical Laboratory, Dayton, Ohio, Private Commumication, 1983.

60. H. J. Rack, J. G. Goree, J. Albritton and P. Ratnarparki, Clemson University, Clemson, South Carolina, Unpublished Research, 1988.

61. M.Y. Wu and O. D. Sherby, Scripta Metallurgica, 18, 773 (1984).

62. T. G. Nieh, C. A. Henshall and J. Wadsworth, Scripta Metallurgica, 18, 1405 (1984).

63. J. Wadsworth, C. A. Henshall, T. G. Nieh, A. R. Pelton and P. S. Gilman in G. J. Hildeman and M. J. Koczak (in ref. 35), pp. 137 - 154.

64. M. W. Mahoney and A. K. Ghosh, Metallurgical Transactions, 18A, 653 (1987).

65. M. W. Mahoney, A. K. Ghosh and C. C. Bampton in F. L. Matthews, N. C. R. Buskell, J. M. Hodgkinson and J. Morton (in ref. 41), pp. 2.372 - 2.389.

66. H.J. Rack, in F. L. Matthews, N. C. R. Buskell, J. M. Hodgkinson and J. Morton (in ref. 41), pp. 2.382 - 2.389.

67. T. Christian and S. Suresh, Microstructural Development in an Aluminum Alloy-SiC Whisker Composite, Brown University Report No. NSF-ENG-8451092/1/87, June, 1987.

68. I. Dutta and D. L. Bourell, in H. L. Marcus and L. K. Rabenberg, eds., Interfacial Characteristics and the Mechanical Properties of Metal Matrix Composites, University of Texas - Austin Report UTCMSE-87-3, September, 1987.

69. T. G. Nieh and R. F. Karlak, Scripta Metallurgica, 18, 25 (1984).

70. H. J. Rack and R. W. Krenzer, Metallurgical Transactions, 8A 335 (1977).

71. R. J. Arsenault and R. M. Fisher, Scripta Metallurgica, 17, 67 (1983).

72. M. Rosen, E. Horowitz, L. Swartzendruber, S. Fick and R. Mehrabian, Materials Science and Engineering, 53, 191 (1982).

73. G. W. Lorimer, in K. C. Russell and H. I. Aaronson, eds., Precipitation Processes in Solids, The Metallurgical Society, Warrendale, Pa., 1978, pp. 87 - 117.

74. J. M. Silcock, Journal of The Institute of Metals, 89, 203 (1960-61).

75. M. Vogelsang, R. J. Arsenault and R. M. Fisher, Metallurgical Transactions, 17A 379 (1986).

76. K. K. Chawla and M. Metzer, Journal of Materials Science, 7, 34 (1972).

77. K. K. Chawla, Fiber Science and Technology, 8, 49 (1975).

78. J. E. Hatch, Aluminum: Properties and Physical Metallurgy, American Society for Metals, Metals Park, Ohio, 1984, pp. 134 -199.

79. H. J. Rack, Materials Science and Engineering, 29, 179 (1977).

80. D. J. Chellman, H. C. Slaughter and A. H. Shabaik, Lockheed-California Company, Burbank, Cal., Unpublished Research, Presented 112th AIME Annual Meeting, Atlanta, Ga. March, 1983.

81. S. V. Nair, J. K. Tien and R. C. Bates, International Metals Review, 30, 275 (1985).

82. D. L. McDanels, Metallurgical Transactions, 16A, 1105 (1985).

83. W. A. Logsdon and P. K. Liaw, Engineering Fracture Mechanics, 24 737 (1986).

84. C. R. Crowe, R. A. Gray and D. F. Hasson, in W. C. Harrigan, Jr., J. Strife and A. K. Dhingra, eds. (in ref. 37), pp. 843 - 866.

85. D. L. Davidson, Metallurgical Transactions, 18A, 2115 (1987).

86. J. K. Shiang and R. O. Ritchie, Materials Science and Engineering, in press.

87. S. R. Nutt and J. M. Duva, Scripta Metallurgica, 20, 1055 (1986).

88. S. R. Nutt and A. Needleman, Scripta Metallurgica, 21, 705 (1987).

89. S. S. Yau and G. Mayer, North Carolina State University, Raleigh, N. C., Unpublished Research, 1985.

90. S. L. Langenbeck and L. S. Castro, Preliminary Investigation of Fatigue Crack Growth Behavior of Silicon Carbide Reinforced Powder Metallurgy Aluminum, Lockheed-California Company, Report LR 30083, 15 April, 1982.

91. R. J. Arsenault, in K. Kawata, S. Umekawa and A. Kobayashi, eds., Composites '86:Recent Advances in Japan and the United States, 1986, pp. 521-527.

92. F. Kloucek and R. F. Singer, Proceedings 31st. International SAMPE Symposium, SAMPE, Covina, Cal., 1986, pp. 1701-1712.

93. A. Marchant, J. Duffy, T. A. Churchman and S. Suresh, An Experimental Study of the Dynamic Mechanical Properties of an Al-SiC$_w$ Composite, Brown University Technical Report, December, 1986.

94. T. Churchman and S. Suresh, Materials Science and Engineering, submitted January 1988.

95. S.Suresh and R. E. Lewis, in W. C. Harrigan, Jr., J. Strife and A. K. Dhingra, eds. (in ref. 37), pp. 315-330.

96. V. Nardone, in Proceedings Ninth Discontinuous Metal Matrix Composites Working Group, Office of Naval Research, Park City, Utah, 1987.

97. S. R. Nutt, in A. K. Dhingra and S. G. Fishman, eds., Interfaces in Metal Matrix Composites, The Metallurgical Society, Warrendale, Pa, 1986, pp. 157 - 167.

98. C. P. You, A. W. Thompson and I. M. Bernstein, Scripta Metallurgica, 21, 181 (1987).

99. R. J. Arsenault, Materials Science and Engineering, 64, 171 (1984).

100. F. W. Wawner, in ref 96.

101. J. G. Goree, Journal of Composite Materials, 1 404 (1967).

102. C. R. Crowe and D. F. Hasson, in R. C. Grifkins, ed., Strength of Metals and Alloys, Pergamon Press, New York, 1983, pp. 859 - 865.

103. R. O. Ritchie and W. Yu, in R. O. Ritchie and J. Lankford, eds., Small Fatigue Cracks, The Metallurgical Society, Warrendale, Pa., 1986, pp. 167 - 189.

104. P. Hood, Advanced Composite Materials Corporation, Greer, South Carolina, Private Communication, February, 1988.

TABLE 1

BULK CHEMICAL COMPOSITION FOR SiC REINFORCEMENTS

	WHISKERS					PARTICULATE	SPHERICAL
	ACMC	EP	LANL	TATEHO	TOKAI	SUPERIOR	IBIDEN
Element (ppm)							
Ca	3700	2000	5000		1300	20	210
Mn	2400	3500	<50		<25	5	50
Al	1300	1500	800	600	500	100	310
Mg	800	485	120	1500	50	40	<25
Fe	500	670	50		1000	200	15200
Cr	<50	-	<25		200	10	70
Ni	<50	<10	50		150	40	-
K	<50	<10	<300		<300	-	-
Na	<50	<10	<100		400	-	40
Cu	<25	<25	400	3800	30	40	-
B	<10	<10	<10			-	-
Li	<10	<10	<30			-	-
Ti	<10	<10	<50		150	40	-

TABLE 2

CHEMICAL COMPOSITIONS OF ALUMINUM MATRIX POWDERS

	Element							
	Cu	Mg	Zn	Si	Mn	Cr	Fe	Other
Al-Cu								
2219	6.74	–	–	–	0.4	–	0.05	0.12V
Al-Cu-Mg								
2124	4.65	1.60	0.01	0.04	0.9	–	0.3	–
2124HP	4.65	1.5	0.02	–	–	–	0.1	–
2048	3.73	1.77	–	–	–	–	0.03	–
ACM1	2.95	1.37	–	–	–	–	–	–
ACM2	3.26	1.25	–	–	–	–	–	0.1 Zr
ACM3	3.67	1.84	–	0.14	0.2	–	0.2	0.6 Zr
Al-Mg-Si								
6061	0.35	1.19	0.02	0.77	–	0.22	0.32	–
6013	0.75	1.15	–	0.94	0.22	–	0.1	–
Al-Zn-Mg-Cu								
7075	1.5	2.5	5.5	–	–	0.30	–	–
7090	1.2	2.5	7.8	0.05	–	–	–	1.4 Co
7091	1.6	2.4	5.65	0.02	0.01	–	0.27	0.44 Co
SXA 60	1.33	2.35	9.7	0.1	–	–	0.06	–
SXA 90	1.31	2.49	7.8	–	0.02	–	0.03	–
AZMC1	–	0.79	3.56	–	–	–	–	–

AZMC2	0.68	0.98	4.18	–	–	–	–	–
MB78	2.0	2.0	7.0	–	–	–	–	0.14 Zr
Al-Li								
AL1	–	–	–	–	–	–	–	1.0
AL2	–	–	–	–	–	–	–	2.0
AL3	–	–	–	–	–	–	–	3.0
Al-Mg								
5082	–	4.5	–	–	0.7	–	–	–
Al-Cu-Mg-Li								
ACML1	0.91	0.85	–	–	–	–	–	1.66 Li
ACML2	0.63	0.68	–	–	–	–	–	1.0 Li
ACML3	1.5	1.0	–	–	–	–	–	2.8 Li
ACML4	3.0	1.0	–	–	–	–	–	1.6 Li
Other								
Al-Fe-Ce	–	–	–	–	–	–	7.7	4.2 Ce, 0.3 W
	–	–	–	–	–	–	5.6	4.6 Ce
Al-Fe-Mo	–	–	–	–	–	–	6.1	1.5 Mo
Al-Fe-X	–	–	–	–	–	–	4.5	4.5 Ni, 1.5Cr
Al-Cr-X					0.8	3.8		1.3 Zr

TABLE 3

CHEMICAL REACTIONS OCCURRING DURING HEATING OF ALUMINUM POWDERS(20)

$$Al_2O_3 \cdot 3H_2O \xrightarrow{> 100^\circ C} Al_2O_3 \cdot H_2O + H_2O(g)$$

$$Al_2O_3 \cdot H_2O \xrightarrow{> 400^\circ C} Al_2O_3 + H_2O(g)$$

$$2Al + 3H_2O \xrightarrow{> 200^\circ C} Al_2O_3 + 3H_2(g)$$

$$2Al + 6H_2O \longrightarrow Al_2O_3 \cdot 3H_2O + 3H_2(g)$$

TABLE 4

WHISKER ASPECT RATIO AS A FUNCTION OF PROCESSING (59)

Material	L/D
Powder/whisker blend	19.8
36:1 Extrusion Ratio Round-to-Round Through Streamline Flow Die	18.0

LIST OF FIGURES

FIG. 9 - Schematic representation of vacuum hot pressing.

FIG. 10 - Residual gas analysis of outgassing reactions in (a) SiC_p and (b) SiC_w reinforced 6061 aluminum(20).

FIG. 11 - Optical micrograph of 11.5:1 extruded 7091 aluminum reinforced with 20 volume percent SiC whiskers.

FIG. 12 - Influence of temperature and strain rate on the deformation efficiency(57).

FIG. 13 - Comparison of (a) shear and (b) streamline flow extrusion die configurations.

FIG. 14 - SiC whisker distribution in extruded 2124 - 20 volume percent SiC_w aluminum: (a) surface orientation, (b) through thickness orientation. Extrusion ratio 11.5:1.

FIG. 15 - Elastic modulus of SiC reinforced aluminum alloys.

FIG. 16 - Elongation and flow stress as a function of strain rate for 2124 reinforced with 20 volume percent SiC whiskers(63).

FIG. 17 - Artificial aging response of unreinforced and reinforced (20 volume percent SiC_w) 6061 aluminum solution treated for 1 hour at 538°C, water quenched and direct aged(18).

FIG. 18 - Transmission electron micrograph of unreinforced 6061, solution treated for 1 hour at 560°C, water quenched and aged 12 hours at 160°C(38).

FIG. 19 - Transmission electron micrograph of 6061 reinforced with 20 volume percent SiC_w, solution treated for 1 hour at 538°C, water quenched and aged 12 hours at 155°C.

FIG. 20 - Artificial aging response for unreinforced 2124, solution treated 1 hour at 495°C, water quenched and direct aged.

FIG. 21 - Artificial aging response for 2124 - 20 v/o SiC_w, solution treated 1 hour at 495°C, water quenched and direct aged.

FIG. 22 - S' precipitate size versus aging time at 177°C for unreinforced and reinforced direct quenched and aged 2124(67).

FIG. 23 - Transmission electron micrograph of unreinforced 2124, solution treated at 495°C for 1 hour, water quenched, naturally aged for 24 hours at 25°C and artificially aged for 100 hours at 100°C.

FIG. 24 - Transmission electron micrograph of 2124 reinforced with 20 volume percent SiC_w, solution treated 1 hour at 495°C, water quenched, stored for 2 hours at -196°C, naturally aged 24 hours at 25°C and aged for 64 hours at 175°C.

FIG. 25 - Schematic representation of the effect of dislocation substructure on the steady state nucleation rate.

FIG. 26 - Influence of SiC content on the tensile properties of 1100 aluminum composites(80).

FIG. 27 - Fracture toughness of particulate and whisker reinforced 2124 aluminum metal matrix composites(33).

FIG. 28 - Scanning electron micrographs of tensile fracture initiation from (a) a large SiC particle and (b) Al,Cu rich constituent particles i 20 volume percent SiC whisker reinforced 7091 and 2124, respectively.

FIG. 29 -Schematic void inititation model for SiC whisker reinforced aluminum metal matrix composites(97).

FIG. 30 S-N curves for SiC reinforced 6061 aluminum(102).

FIG. 31 - Variation in fatigue crack growth rates (da/dN) with nominal stress-intensity range (ΔK) at R = 0.1 for SiC particulate reinforced MB78 in peak aged condition(86).

FIG. 32 - Variation in fatigue crack growth rates (da/dN) with nominal stress-intensity range (ΔK) at R = 0.1 for SiC whisker reinforced 2124 aluminum(95).

FIG. 33 - Near threshold fatigue crack growth rates for SiC whisker reinforced 2124(94).

FIG. 34 - Scanning electron micrographs of fatigue pre-crack region in L-T oriented (a) 3 mm compact tension and (b) 12 mm thick center cracked 2124 - 20 v/o SiC_w fracture toughness specimens removed from 11.5:1 12.5 in. thick extrusion.

FIG. 35 - Fracture toughness comparison for unreinforced and SiC whisker reinforced aluminum sheet(104).

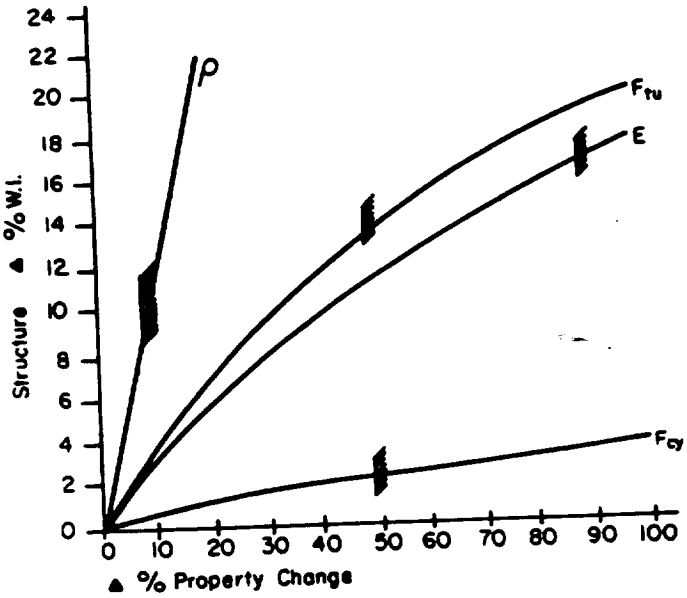

FIG. 1 - Performance enhancement related structural weight reductions in cargo-bomber aircraft applications (1).

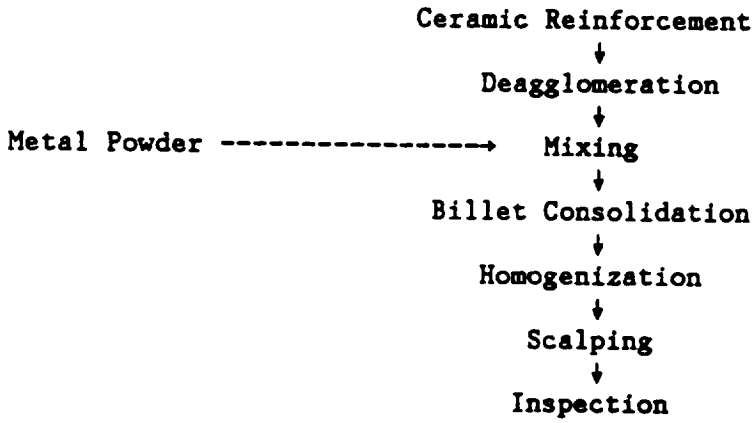

FIG. 2 - Powder-ceramic reinforcement blending sequence for discontinuously reinforced metal matrix composites.

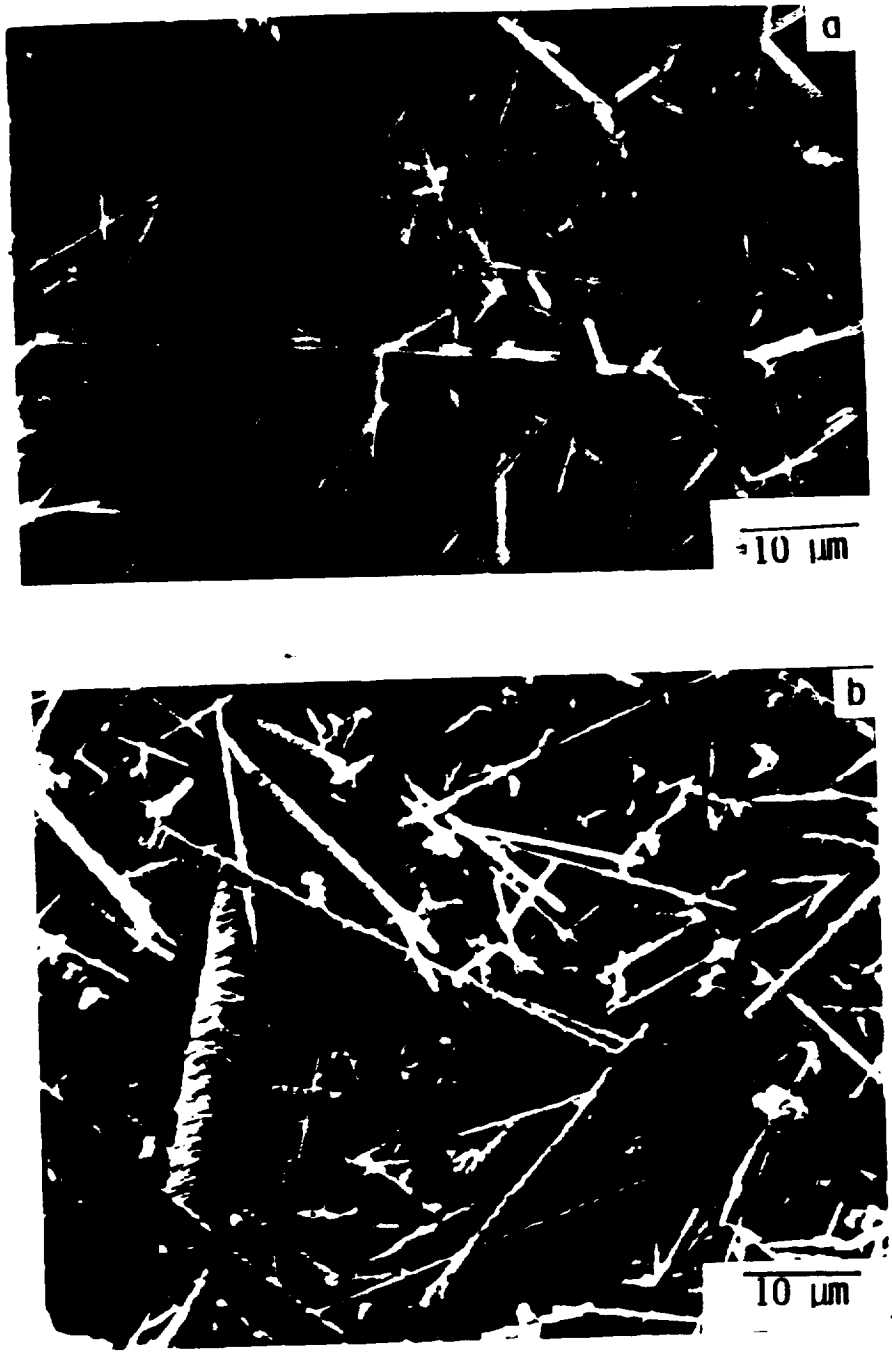

FIG. 3 - Scanning electron micrographs of discontinuous SiC whisker reinforcements (a) ACMC, (b) AMMATRIX and (c) Tokai.

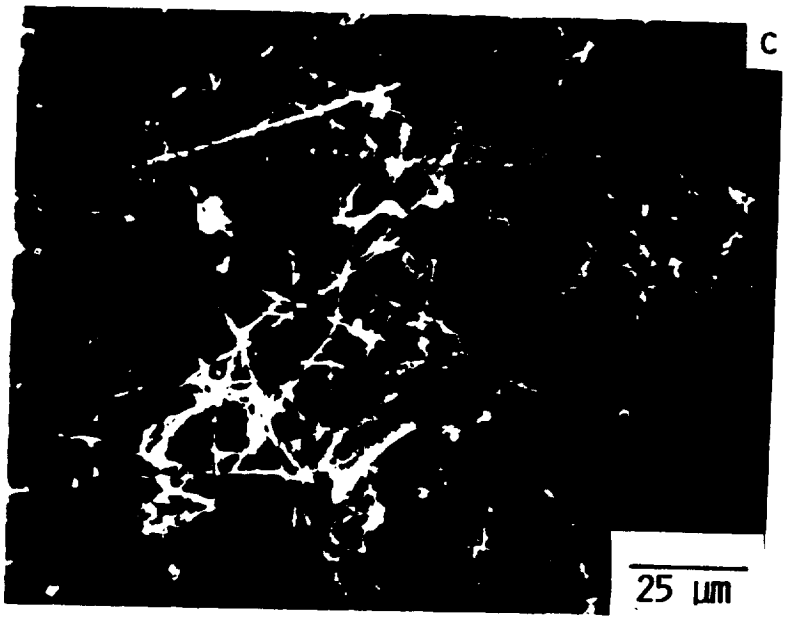

FIG. 3 - Continued

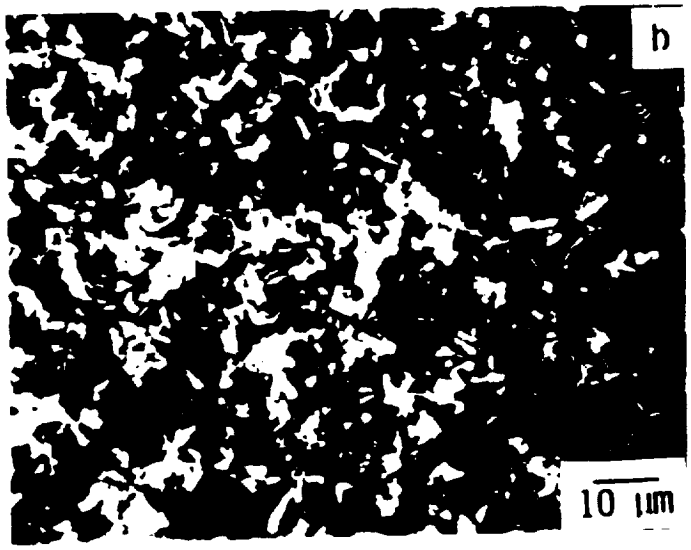

FIG. 4 - Scanning electron micrographs of discontinuous SiC (a) AMMATRIX oblate platelets and (b) Carborundum particulates.

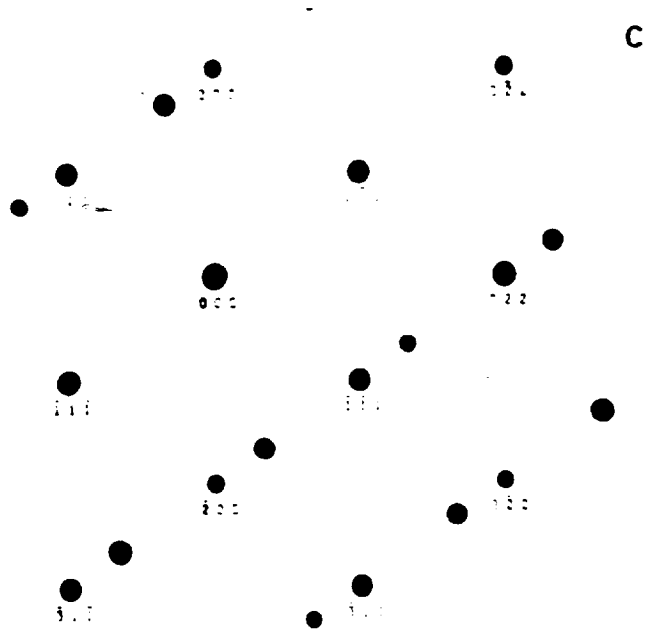

β-SiC (Zinc Blende Structure) twinned on $(1\bar{1}1)$ planes. $\underline{B}$=[011].

FIG 5 - Bright - field transmission electron micrograph of ACMC SiC in as-quenched 2124 matrix, (b) corresponding electron diffraction pattern and (c) calculated electron diffraction pattern for twinned β-SiC structure

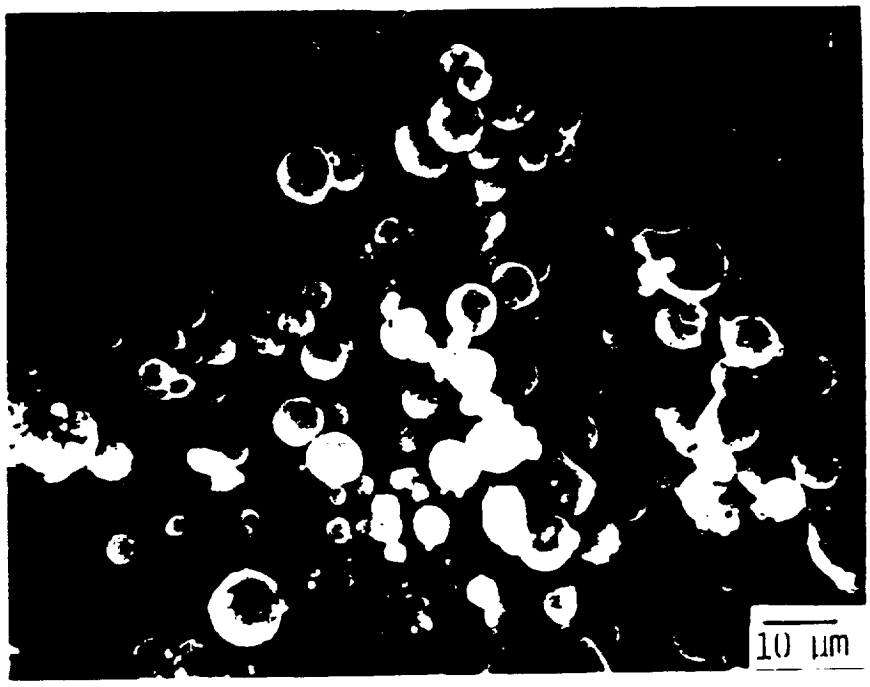

FIG. 6 - Scanning electron micrograph of helium inert gas atomized 7090 aluminum.

FIG. 7 - Silicon carbide whisker - aluminum blend.

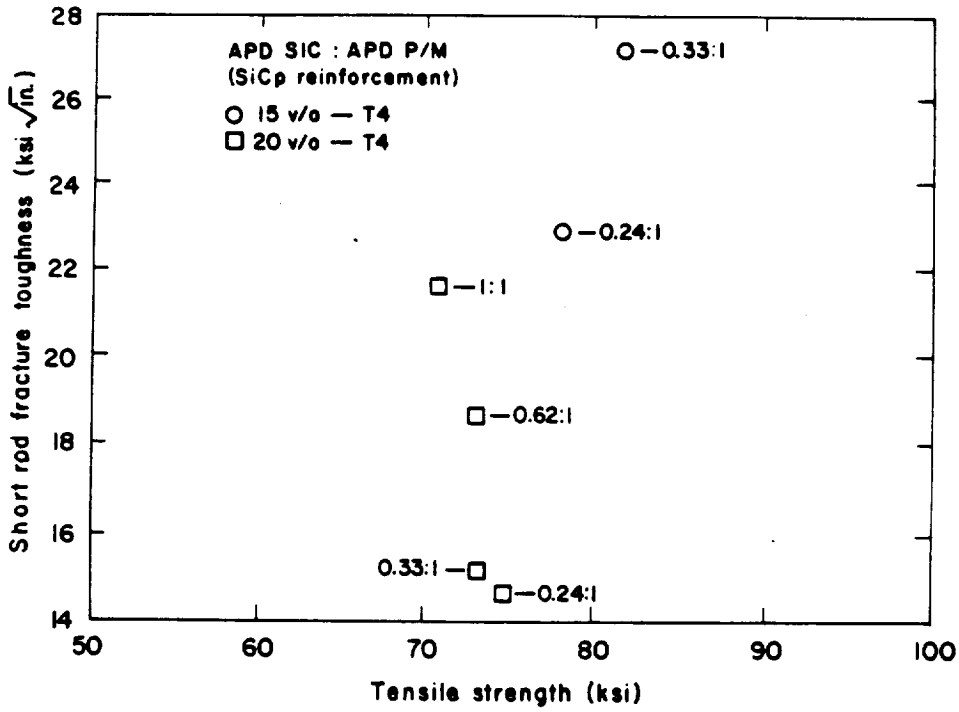

FIG. 8 - Influence of SiC_p/Al size ratio on fracture toughness of MB85(26).

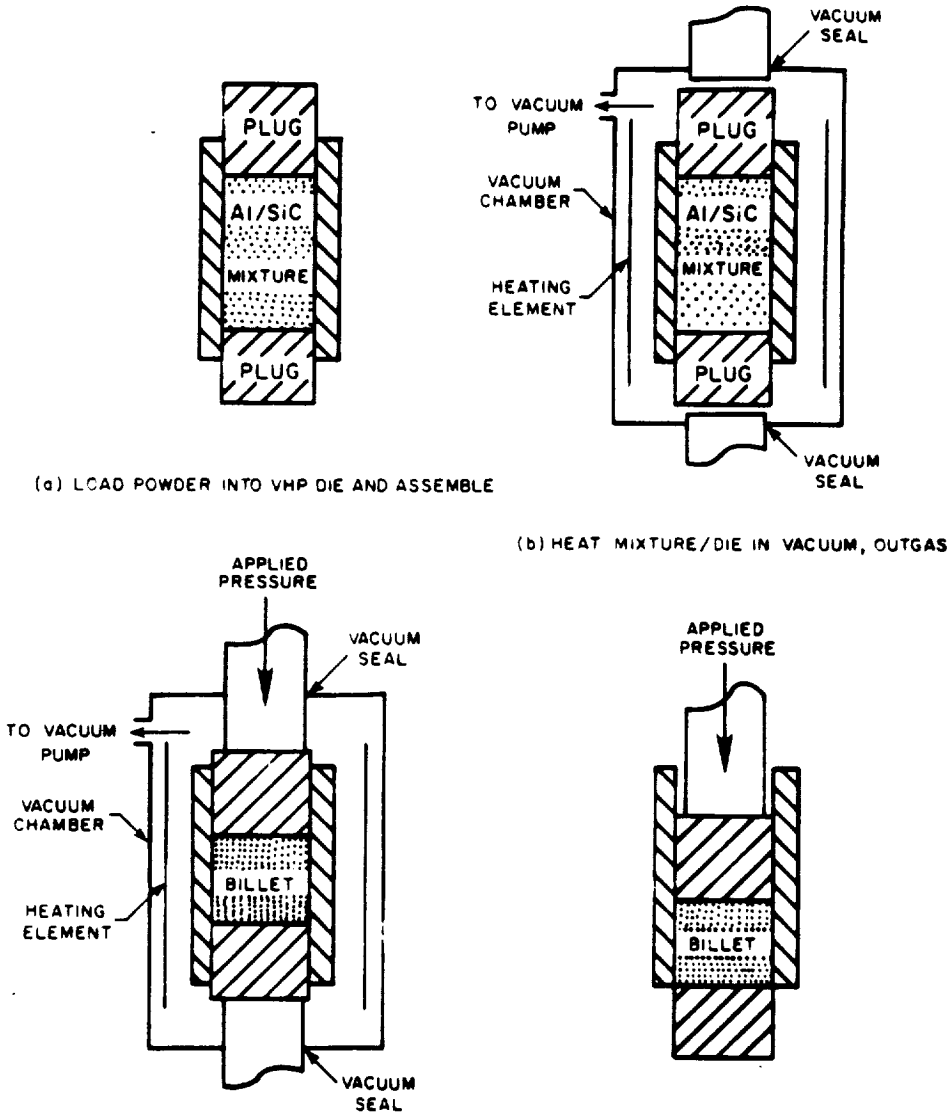

FIG. 9 - Schematic representation of vacuum hot pressing.

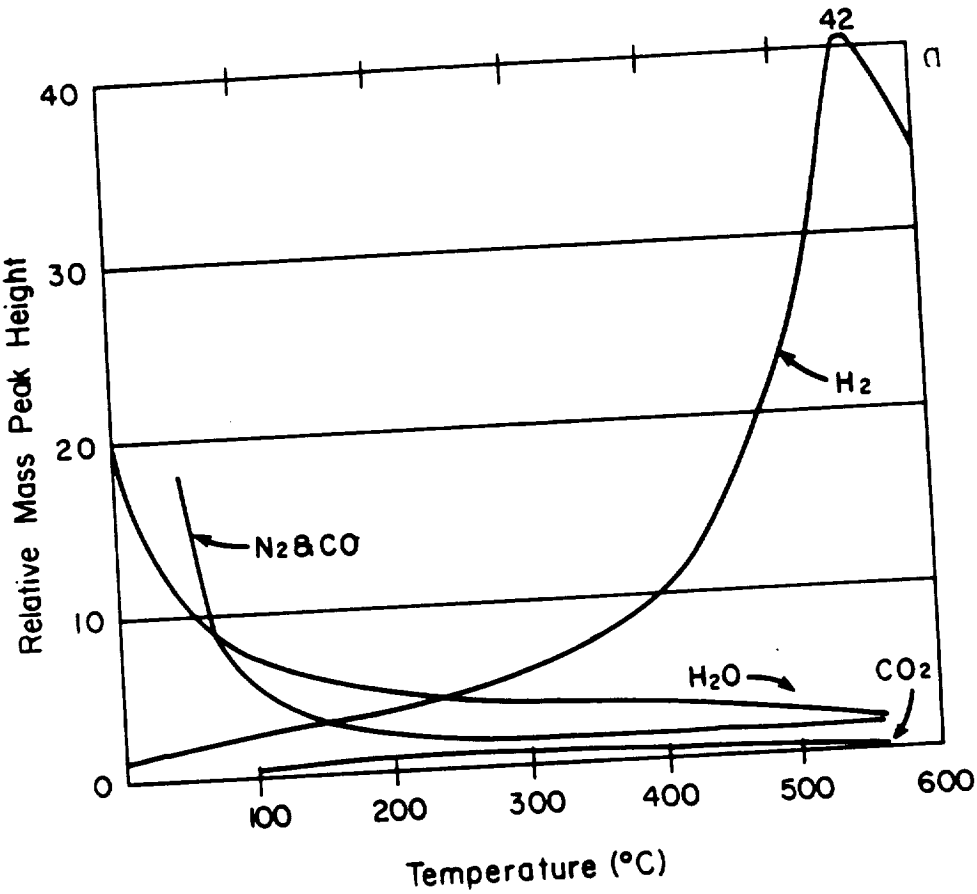

FIG. 10 - Residual gas analysis of outgassing reactions in (a) SiC$_p$ and (b) SiC$_w$ reinforced 6061 aluminum(20).

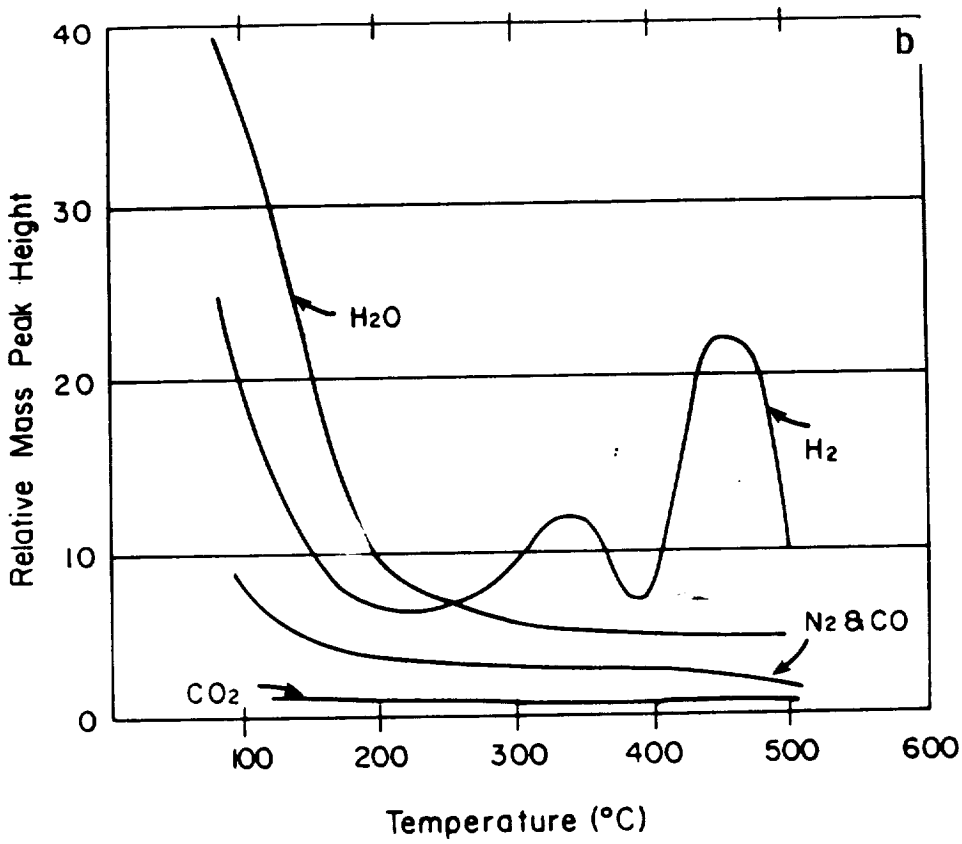

FIG. 10 - Continued

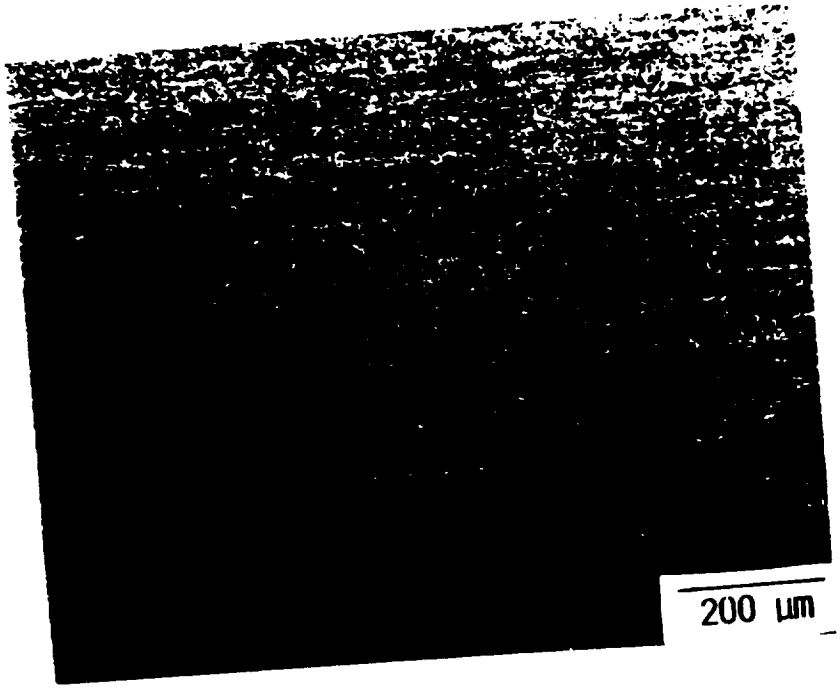

FIG. 11 - Optical micrograph of 11.5:1 extruded 7091 aluminum reinforced with 20 volume percent SiC whiskers.

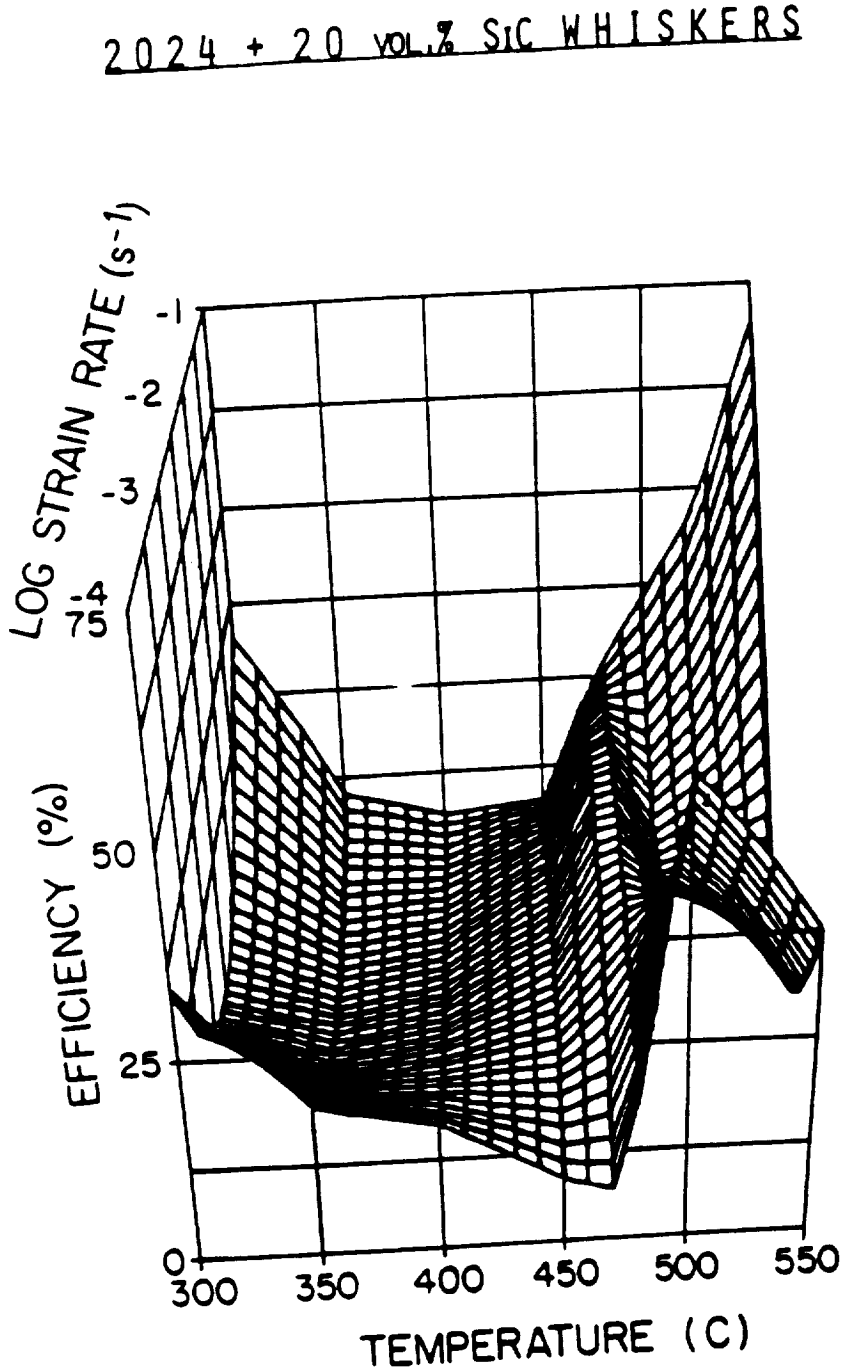

FIG 12 - Influence of temperature and strain rate on the deformation efficiency (30)

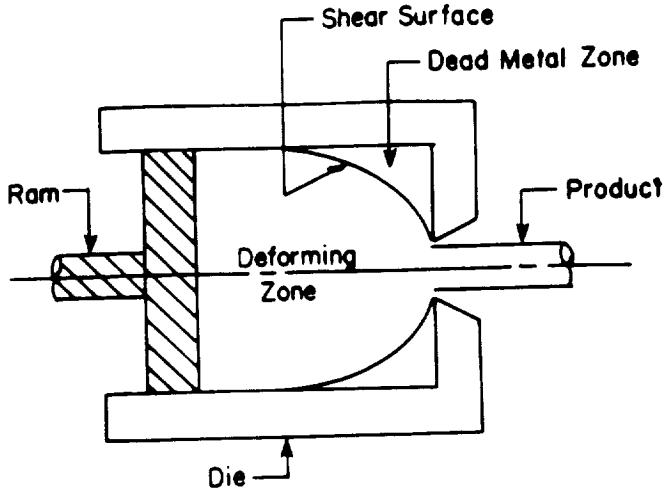

Shear Die

(a)

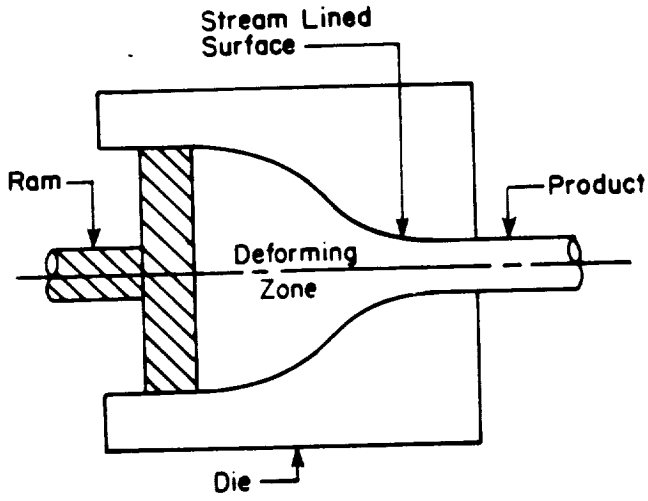

Stream Lined Die

(b)

FIG. 13 - Comparison of (a) shear and (b) streamline flow extrusion die configurations.

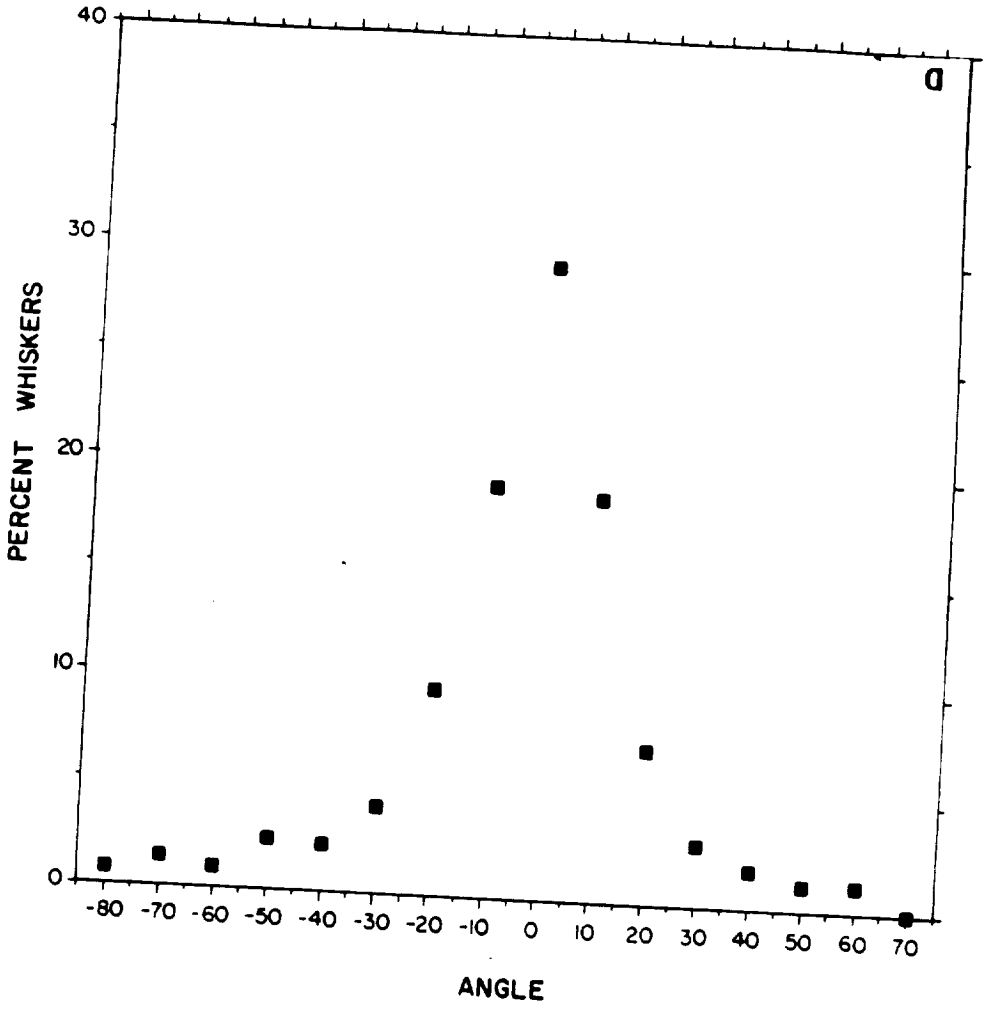

FIG. 14 - SiC whisker distribution in extruded 2124 - 20 volume percent SiC$_w$ aluminum: (a) surface orientation, (b) through thickness orientation. Extrusion ratio 11.5:1.

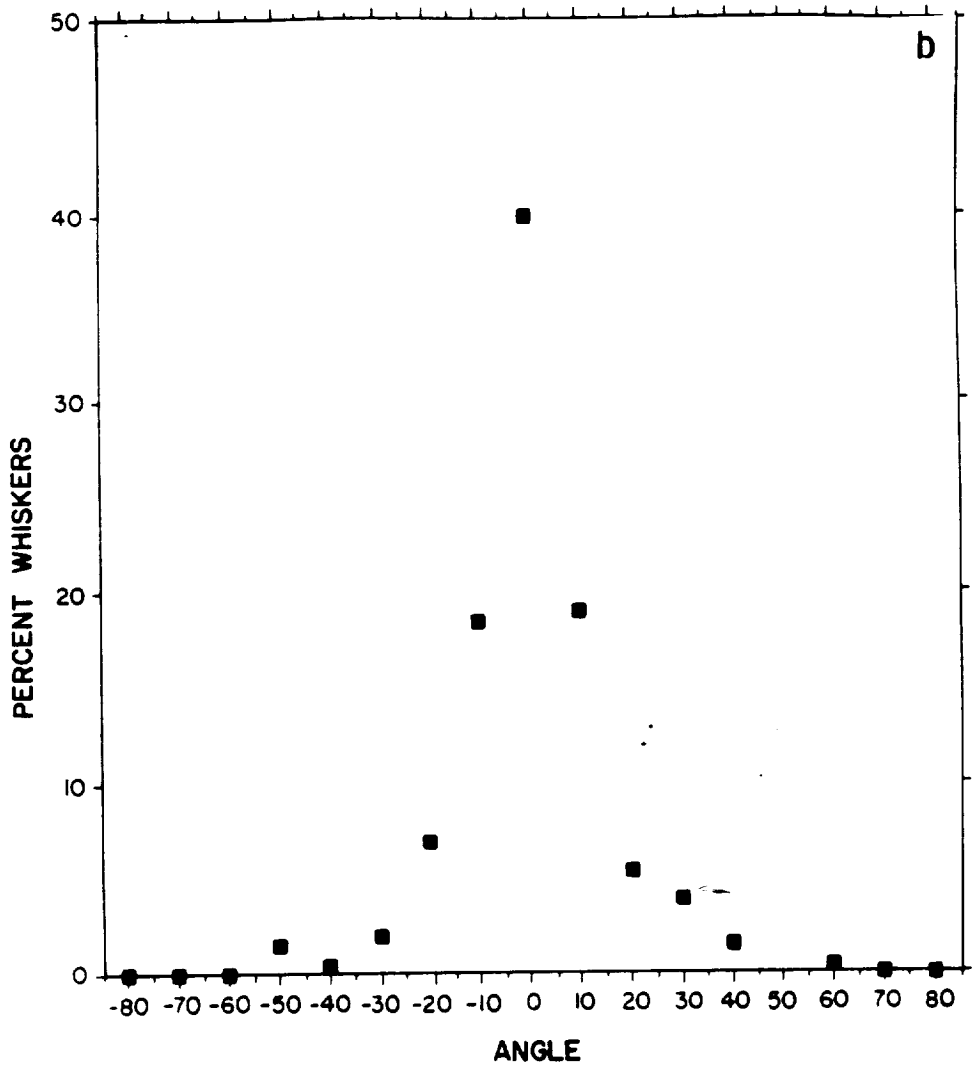

FIG. 14 - Continued

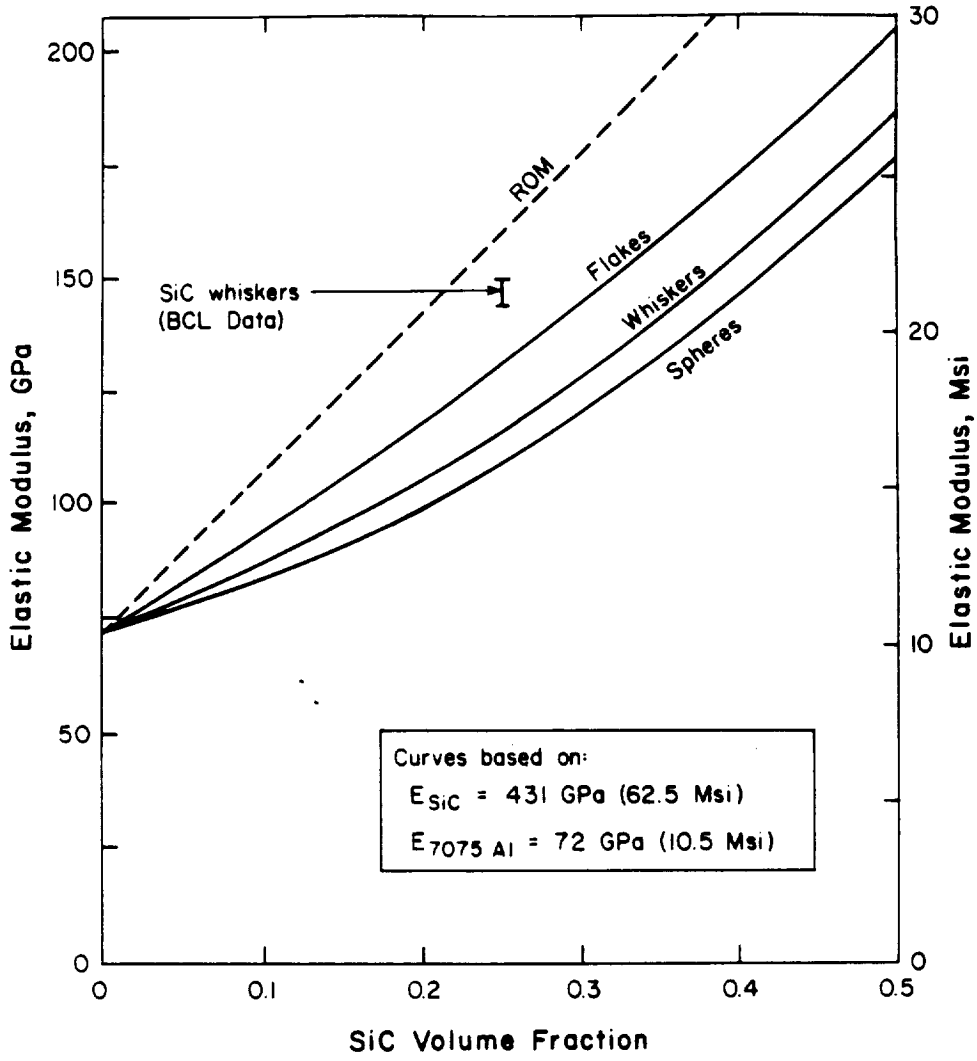

FIG. 15 - Elastic modulus of SiC reinforced aluminum alloys.

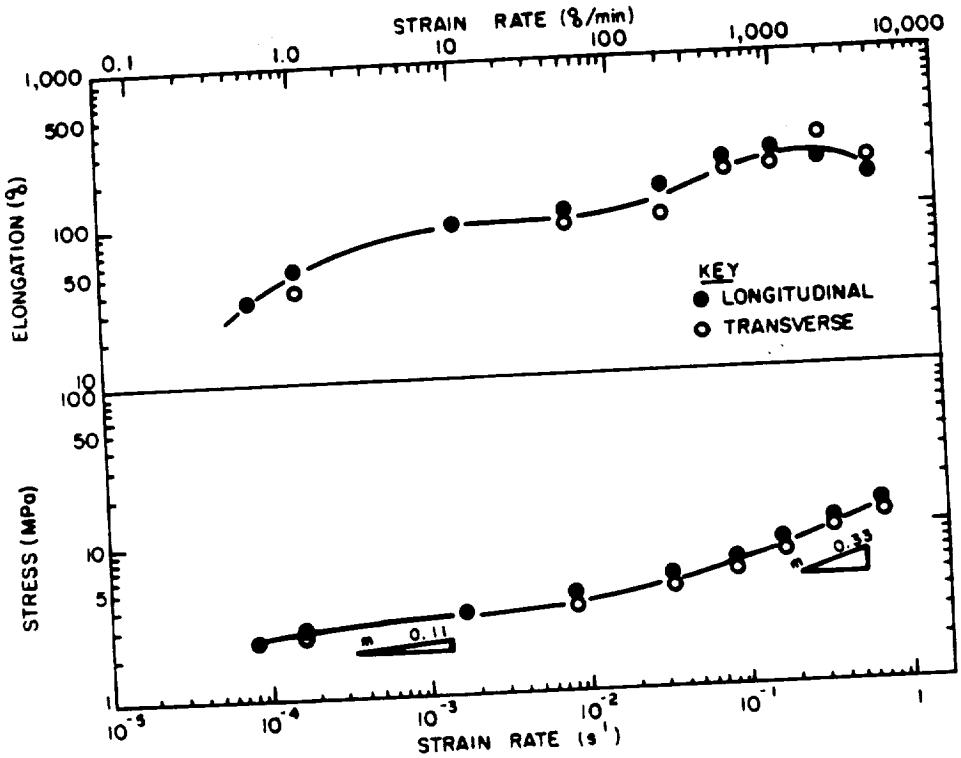

FIG. 16 - Elongation and flow stress as a function of strain rate for 2124 reinforced with 20 volume percent SiC whiskers(63)

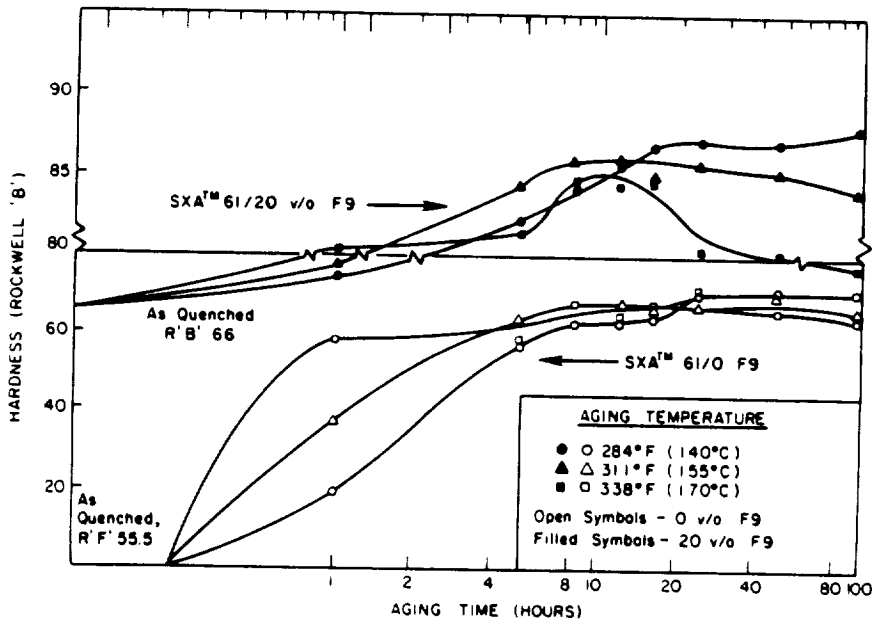

FIG. 17 - Artificial aging response of unreinforced and reinforced (20 volume percent SiC_p) 6061 aluminum solution treated for 1 hour at 538°C, water quenched and direct aged(18).

FIG. 18 - Transmission electron micrograph of unreinforced 6061, solution treated for 1 hour at 560°C, water quenched and aged 12 hours at 160°C(38).

FIG. 19 - Transmission electron micrograph of 6061 reinforced with 20 volume percent SiC_p, solution treated for 1 hour at 538°C, water quenched and aged 12 hours at 155°C.

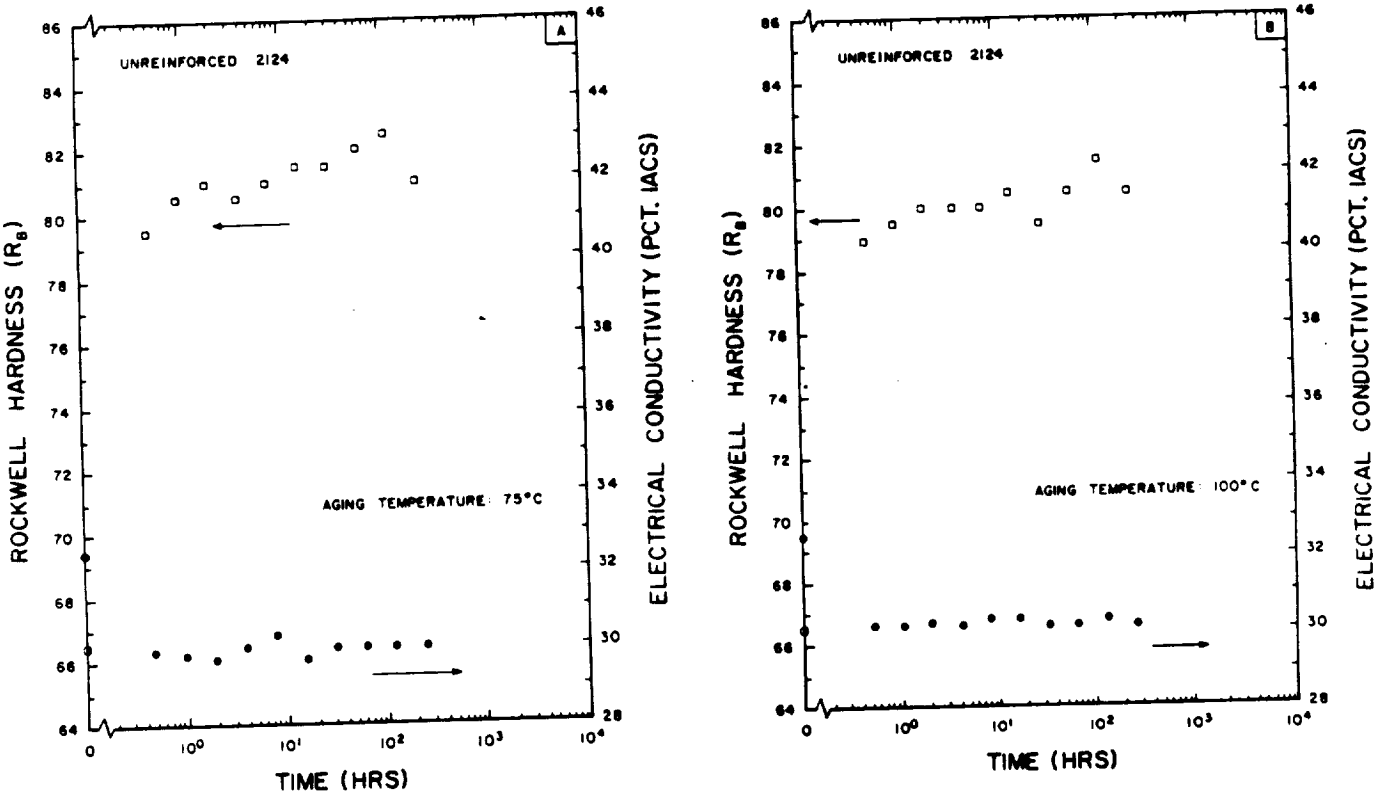

FIG. 20 - Artificial aging response for unreinforced 2124, solution treated 1 hour at 495°C, water quenched and direct aged.

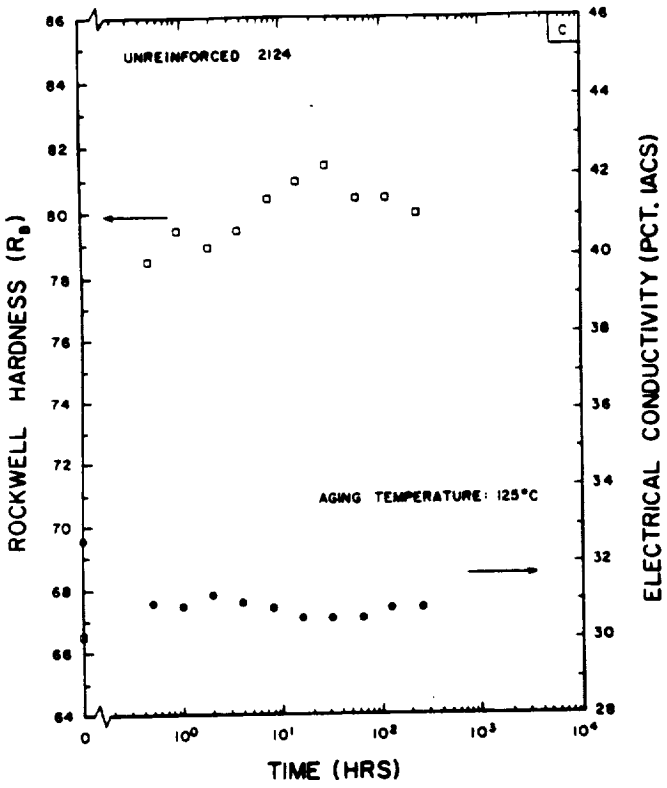

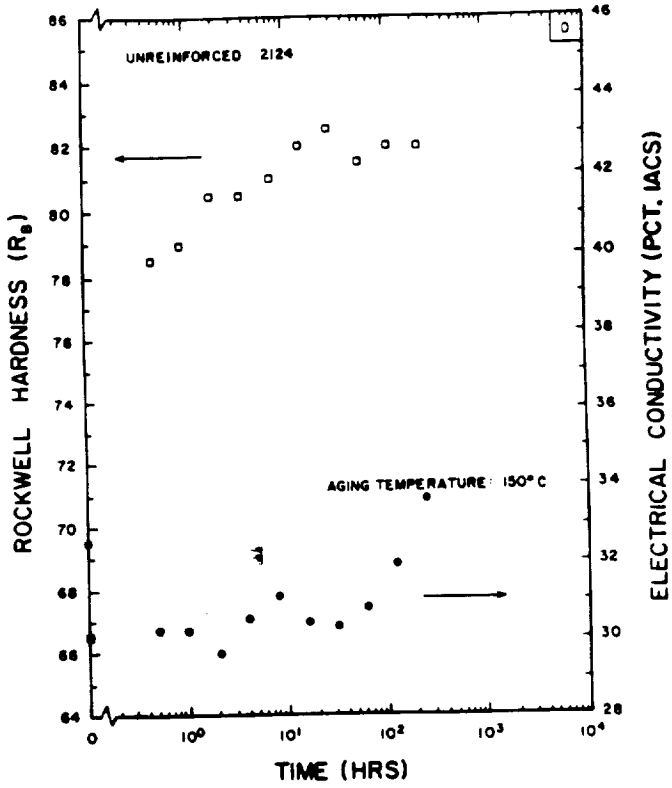

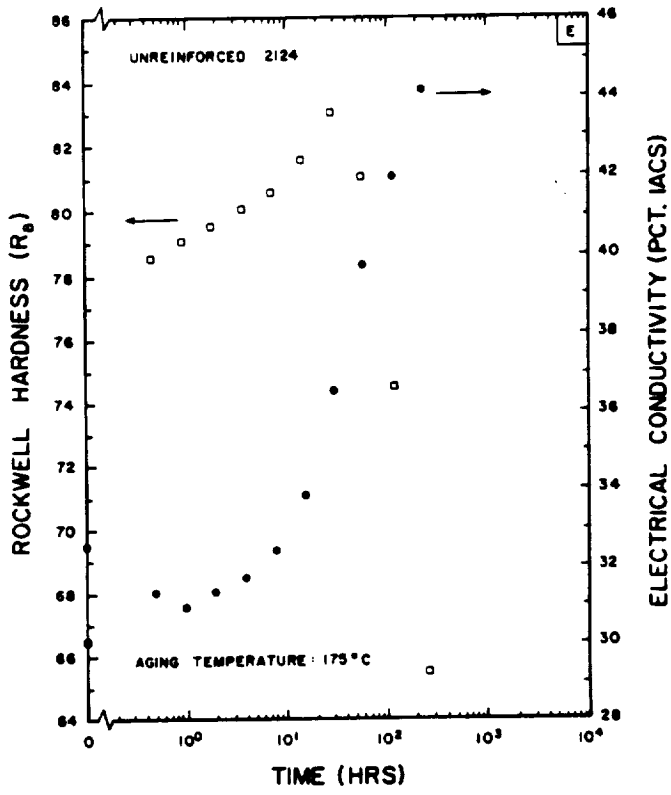

FIG. 20 - continued

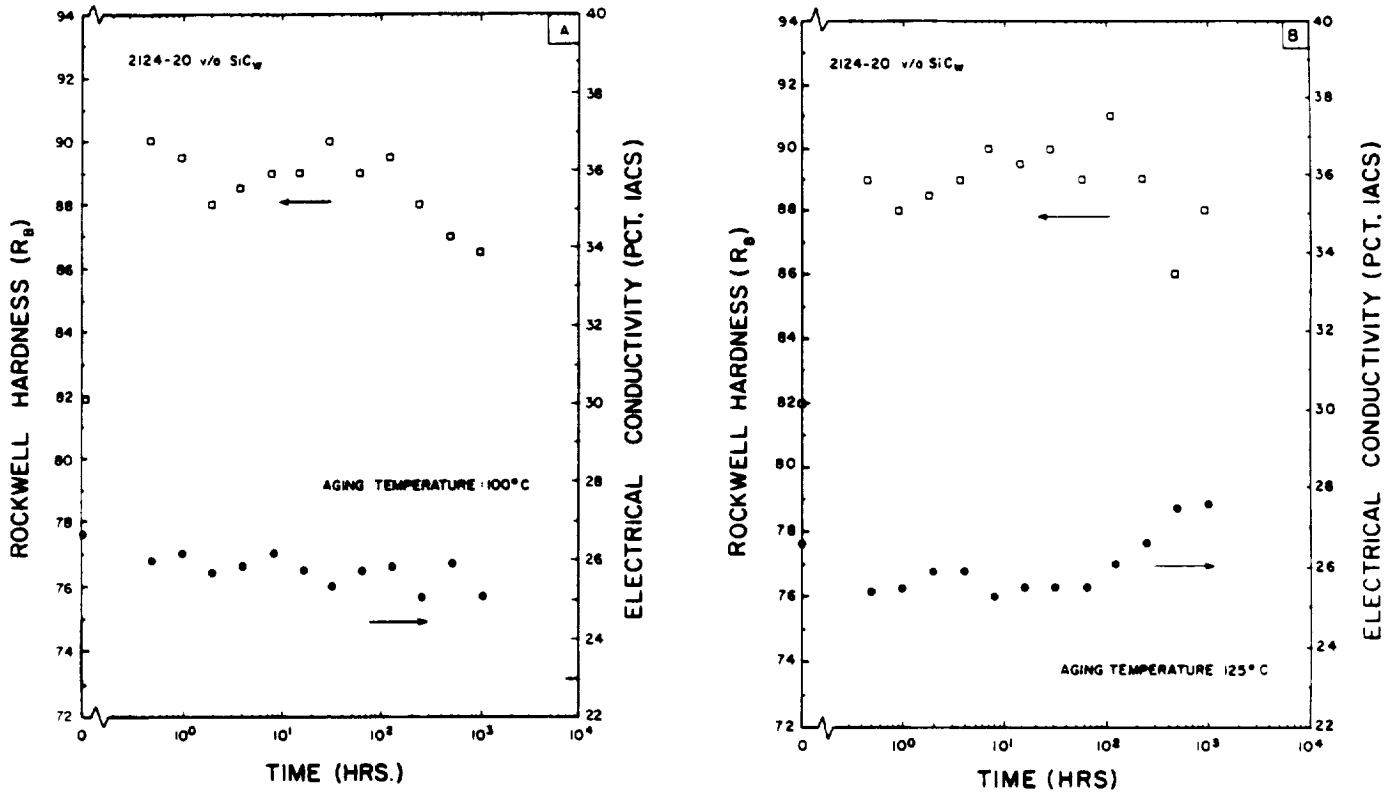

FIG. 21 - Artificial aging response for 2124 - 20 v/o SiC_w, solution treated 1 hour at 495°C, water quenched and direct aged.

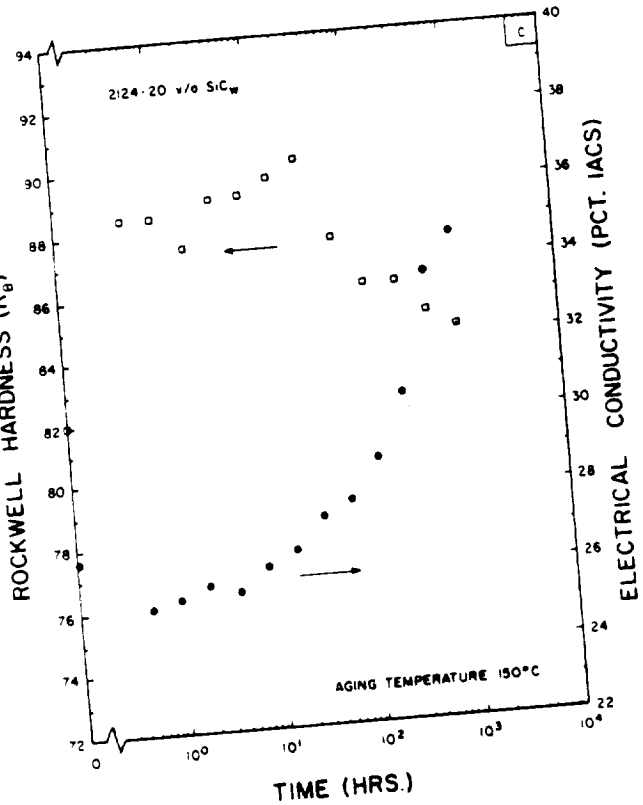

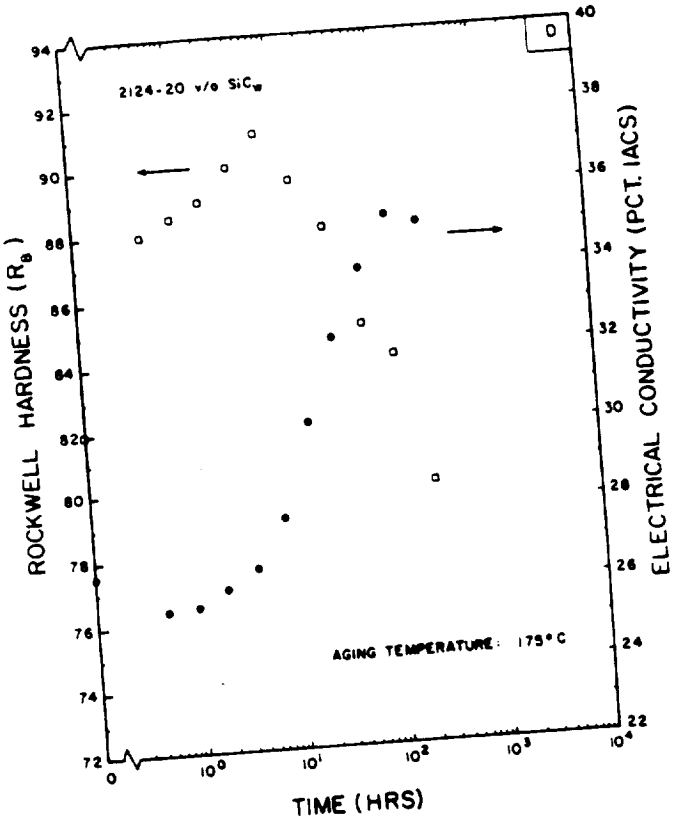

FIG. 21 - continued

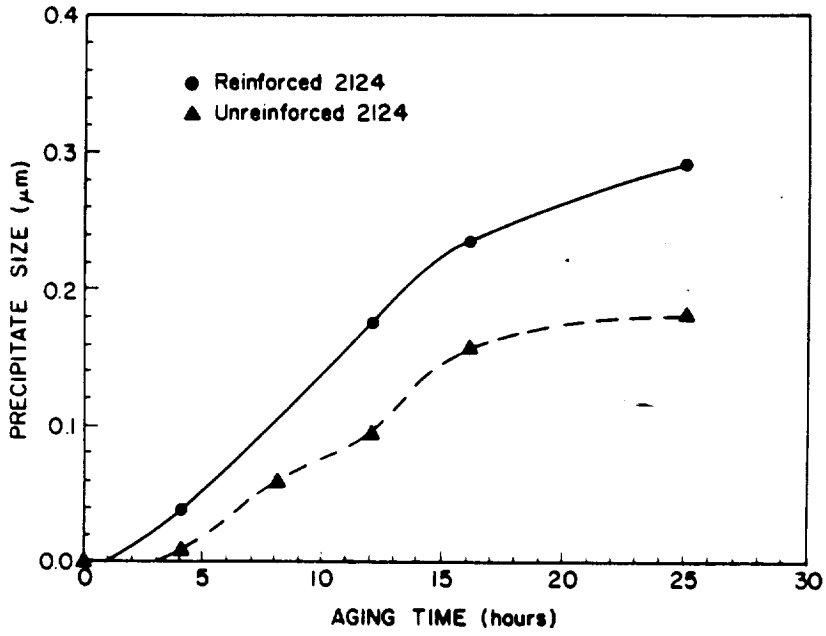

FIG. 22 - S' precipitate size versus aging time at 177°C for unreinforced and reinforced direct quenched and aged 2124(67).

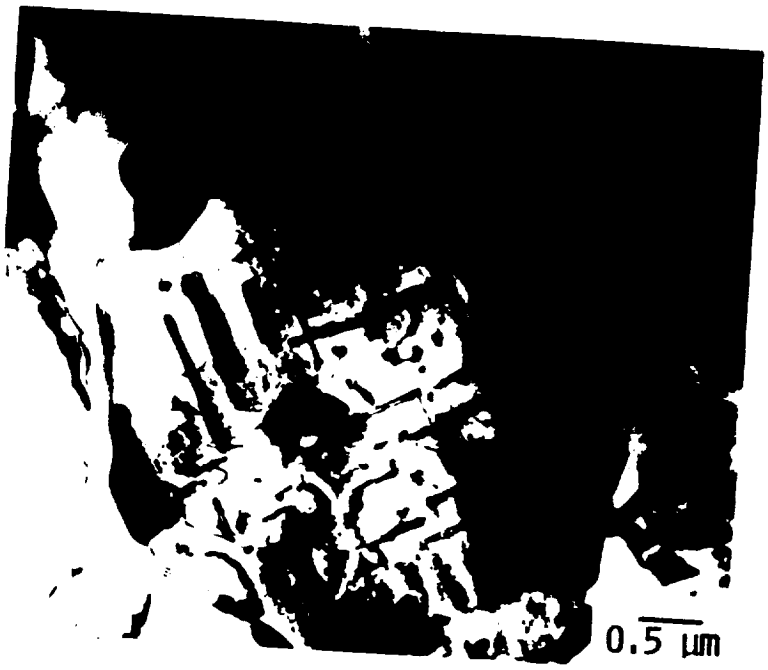

FIG. 23 - Transmission electron micrograph of unreinforced 2124, solution treated at 495°C for 1 hour, water quenched, naturally aged for 24 hours at 25°C and artificially aged for 100 hours at 100°C.

FIG. 24 - Transmission electron micrograph of 2124 reinforced with 20 volume percent SiC_w, solution treated 1 hour at 495°C, water quenched, stored for 2 hours at -196°C, naturally aged 24 hours at 25°C and aged for 64 hours at 175°C.

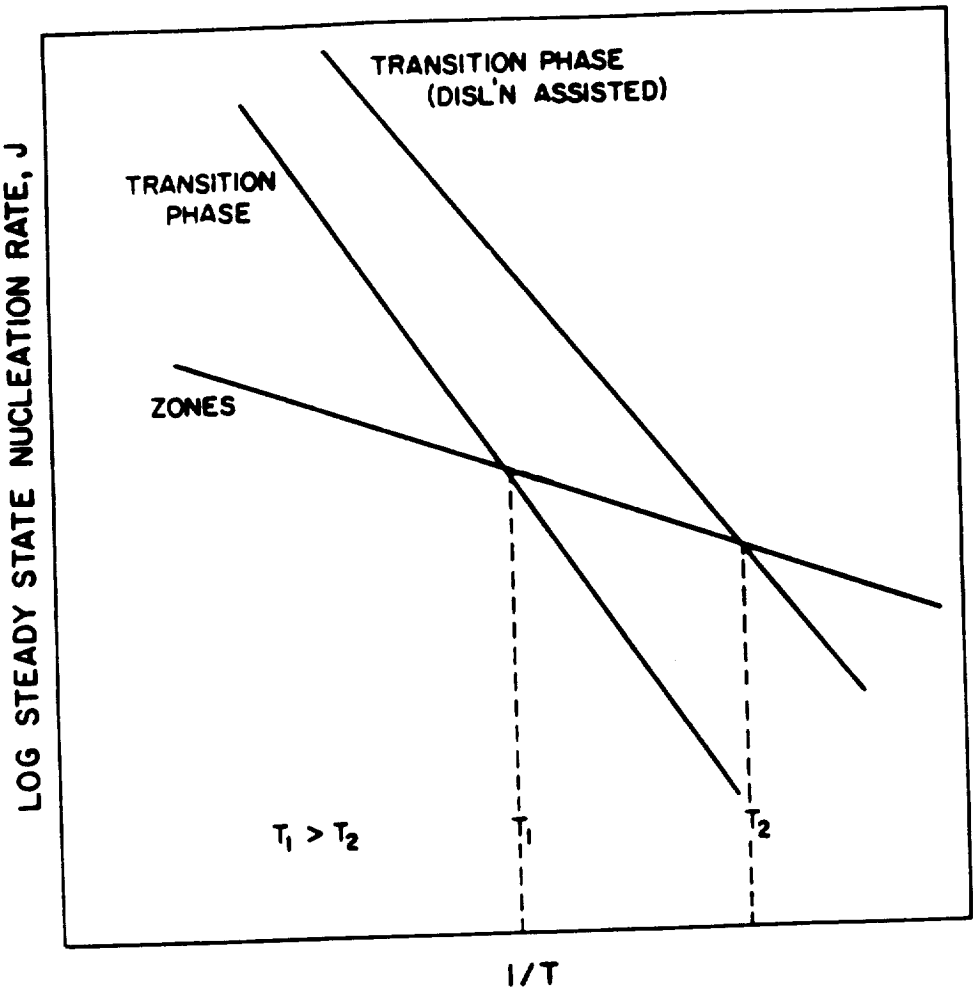

FIG. 25 - Schematic representation of the effect of dislocation substructure on the steady state nucleation rate.

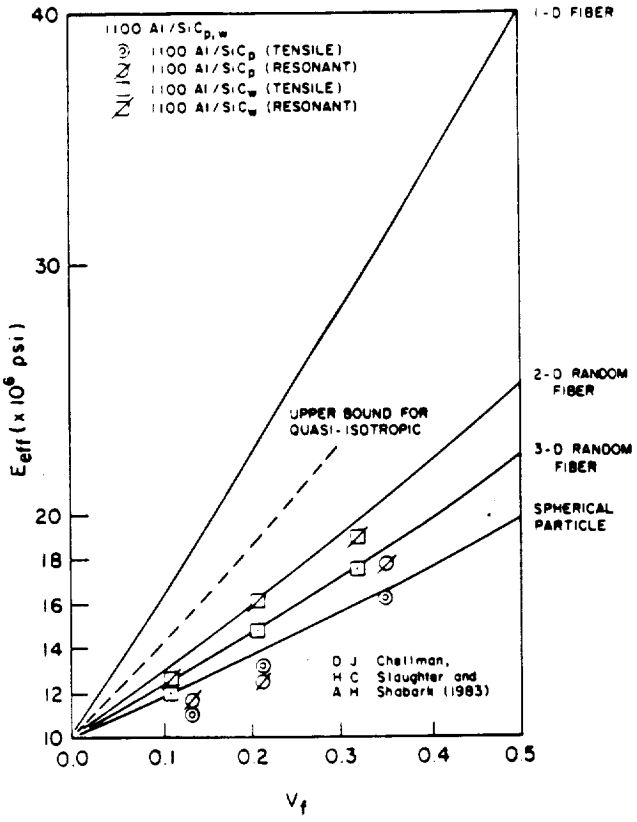

FIG. 26 - Influence of SiC content on the tensile properties of 1100 aluminum composites(80).

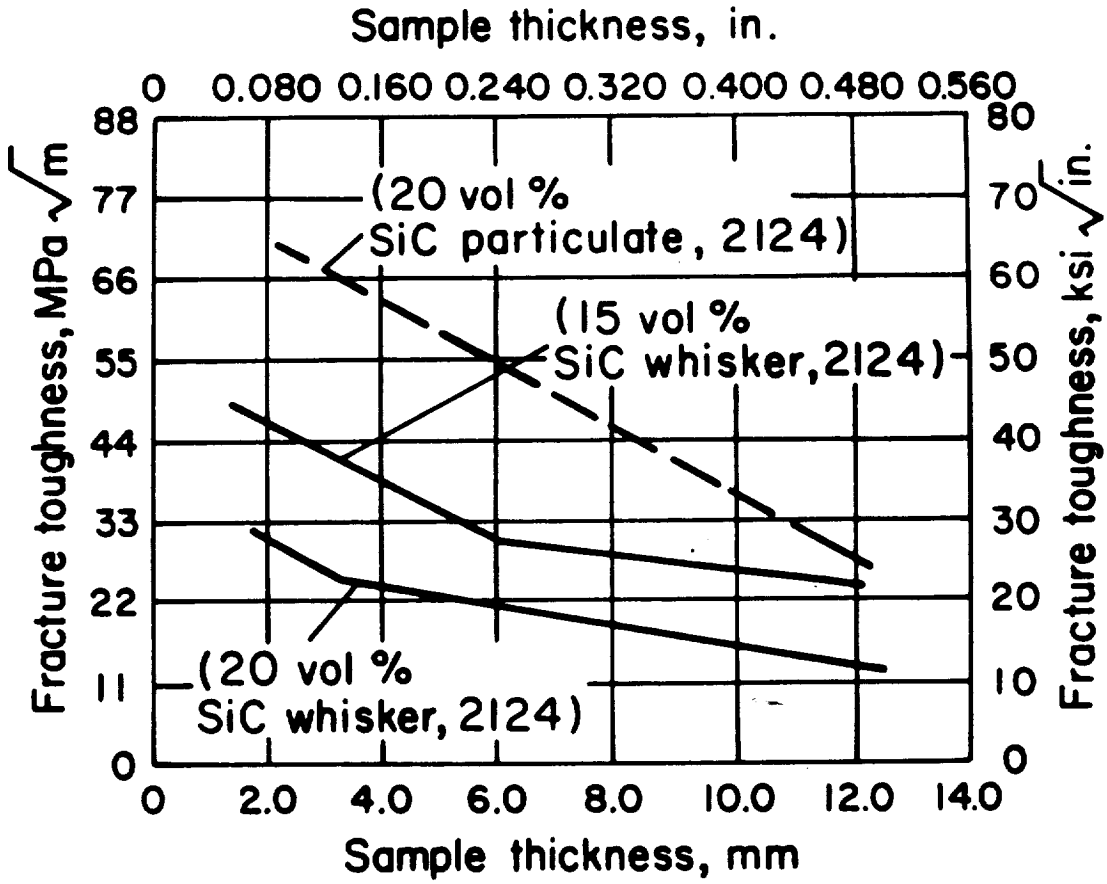

FIG. 27 - Fracture toughness of particulate and whisker reinforced 2124 aluminum metal matrix composites(33).

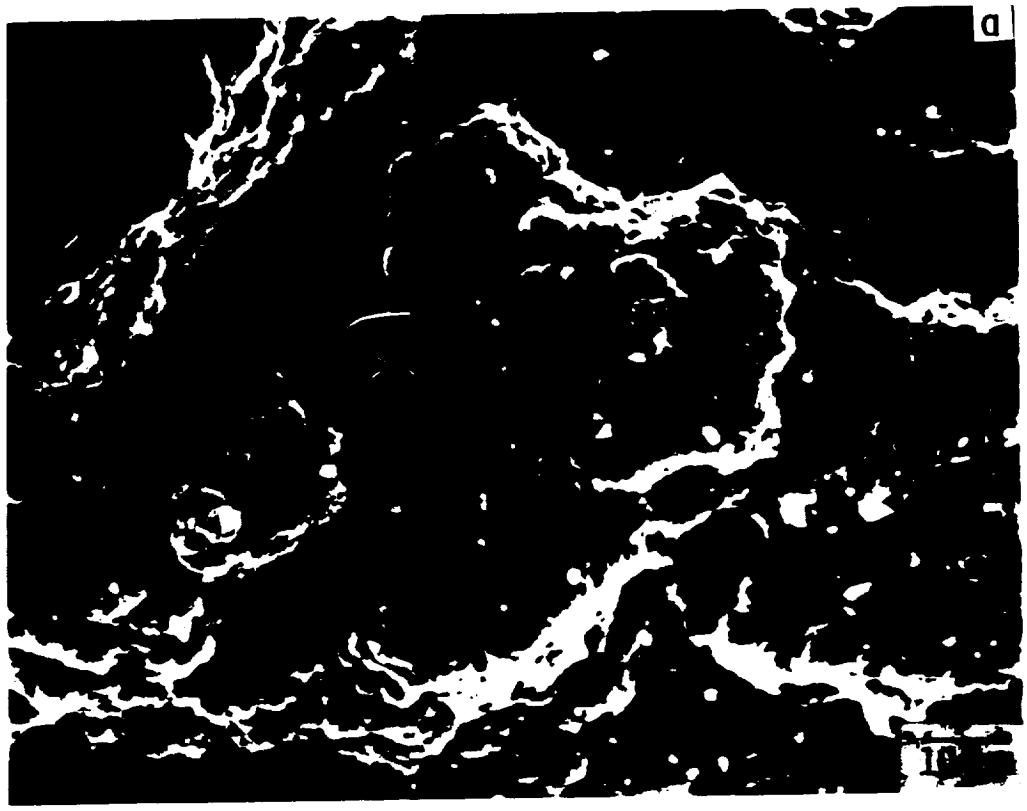

FIG. 28 - Scanning electron micrographs of tensile fracture initiation from (a) a large SiC particle and (b) Al,Cu rich constituent particles in 20 volume percent SiC whisker reinforced 7091 and 2124, respectively.

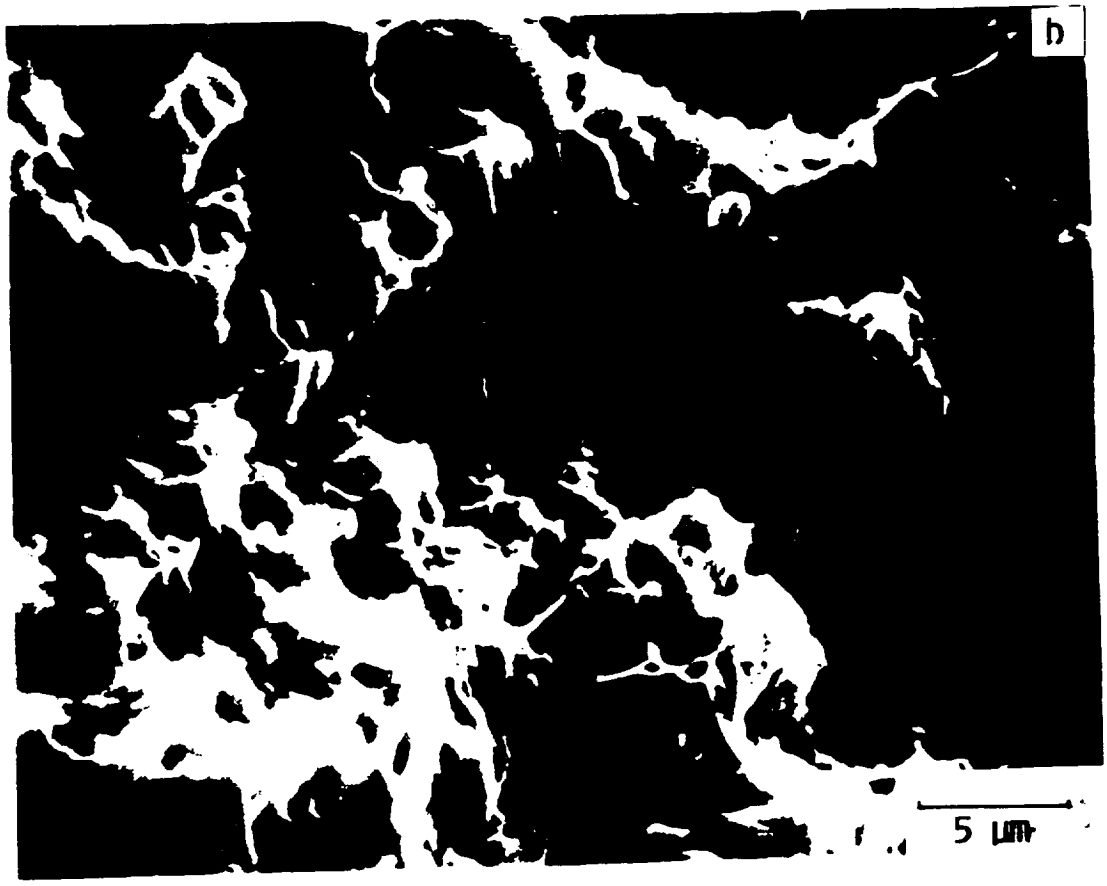

FIG. 28 - Continued

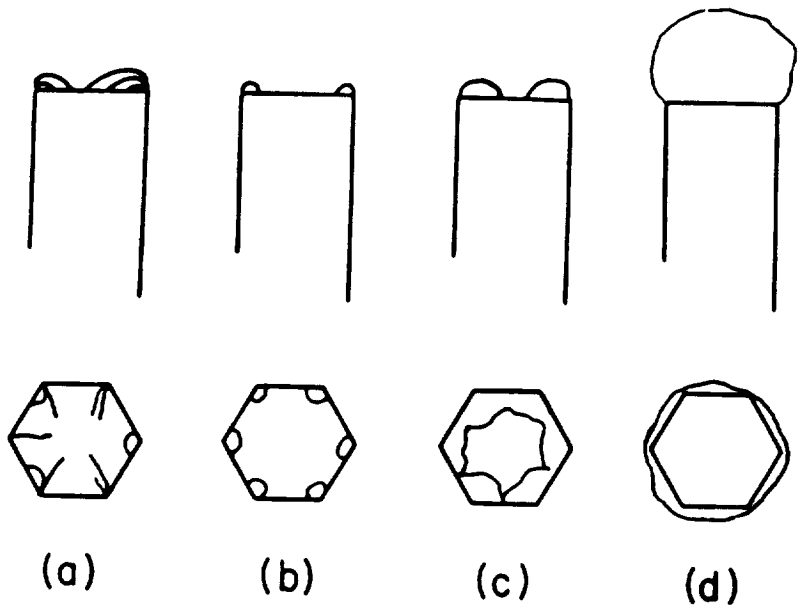

FIG. 29 -Schematic void inititation model for SiC whisker reinforced aluminum metal matrix composites(97).

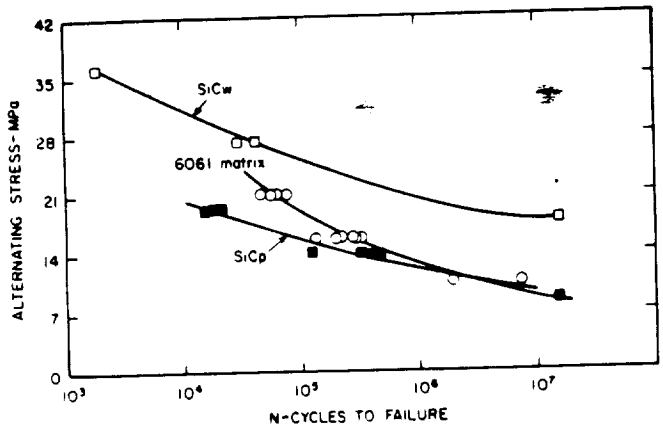

FIG. 30 S-N curves for SiC reinforced 6061 aluminum(102).

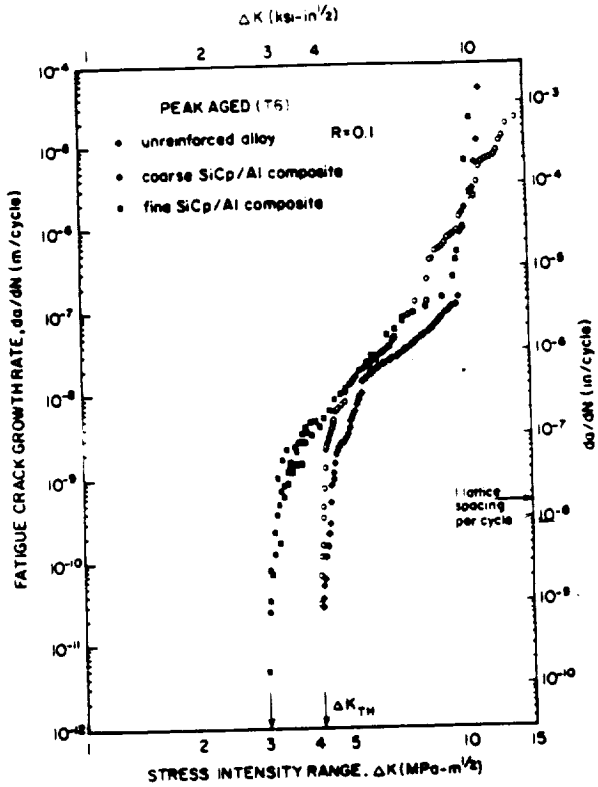

FIG. 31 - Variation in fatigue crack growth rates (da/dN) with nominal stress-intensity range (ΔK) at R = 0.1 for SiC particulate reinforced MB78 in peak aged condition(86).

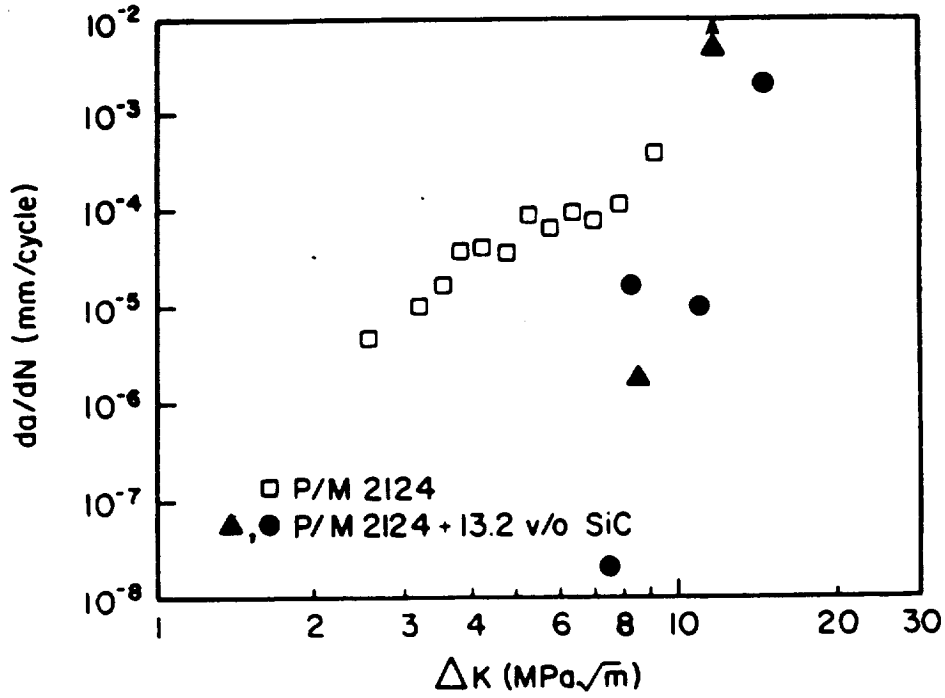

FIG. 32 - Variation in fatigue crack growth rates (da/dN) with nominal stress-intensity range (ΔK) at R = 0.1 for SiC whisker reinforced 2124 aluminum(95).

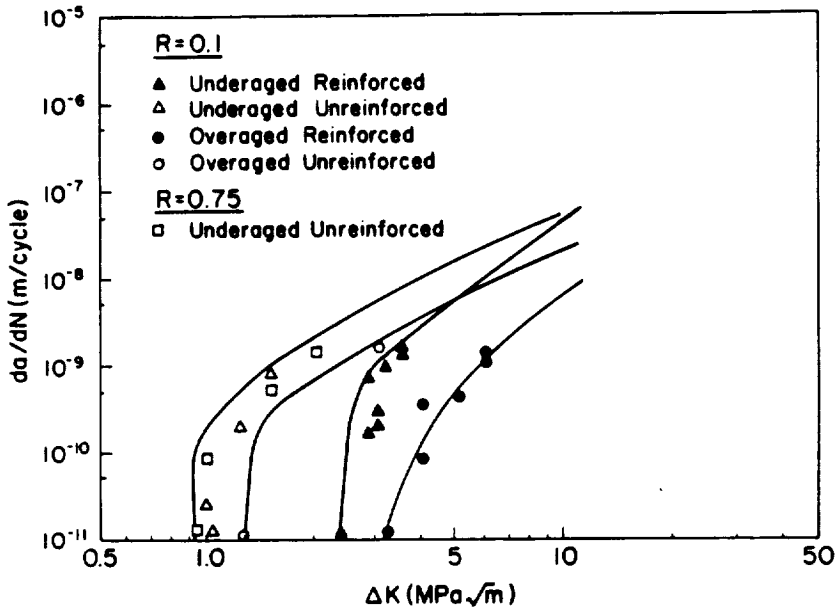

FIG. 33 - Near threshold fatigue crack growth rates for SiC whisker reinforced 2124 (94)

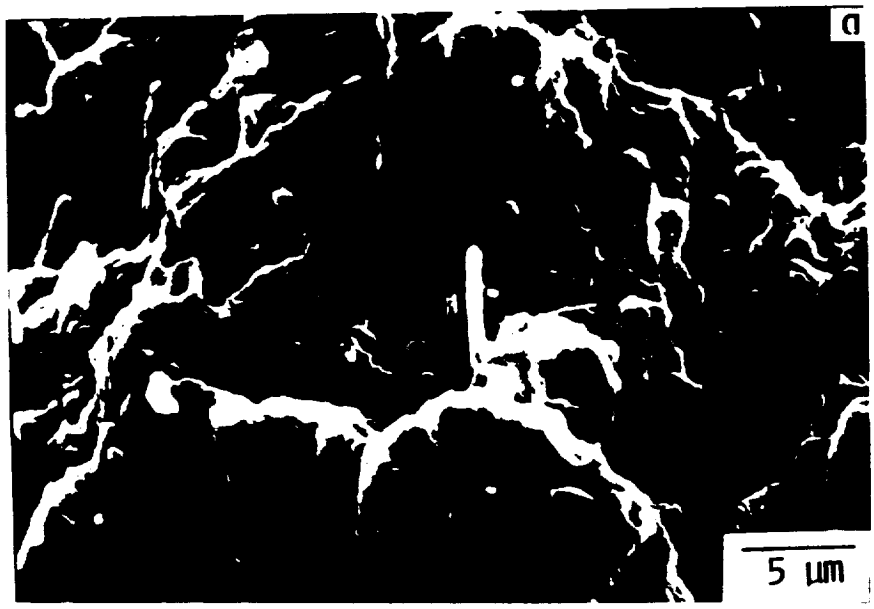

FIG. 34 - Scanning electron micrographs of fatigue pre-crack region in L-T oriented (a) 3 mm compact tension and (b) 12 mm thick center cracked 2124 - 20 v/o SiC$_p$ fracture toughness specimens removed from 11.5:1 12.5 in. thick extrusion.

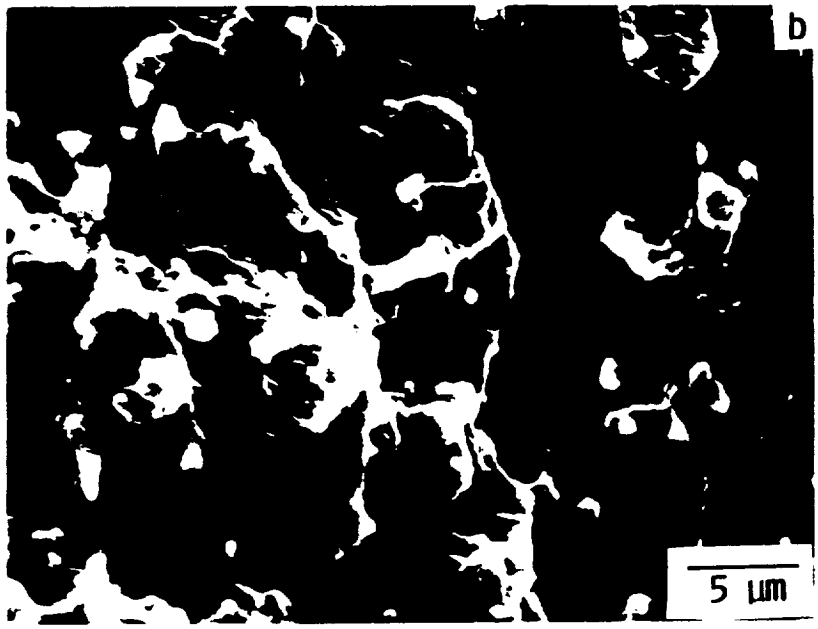

FIG. 34 - Continued

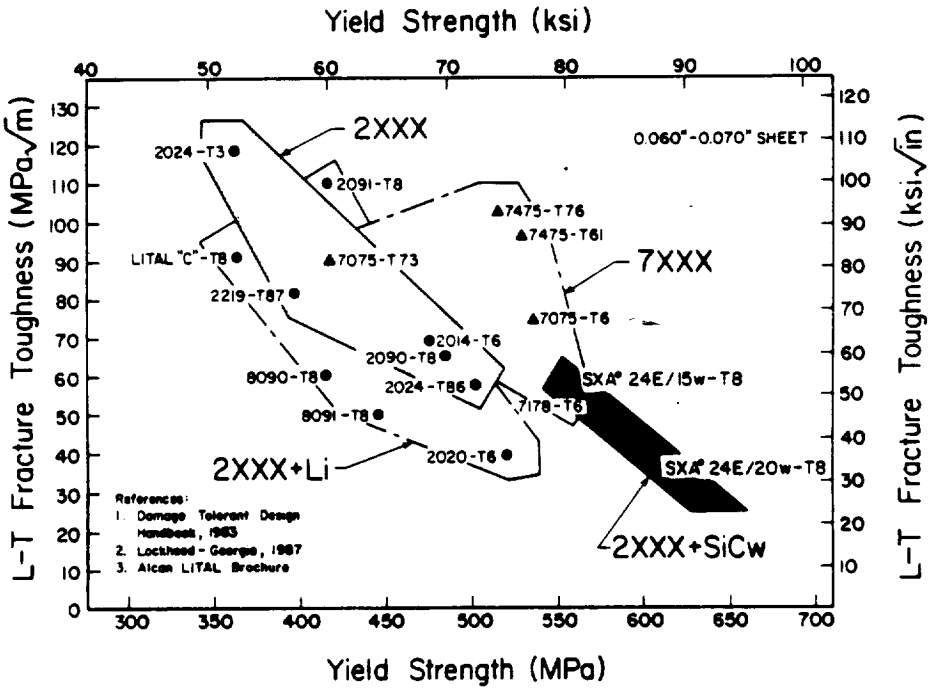

FIG. 35 - Fracture toughness comparison for unreinforced and SiC whisker reinforced aluminum sheet(104).

APPENDIX C

Fracture of Silicon Carbide Whisker Reinforced Aluminum

J. R. Albritton

and

J. G. Goree

To be Published

Proceedings of the Seventh International Conference
on Fracture, 1989(ICF 7)

Houston, Texas

March 20-24, 1989

FRACTURE OF SILICON CARBIDE WHISKER REINFORCED ALUMINUM[1]

James R. Albritton[2]
Graduate Student in Engineering Mechanics

James G. Goree
Professor of Mechanical Engineering and Engineering Mechanics

Mechanical Engineering Department
Clemson University
Clemson, South Carolina 29634-0921

ABSTRACT

This paper discusses the results of an investigation into the appropriateness of using standard fracture toughness testing procedures (developed for metals) for whisker reinforced metal matrix composites. Results of tests of ten and twenty volume percent silicon carbide whisker reinforced 2124 aluminum extruded plate are presented. Test coupons in the form of compact-tension, center-notched, and edge-notched specimens were used, with the loading direction either parallel or perpendicular to the extrusion direction. Testing was in the as-extruded condition.

None of the tests were found to give a valid fracture toughness (K_{IC}) according to the criteria of the ASTM Standard E-399. For an extrusion direction aligned with the loading, the compact-tension, plane-strain coupon, did not even produce self-similar fatigue pre-crack growth. The center-notched coupon gave the most consistent results and was indicated to be useful in comparing different materials or to quantify improvements made in a material by changes in processing. Linear elastic fracture mechanics did not correlate the fracture behavior for these materials and tests. Even when the fiber direction was held constant the measured fracture toughness values obtained from the different coupons differed by as much as a factor of two.

INTRODUCTION

In the development of discontinuously reinforced metal matrix composites (MMC), it has been found to be relatively easy to make significant improvements in the unnotched strength and the stiffness over that of the unreinforced matrix. Also, it is possible to determine well defined material property values for strength and stiffness. Unfortunately, it is considerably more difficult to decrease the notch sensitivity (or increase the fracture toughness). Indeed, in almost all cases the fracture toughness, or at least the ultimate load at which a notched coupon will fail, decreases.

---

[1]Supported by NASA-Langley Research Center under NASA Grant NSG-1-724, Grant Monitors W.S. Johnson and W.D. Brewer.

[2]This work was part of the first authors M.S. thesis. Mr. Albritton is now a research engineer with General Dynamics in Fort Worth, Texas.

There are, however, no standard procedures available for determining consistent fracture toughness properties. It is, in fact, not at all clear what is meant by "the fracture toughness" of MMC, although at the present time most of the toughness values reported in the literature are obtained using standard test methods developed for metals.

For most isotropic metals a plane-strain mode I (K_{IC}), fracture toughness obtained by following the test procedures outlined in ASTM E-399 [1] has essentially the same validity as other material properties such as the extensional modulus. The same degree of consistency does not appear to exist for some MMC systems, and while particular difficulties have been discussed in the literature, [2,3,4], to the authors' knowledge no comprehensive comparative study has been presented. The primary purpose of the investigation reported here was to provide a detailed record of the fracture behavior of the whisker reinforced material when tested using E-399 guidelines.

It is reasonable to expect the fracture toughness for the MMC to change with fiber orientation just as the strength and stiffness does. It is not as clear that test specimen geometry should make a significant difference. Some studies though, [2,3] for example, have indicated that this is the case and it has been suggested that a compact-tension test specimen is not as "good" as a center-notched coupon. While it is possible to use only center-notched coupons in the laboratory, edge cracks do form in structures. Questions that must be asked then are: do the standard linear elastic fracture mechanics (LEFM) test methods work for this material, even if we accept different behavior depending on fiber direction, and how do we obtain fracture data to use in design?

One of the fundamental precepts of LEFM is that the stress field in the very near vicinity of the crack tip controls the fracture behavior. In particular, the stresses have a square-root singular form and this singular term alone is sufficient to predict fracture. Under a pure opening (Mode I) stress field the three test specimens used in this study, compact-tension, center-notched and edge-notched, have an explicit relationship between the coefficients of this singular stress term (i.e. the stress intensity factor). For many metals one can accurately predict fracture for all of the specimens by testing only one geometry.

If the whisker reinforced composite is viewed as an orthotropic continuum, the stresses are also square-root singular [5], and again the coefficient of the singular term for an edge-notch is directly related to the corresponding coefficient in a center-notched panel. In fact, the mode I stress intensity factor is exactly the same as for the isotropic case. If LEFM is applicable for this orthotropic material, the test results should also be consistent with the analytical stress intensity factors.

Some early work by Reedy [6] using continuous fiber unidirectional boron/aluminum MMC laminates pointed out the inability of LEFM to predict the fracture toughness of the continuous system. Reedy found that drastically different values of fracture toughness could be obtained in those composites through variations in test specimen geometry. This paper extends Reedy's work to give a similar comparison of the crack growth and fracture behavior for a whisker reinforced material, using ASTM E-399 [1] procedures for the testing.

A parallel study is also underway, as part of the research in [7], to consider a more complete fracture criterion. It has been shown by Sih [8] that mixed mode fracture for isotropic materials can be predicted by a strain energy criterion. A related strain energy criterion is being investigated and will be compared with the present experimental results. In addition to this mechanics based research, a materials phase of [7] is being considered under the direction of Professor Rack at Clemson. The results of that effort will be reported elsewhere.

EXPERIMENTAL PROCEDURE

The material used in this study was 2124 aluminum reinforced with 10 and 20 volume percent F-9 SiC whiskers. The fabrication was a powder metallurgy process as described in [9]. The material was produced in billets and then extruded into 127 mm wide by 12.7 mm thick plates. The extrusion ratio was 11.5:1, resulting in a very uniform alignment of the SiC whiskers in the extrusion direction, both with respect to width and thickness. A detailed description of the fiber distribution will be given in the final report of [7]. The material was tested in the as-extruded (F) temper.

For metals, the compact-tension specimen is an accepted design used to determine the mode I, plane strain, fracture toughness, K_{IC}. Very specific guidelines and test procedures are given in [1]. The center-notched and edge-notched coupons are not covered in [1], but the same procedures were used for those specimens. That is, the criteria for obtaining "valid" fracture toughness results were applied to all three specimens.

Figure 1 shows the test coupon geometries with the compact-tension (CT) specimen designed according to ASTM-E-399. The CT coupons were tested with thicknesses of 12.7 mm (plane-strain) and 2.54 mm (plane-stress). The thin specimens were obtained by machining both sides of the 12.7 mm stock. As indicated above, work by Rack and Prabodh [7] found the fiber distribution to be very uniform through the thickness for this material. The 2.54 mm coupons were then essentially the same material as the plane-strain coupon. The center-notched (CCT) and edge-notched (SENT) coupons were only tested in 12.7 mm thickness. All specimens had straight-through starter notches.

The fatigue loading during pre-cracking was done at between 20 and 40 cycles per second, starting with a maximum load equal to 50 percent of the estimated fracture load. The loads were gradually increased, maintaining a load ratio of minimum to maximum value of 0.1, until crack initiation was detected. Crack growth was monitored with a traveling microscope and a COD gage. A strobe light was used to assist in following the fatigue pre-cracks as they were extremely tight, especially at short lengths. In general, all specimens were much more difficult to pre-crack than an all-aluminum coupon. The difference between the maximum load (or K) required to initiate a fatigue crack and the load giving unstable growth (fracture) was very small. That is, the da/dn vs ΔK curve was steep. All tests were run under load control and a load reduction procedure was used during fatigue pre-cracking. Most of the testing was done using an MTS-880 servo-hydraulic machine; however, some of the 20 volume percent CCT coupons were tested in an Instron 800 machine.

The detailed procedures of E-399 were followed in all tests and those requirements on the size of the specimen and manner of testing were all met. In order for the tests to give a valid fracture toughness measure, specific requirements were imposed on the results. The most fundamental of these are listed below, and will be compared to the test results.

1) Self-similar crack growth (8.2.4 of E-399).

2) The crack front at the end of the fatigue pre-crack stage should be relatively flat. The difference between surface crack length and the average crack length should be no more than 15% of the average, with $0.45W<a<0.55W$. (8.2.2 of E-399).

3) The maximum value of the mode I stress intensity factor, K, during the terminal fatigue crack growth stage must be less than 60% of K at fracture. (A.2.4 of E-399).

4) From the test record of the load vs COD results, the 95% tangent line (i.e. having 95% the slope of the tangent to the initial linear part of the curve) must intersect the curve at a point P_Q such that $P_{max}/P_Q \leq 1.10$. (9.1.1 and 9.1.2 of E-399).

The equations used to calculate K, the mode I stress intensity factor, for the three different specimen geometries, are given in the following references. For the compact-tension specimen the equations in section A4.5 of E-399, [1] were used. The equation for the center-notched coupon (CCT) with clamped ends and a free length-to-width ratio of 1.5 was taken from reference [10], and is accurate for $2a/W \leq 0.6$. The appropriate equation for the single edge-notched coupon (SENT) is given in reference [11], and is accurate for $a/W<0.6$. These equations are for isotropic materials but, as discussed above, the mode I stress intensity factors are the same in an orthotropic material. In all cases the stress intensity factor K is of the form $K=PF(a,W)$. Values of K corresponding to P_Q and P_{max} were then obtained from the appropriate equations and are designated K_Q and K_M respectively. For a metal, if all the criteria are met, the conditional value K_Q is then denoted by K_{IC} and is called the plane-strain factor toughness for the material.

RESULTS

The test program with resulting values of K_Q and K_M is given in Table 1, where the L-T designation indicates that the loading was in the extrusion direction and the machined notch in the transverse direction. The T-L designation corresponds to loading perpendicular to the extrusion direction with the initial notch being parallel to the extrusion direction. The coupons designated CT (CCT) were special compact-tension coupons that were cut from pre-cracked center-notched coupons. Material property values are given in Table 2.

All specimens tested had self-similar fatigue pre-crack growth except the plane strain, compact-tension coupons with L-T orientation, (i.e. tests 1,3,9, and 10). In these four coupons the fatigue crack initiated at the end of the notch and grew at an angle with respect to the transverse direction.

In none of these four cases was there any transverse growth. Note that specimens 1 and 3 had machined notches while in 9 and 10 the machined notch had been extended as a sharp self-similar crack by first fatiguing a center-notched coupon and cutting the CT specimen from it. The sharpness of the notch had no measureable influence, and the cracks initiated at a 45° angle in the 10% material and at a 70° angle in the 20% material. Several 20% CT(L-T) coupons with chevron starter notches were also tested and the fatigue crack still turned. It was much more difficult to observe the crack so the remaining tests had straight-through starter notches. A photograph of a failed 20% CT(L-T) coupon is shown in Figure 2. Having these results, it was very interesting that when the thickness of the CT coupon was reduced (by machining) to 2.54 mm the crack did not turn. Also note that the SENT coupon gave self-similar crack growth. The SENT coupon is similar to a CT coupon except that the location of the pin loaded holes gives different contributions of stress due to bending and axial loading. For the geometry of Figure 1, the bending moment about the center-line of the net-section ligament is Pa/2 for the SENT coupon and P(25.4 + a)/2 for the CT geometry. The CCT specimen has no net bending moment.

TABLE 1. Testing Program and Results

All specimens were 2124 aluminum reinforced with either 10 or 20 volume percent SiC whiskers, and were tested in the as-extruded, F-temper. The results are the average of 2 or 3 replicate tests in most cases.

No.	Geometry	Thickness	Orientation	%Fiber	K_Q[1]	K_M[1]
1	CT	12.7 mm	L-T	10	13.7[2]	19.6[2]
2	CT	12.7 mm	T-L	10	12.7	17.9
3	CT	12.7 mm	L-T	20	17.1[2]	18.2[2]
4	CT	12.7 mm	T-L	20	15.8	17.7
5	CT	2.54 mm	L-T	10	12.5	22.9
6	CT	2.54 mm	T-L	10	12.7	17.9
7	CT	2.54 mm	L-T	20	15.9	22.2
8	CT	2.54 mm	T-L	20	14.7	20.5
9	CT(CCT)	12.7 mm	L-T	10	15.3[2]	21.2[2]
10	CT(CCT)	12.7 mm	L-T	20	17.0[2]	17.0[2]
11	CCT	12.7 mm	L-T	10	17.9	20.9
12	CCT	12.7 mm	T-L	10	20.3	20.3
13	CCT	12.7 mm	L-T	20	17.3	18.2
14	CCT	12.7 mm	T-L	20	13.0	16.2
15	SENT	12.7 mm	L-T	10	20.0	26.3

[1] the units of K_Q and K_M are MPa $\sqrt{m}$
[2] in these specimens the fatigue crack turned, K was computed using the horizontal projection of the crack length

TABLE 2. Material Properties

% fiber	E_1 (GPa)	E_2 (GPa)	σ_{ys} (MPa)	K_{IC} (MPa $\sqrt{m}$)
0%	73	73	300	≈40
10%	95	73	≈350	?, see Table 1
20%	128	101	≈390	?, see Table 1

None of the compact-tension specimens met the second condition. The crack front was very uniformly rounded, (nearly a circular arc) with the surface crack length differing from the average length by about 20%. The CCT and SENT coupons were fatigued to give a longer crack length in order to be able to fracture the specimens and the percent difference was about 10%, but the crack front was essentially the same shape as the CT coupons.

The third criteria was marginal (i.e. on the order of 65%) in most cases, when the requirement was based on the maximum value of K, i.e. K_M in Table 1. In those cases of considerable non-linearity in the load-COD record the value of K maximum during the final fatigue cycle was frequently as large as K_Q.

The fourth critera imposes a limitation on the degree of non-linearity in the load-COD results. Only tests 3,10,12 and 13 satisfied this condition of $K_M/K_Q \leq 1.1$, and in tests 3 and 10 the fatigue crack was not self-similar. A typical load-COD curve is given in Figure 3.

The difference in behavior (crack branching) observed between the thick and thin compact-tension coupons and between the thick compact-tension and edge-notched specimens is the most significant difficulty in attempting to use these tests to develop fracture data. The observed response is apparently due to the influence of the different stress states: plane strain vs. plane stress and the stress gradient due to the different bending components. A series of tests using a standard edge-notched coupon with different pinhole locations are now underway to investigate this behavior.

The variation in the averaged values given in Table 1 (with fiber orientation and specimen geometry) covers a range of K_Q or K_M of over 20%. These were the average of several tests for each particular specimen configuration. The variation within a given series was also on the order of 25%, giving a large scatter in the full set of data. For example, for a 10% T-L material the minimum value of K_Q recorded was 11.8 Mpa$\sqrt{m}$ for a CT specimen, and a maximum value of 21.6 Mpa$\sqrt{m}$ was obtained from a CCT coupon. This was typical of all the tests, with the CT coupon giving the lowest value of toughness, the CCT next, and the SENT the highest. As indicated however, it appears that the SENT results depend on the pin location.

CONCLUSIONS

Following the E-399 guidelines, it must be concluded that none of the tests gave a valid K_{IC}.

There is no real reason to feel that the above criteria must be applied to the composite. If the results were such that a consistent value of K (either K_Q or K_M) emerged, then there would be some justification for using it as a material property in design. Unfortunately, the results do not show such consistency.

It seems that the best one can say for these testing methods is that the center-notched coupon is the most consistent and is the most suitable specimen to use to compare different materials or to quantify improvements made in a material by changes in processing. These tests do not indicate that an increased K value using a CCT test will necessarily correspond to the same improvement in a different specimen geometry.

The singular crack-tip stress field (stress intensity factor) and the standard application of LEFM does not represent the fracture behavior of these materials. No single value of toughness was found, even when the fiber orientation was fixed.

REFERENCES

1. Annual Book of ASTM Standards, 1983, Section E-399.

2. Hayes, S. V. and Knight, R. C., "Metal Matrix Composite Structural Demonstration for Missiles," LTV Aerospace and Defense Company, AFWAL-TR-86-3097, 1987, sec. 3, pp. 29-35.

3. Crowe, R. C. and Gray, R. A., "The Effect of Notch Root Radius on Crack Initiation in SiC_d/Al," Proceedings of the 39th Meeting of the Mechanical Failures Prevention Group, N.B.S., Editors, Early, Shires, and Smith, Cambridge University Press, 1984, pp. 157-166.

4. Hasson, D.F., Hoover, S.M., and Crowe, C.R., "Effect of Thermal Treatment on the Mechanical and Toughness Properties of Extruded SiC_w/aluminum 6061 Metal Matrix Composite," Journal of Material Science, Vol. 20, 1985, pp. 4147-4154.

5. Paris, P.C. and Sih, G.C., "Stress Analysis of Cracks, Fracture Toughness Testing and its Applications," ASTM, STP No. 381, 1965, pp. 30-85.

6. Reedy, E. D., "On the Specimen Dependence of Unidirectional Boron/Aluminum Fracture Toughness," Journal of Composite Materials Supplement, Vol. 14, 1980, pp. 118-131.

7. Rack, H. J. and Goree, J. G., "Fracture Criteria for Discontinuous Metal Matrix Composites," NASA Grant NSG-1-724, November 18, 1986 to February 16, 1989.

8. Sih, G.C., "A Special Theory of Crack Propagation," Methods of Analysis and Solutions of Crack Problems, Edited by Sih, G. C., Vol. 1 of Mechanics of Fracture, Noordhoff, 1973.

9. Rack, H. J., "Light-weight, High-Performance Metal Matrix Composites," Powder Metallurgy Composites, Editors, Kumar, Vedula, and Ritter, AIME, Warrendale, PA. In press.

10. Isida, M., "Effect of Width and Length on Stress-Intensity Factors of Internally Cracked Plates Under Various Boundary Conditions," International Journal of Fracture Mechanics, Vol. 7, No. 3, 1971, pp. 301-316.

11. Brown, W. F., Jr. and Srawley, J. E., "Plane Strain Crack Toughness Testing of High Strength Metallic Materials," ASTM, STP No. 410, 1966.

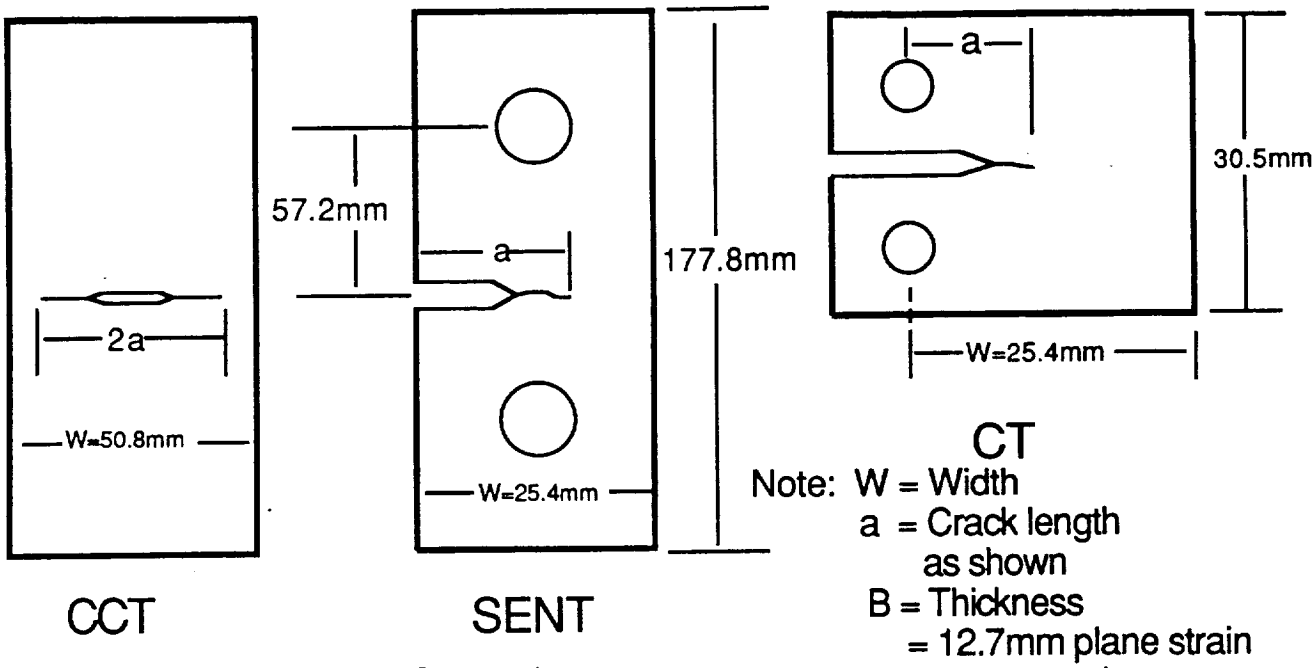

Figure 1. Specimen Geometries

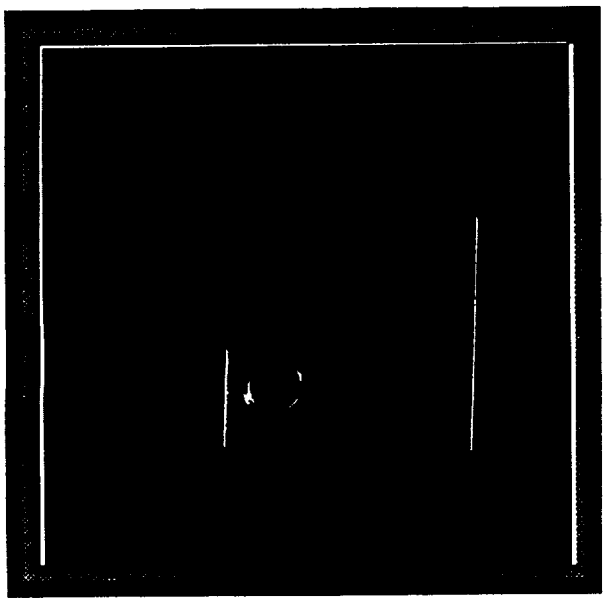

Figure 2. Crack Deflection in a 20% L-T, Plane Strain Specimen

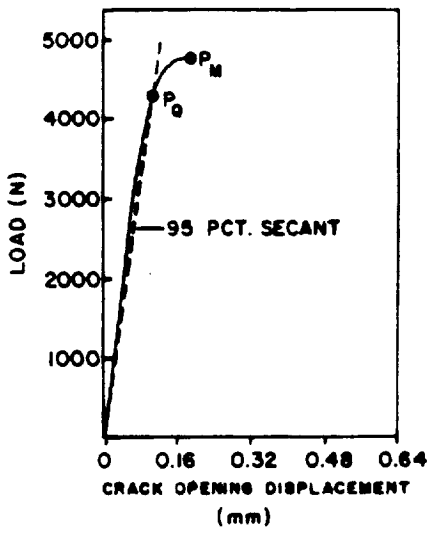

Figure 3. Load-COD Curve for a 20% CT, T-L Specimen